

© 2019

Yee Chen Low

ALL RIGHTS RESERVED

**APPLICATIONS OF BIOTECHNOLOGY FOR CROP ENHANCEMENT IN
DISEASE RESISTANCE AND NUTRITION**

By

YEE CHEN LOW

A dissertation submitted to the

School of Graduate Studies

Rutgers, The State University of New Jersey

In partial fulfillment of the requirements

For the degree of

Doctor of Philosophy

Graduate Program in Plant Biology

Written under the direction of

Professor Rong Di

And approved by

New Brunswick, New Jersey

OCTOBER 2019

ABSTRACT OF THE DISSERTATION

APPLICATIONS OF PLANT BIOTECHNOLOGY FOR CROP ENHANCEMENT IN DISEASE RESISTANCE AND NUTRITION

By YEE CHEN LOW

Dissertation Director:

Professor Rong Di

Developments in plant biotechnology are providing solutions for addressing the problems and challenges of sustainable agriculture and providing healthy food. Engineering disease resistant and nutritionally improved agricultural crops is integral to the application of plant biotechnology. In this thesis study, our core interests are on (i), studying and manipulating the economically important plant disease *Fusarium* head blight (FHB) by generating CRISPR-edited *Arabidopsis* resistant mutant plants; and (ii), producing nutritionally enhanced tomato plants with a two-in-one strategy.

FHB caused by *Fusarium graminearum* (*Fg*) is a devastating disease of crops especially wheat and barley, resulting in significant yield loss and reduced grain quality. *Fg* also produces mycotoxins, which are chemicals that are toxic to humans and livestock upon consumption. In order to examine potential susceptibility genes in barley and to enhance host resistance to FHB, two susceptibility genes, *2-oxoglutarate Fe(II)-dependent*

oxygenase (2OGO) and *ethylene insensitive 2 (EIN2)* genes were chosen for this study. Mutation of the *2OGO* gene has been shown to enhance plant defense genes' expression, leading to FHB resistance in Arabidopsis, indicating that *2OGO* is a plant immunity suppressor. Previous reports showed that both loss-of-function Arabidopsis *EIN2* gene and attenuated expression of wheat *EIN2* gene conferred resistance to *Fg*, leading to the speculation that the ethylene signaling pathway is hijacked by *Fg*. We have used CRISPR/Cas9-gene editing to precisely mutate these two Arabidopsis FHB susceptibility genes. Our results indicated that both *At2OGO*- and *AtEIN2*-gene knocked-out (KO) mutants were resistant to FHB such that *Fg* growth was greatly impeded. A critical part of this study is that phenotype could be restored in gene complementation assays using the barley gene orthologues *Hv2OGO* and *HvEIN2* in the *At2OGO*- and *AtEIN2*-KO mutants, thus demonstrating their involvement in FHB susceptibility, and indicating the molecular targets for similar gene editing of these genes in barley plants.

Genistein is one of the major isoflavones found abundantly in soybeans. It is a promising medicinal compound with anti-inflammatory, anticarcinogenic, anti-Alzheimer's and anti-osteoporosis effect due to its phytoestrogenic and antioxidant properties. Since soy products are not commonly consumed in the western diet as compared to the eastern diet, genetically engineered Moneymaker tomato which produces genistein provides a natural route to increase the intake of genistein in food without relying on supplements. We have successfully engineered Moneymaker tomato to produce a level of genistein, that is up to 250-fold the levels found in the wildtype (WT) tomato plants. Transgenic tomatoes expressing genistein, were used to study the compound's anti-Alzheimer's effects on the

amyloid β -expressing *C. elegans* disease model. Our results show that a combination of feeding genistein and lycopene can significantly delay Alzheimer's disease progression and reduce neuronal damage.

ACKNOWLEDGEMENT

I would like to express my sincere gratitude to my advisor, Dr. Rong Di, for her invaluable guidance and patience throughout the course of my PhD studies. I would like to specially thank my committee members, Dr. Michael A. Lawton, Dr. Faith C. Belanger, Dr. Juan Dong and Dr. Samuel I. Gunderson for their encouragement, comments and time. I am also thankful to my colleagues in Di and Lawton research lab and Department of Plant Biology. I am also very grateful to the Department of Plant Biology for the TA assistantship. In addition, thank you to my supervisor, Wilson, who is a great leader and mentor. Last but not least, I am deeply thankful to my family for their endless care and encouragement.

Now to him who is able to do immeasurably more than all we ask or imagine, according to his power that is at work within us. – *Ephesians 3:20*

TABLE OF CONTENTS

	Page
Abstract of the Dissertation	ii
Acknowledgement	v
List of Tables	xii
List of Illustrations	xiii
Chapter 1	1
Introduction	2
<i>Fusarium</i> head blight – the cereal killer	3
Modes of action of <i>Fusarium graminearum</i>	5
Plant responses to <i>Fusarium graminearum</i>	6
Transgenic approach for FHB resistance	7
Genistein – plant-based phytoestrogen	9
Effect of genistein on Alzheimer’s disease and other neurodegenerative disorders	10
Thesis objectives	11
References	13
Chapter 2	19
The DMR6-edited <i>Arabidopsis</i> expressing a barley <i>2-oxoglutarate</i> <i>Fe(II)-dependent oxygenase</i> orthologue validates the gene’s involvement in <i>Fusarium</i> head blight susceptibility	
Introduction	20
Materials and methods	22

TABLE OF CONTENTS (cont.)

	Page
<i>Arabidopsis thaliana</i> plant growth	22
Construction of <i>At2OGO</i> CRISPR-editing vector	23
<i>Arabidopsis thaliana</i> plant transformation and mutant selection	24
Genomic DNA (gDNA) isolation of <i>Arabidopsis</i> mutant plants	24
Mutant analysis: mutant confirmation, restriction fragment length polymorphism (RFLP) and T7 endonuclease I (T7E1) assays	25
Complementation of <i>At2OGO</i> -KO line with <i>Hv2OGO</i>	26
<i>Fg</i> inoculation on detached <i>Arabidopsis</i> inflorescences and quantitative assays for disease development	27
Relative gene expression profiling on plant defense mechanism	28
Results	30
Generating <i>DMR6</i> mutants in <i>Arabidopsis</i> using CRISPR/Cas9 system	30
Molecular characterization of <i>At2OGO</i> -KO (<i>dmr6</i>) mutants and identification of homozygous progeny	31
Identification of <i>DMR6</i> (<i>2OGO</i>) orthologue from barley cultivar Conlon for complementation test	35
Characterization of disease phenotype on <i>At2OGO</i> -KO and <i>At2OGO</i> -KO/ <i>Hv2OGO</i> -complemented homozygous plants	38

TABLE OF CONTENTS (cont.)

	Page
Gene expression profiling on plant defense signaling pathway -related genes	42
Discussion	47
References	51
Chapter 3	55
The <i>Ethylene Insensitive 2 (EIN2)</i>-edited <i>Arabidopsis</i> expressing a barley <i>EIN2</i> orthologue validates the gene's involvement in <i>Fusarium</i> head blight susceptibility	
Introduction	56
Materials and methods	58
<i>Arabidopsis thaliana</i> plant growth	59
Construction of <i>AtEIN2</i> CRISPR-editing vector	59
<i>Arabidopsis thaliana</i> plant transformation and mutant selection	60
Genomic DNA (gDNA) isolation of <i>Arabidopsis</i> mutant plants	61
Mutant analysis: mutant confirmation, restriction fragment length polymorphism (RFLP) and TaqMan assays	61
Complementation of <i>AtEIN2</i> -KO line with <i>HvEIN2</i>	62
<i>Fg</i> inoculation on detached <i>Arabidopsis</i> inflorescences and quantitative assays for disease development	63
Relative gene expression profiling on plant defense mechanism	65
Results	66

TABLE OF CONTENTS (cont.)

	Page
Generating <i>EIN2</i> mutants in Arabidopsis using CRISPR/Cas9 system	66
Molecular characterization of <i>AtEIN2</i> -KO mutants and identification of homozygous progeny	67
Identification of <i>EIN2</i> orthologue from barley cultivar Conlon for complementation test	73
Characterization of disease phenotype on <i>AtEIN2</i> -KO and <i>AtEIN2</i> -KO/ <i>HvEIN2</i> -complemented homozygous plants	74
Gene expression profiling on plant defense signaling pathway-related genes	79
Discussion	81
References	85
Chapter 4	89
Overexpression of genistein in transgenic Moneymaker tomato and its anti-Alzheimer's effect on amyloid β-expressing <i>C. elegans</i>	
Introduction	90
Materials and methods	93
Plasmid construction of <i>isoflavone synthase (IFS)</i> and <i>chalcone isomerase (CHI)</i> gene transformation vectors	93
Tomato seedling growth for <i>Agrobacterium tumefaciens</i> transformation	93

TABLE OF CONTENTS (cont.)

	Page
Generation of transgenic tomatoes <i>via</i> tissue culture selection	94
Transgenic line confirmation and homozygous line segregation	95
Quantitation of gene expression of <i>IFS</i> and <i>CHI</i> genes in homozygous tomato fruit peel and flesh	96
Lyophilization of transgenic fruit peel and flesh tissues	97
Extraction and analysis of isoflavones in transgenic tomato	98
<i>C. elegans</i> strain and maintenance	99
Serotonin (5-HT) sensitivity assay in transgenic <i>C. elegans</i>	99
Quantitative fluorescence staining of A β aggregates with thioflavin-T	100
Results	101
Construction of pIFS/CHI and pIFS plasmid vectors for the expression of <i>IFS</i> and <i>CHI</i> genes	101
Generation of homozygous transgenic tomato plants expressing both the pIFS/CHI and pIFS vectors	105
Quantitation of transgene expression in homozygous transgenic tomato plants	108
Chemical quantitation analysis of isoflavones in homozygous transgenic tomato lines	111
Serotonin (5-HT) sensitivity assay in transgenic <i>C. elegans</i>	116

TABLE OF CONTENTS (cont.)

	Page
Quantitative fluorescence staining of A β aggregates with thioflavin-T	119
Discussion	121
References	127
Chapter 5	132
Summary	133

LIST OF TABLES

	Page
Table 2.1. List of primers used in the RT-qPCR gene expression assay	31
Table 3.1. List of primers used in the RT-qPCR gene expression assay	66
Table 3.2. TaqMan qPCR assay to confirm putative CRISPR-edited <i>AtEIN2</i> (RD182) mutants	70
Table 3.3. TaqMan qPCR assay to confirm homozygous <i>AtEIN2</i> -KO (RD182-KO) mutants	71
Table 4.1. The record of transgenic tomato lines from T ₁ to T ₂ generation	108
Table 4.2. Chemical quantification analysis of isoflavone content on the dry weight basis	114
Table 4.3. Chemical quantification analysis of isoflavone content on the fresh weight basis	115
Table 4.4. List of selected foods that contain significant level of isoflavone	125

LIST OF ILLUSTRATIONS

	Page
Figure 2.1. RFLP and T7E1 assays to confirm putative CRISPR-edited <i>At2OGO</i> (RD207) mutants	32
Figure 2.2. Mutation profiles of <i>At2OGO</i> -KO (RD207) mutants at T ₁ generation and segregated homozygous mutants at T ₂ generation	34
Figure 2.3. Schematic diagram of <i>At2OGO</i> gene in WT and homozygous mutant RD207-15-5	35
Figure 2.4. Pairwise alignment of Conlon and Morex <i>Hv2OGO</i> sequences	37
Figure 2.5. Gel image of PCR-confirmed <i>At2OGO</i> -KO/ <i>Hv2OGO</i> lines	38
Figure 2.6. Illustration of FHB disease progression on detached <i>Arabidopsis</i> inflorescences	40
Figure 2.7. qPCR quantitative assay in measuring disease severity on <i>Fg</i> inoculated inflorescence	40
Figure 2.8. Quantitative assay of spore production on <i>Fg</i> inoculated inflorescence	41
Figure 2.9. Relative gene expression of non-inoculated <i>At2OGO</i> -KO floral and leaf samples	44
Figure 2.10. RT-qPCR analysis of plant defense-related genes relative expression	45
Figure 3.1. RFLP assay to confirm putative CRISPR-edited <i>AtEIN2</i> (RD182) mutants	69

LIST OF ILLUSTRATIONS (cont.)

	Page
Figure 3.2. The mutation profiles of RD182 (<i>AtEIN2</i> -KO) mutants at T ₁ generation and the homozygous mutants at T ₄ generation	71
Figure 3.3. Gel image showed the PCR-confirmed <i>AtEIN2</i> -KO/ <i>HvEIN2</i> lines	74
Figure 3.4. Illustration of FHB disease progression on detached <i>Arabidopsis</i> inflorescences	75
Figure 3.5. qPCR quantitative assay in measuring disease severity on <i>Fg</i> inoculated inflorescence	78
Figure 3.6. Quantitative assay of spore production on <i>Fg</i> inoculated inflorescence	79
Figure 3.7. RT-qPCR analysis of plant defense-related genes relative expression	81
Figure 4.1. Illustration of the plasmid vectors used for tomato transformation	102
Figure 4.2. <i>IFS</i> and <i>CHI</i> protein sequence alignment between alfalfa (<i>Medicago sativa</i>) and soybean (<i>Glycine max</i>)	105
Figure 4.3. Generation of homozygous transgenic tomato plants <i>via</i> tissue culture	107
Figure 4.4. Transgene expression of <i>IFS</i> and <i>CHI</i> in peel and flesh tissue of <i>IFS/CHI</i> homozygous lines	110

LIST OF ILLUSTRATIONS (cont.)

	Page
Figure 4.5. Transgene expression of <i>IFS</i> in peel and flesh tissue of IFS homozygous lines	111
Figure 4.6. Extracted ion chromatogram of IFS/CHI 9-7 and WT tomato	113
Figure 4.7. Serotonin sensitivity assay of <i>C. elegans</i>	118
Figure 4.8. Quantification of A β aggregates by thioflavin-T fluorescence staining	120
Figure 4.9. Simple illustration of the isoflavone synthesis pathway	123

Chapter **1**

Introduction

Chapter 1

Introduction

Plant biotechnology has been in an impetuous development during the past 30 to 40 years. It has become the mainstream technology that allows farmers or plant breeders to introduce desirable and beneficial traits such as disease resistance, pest resistance, insecticide and herbicide tolerance, nutrient enhancement or molecular factory into plants through genetic modification. Genetic engineering method and delivery agents are the two important aspects in generating transgenic plants. One of the key milestones for plant biotechnology field is the advent of *Agrobacterium tumefaciens*, the nature's genetic engineer which has been well-studied over the past 100 years [1]. The ability of *Agrobacterium* to utilize its *vir* genes to transfer its tumor-inducing DNA (T-DNA) into the host plant's genome has revolutionized plant genetic engineering [2]. The properties of *Agrobacterium* allow genes of interest to be integrated into the genome of cultured plant cells. While *Agrobacterium* has been the main delivery agent used for routine plant transformation, the development of biolistic or "gene gun" transformation has improved the transformation efficiency for cells that are not susceptible to *Agrobacterium*, and are otherwise recalcitrant to DNA transfer [3-5]. Biolistic transformation involves the direct delivery of exogenous DNA into plant cells for nuclear integration and can be applied to all types of plant cells [6]. Another delivery agent is the viral-based vector for transducing the DNA into host cell [7, 8]. These three delivery methods are commonly used for RNAi (RNA interference) [9-11], TALENs (transcription activator-like effector nucleases) [12, 13] and most recently the CRISPR

(clustered regularly interspaced short palindromic repeats) [14, 15] applications. The emerging of CRISPR gene editing provides a more precise and efficient way for genetic engineering application as well as accelerates the research in plant biotechnology field such as developing resistance cultivar and improving crop yield.

***Fusarium* head blight – the cereal killer**

Fusarium head blight (FHB) or scab is a devastating disease of cereal crops especially in wheat, barley, oat and maize [16, 17]. It can be caused by several species of the *Fusarium* fungal group but the primary causal agent in North America and Europe is *Fusarium graminearum* (*Fg*) (teleomorph *Gibberella zeae*) [18]. *Fg* is an important hemibiotrophic fungal pathogen, with a short biotrophic phase (feeding on the host) preceding a necrotrophic phase (killing the host for nutrients) [19]. Its growth is favored by warm condition (18-30 °C) with high humidity and it is highly infectious during host flowering season but infection can still occur during kernel formation [20, 21]. The infected cereal crops have disease symptoms of bleaching of spikelets and shriveled, non-viable seeds. Due to the reduced grain quality, FHB has caused billions of dollars of economic loss in the 1990s and early 2000s [22, 23]. In addition to yield cutback, the disease compromises the quality of infected grain due to mycotoxin contamination that is toxic to humans and animals upon consumption [24, 25]. Deoxynivalenol (DON), often referred as vomitoxin, is the most prevalent trichothecene mycotoxin found in *Fg*-infected grains [26]. It is a virulence factor for *Fg* infection and host colonization. DON toxin inhibits protein synthesis in eukaryotic cells by binding to the ribosomal 60S subunit [27]. As a

consequence, cellular integrity is severely disrupted due to ribotoxic stress, apoptosis and the hampering of cell division. In severe cases, consumption of DON-contaminated grains can cause nausea, vomiting, diarrhea and fever in humans while weight loss and death in animals [28]. As a result of DON acute toxic effects, the U.S. Food and Drug Administration (FDA) has set the advisory levels for human and animal daily intake of DON [29]. The advisory level for finished wheat products is 1 ppm (part per million), 10 ppm on grains and grain by-products, and 5 ppm on grain feeds for swine and other animals that do not exceed 20% and 40% of their diet, respectively. Despite the adverse effect of FHB on mammal health and economic output, effective strategies for disease management are currently very limited. One of the control measures is the use of fungicide on cereal crops prior to the appearance of disease symptoms [30]. This large coverage of fungicide spraying can be very costly and unnecessary. In addition, *Fg* is resistant to azole fungicide which renders the complete prevention impossible [31, 32]. Current preventive measures focus mainly on marker-assisted breeding for genetic resistance traits [33-35]. However, the incorporation of well-studied and commonly used QTL such as *Fhb1* into susceptible cultivars is only partially effective and the resulting level of resistance through breeding is often insufficient to control the FHB epidemic [36]. On the grounds that resistant cultivars are desperately needed, novel strategies *via* genetic engineering, chemical application or sophisticated forecasting systems are favorable for enhancing the cultivars' performance in restricting FHB. Prior to that, it is imperative to have a thorough understanding on *Fg* disease development and plant defense responses to *Fg* as well as current advancement in FHB resistance.

Modes of action of *Fusarium graminearum*

Fg reproduces asexually *via* macroconidia or sexually *via* ascospores, which are dispersed through wind and rain [37-39]. The specific G protein-coupled receptors and the expression of *transducin beta-like* gene (*FgFTL1*) allow *Fg* to sense environmental cues and transmit signals for host recognition [40, 41]. Firm macroconidia adhesion is the key step for *Fg* to establish itself on the host surface, usually on plant cuticle. Fungal adhesion, sometimes facilitated by a sticky ascospore cell wall, is an important mechanism for *Fg* to prevent spore displacement from the host [42]. Spore germination is dictated by its surrounding environmental conditions such as temperature, water availability and spore density. Once *Fg* senses the favorable conditions, its macroconidia germinate and form a fungal germ tube for host penetration. *Fg* can enter the host either passively through a natural opening such as an open stomata or actively by direct cuticular penetration. In order to actively gain entry into the host by penetrating the plant cuticle layer, *Fg* transmits a signal through the activation of *FgRAS2 GTPase* and *FgGpmk1* MAPK to drive the expression of hydrolytic enzymes (e.g. cutinase and lipases) to degrade the plant cuticle [43]. At the same time, *Fg* also releases enzymes such as chitin synthases (*FgCHSs*) and sphingolipid glucosylceramide synthase (*FgGCS*) to maintain its integrity of its cell wall and membrane from plant degradation enzymes. In subsequent infection growth, fungal RALF (rapid alkalization factor) initiates the alkalization of the plant apoplast pH to stimulate phosphorylation of MAPK and the initiation of a downstream signaling cascade [44, 45] that can sense the plant polyamines and reactive oxygen species (ROS) and then trigger the synthesis of deoxynivalenol (DON) through the activation of tricothecene (Tri) genes [46,

47]. Further penetration into plant cell wall and membrane requires the synthesis of a vast array of degradation enzymes (e.g. lipases, pectinase, hemicellulases and cellulases) [48, 49]. The release of DON toxin causes oxidative stress in host and the hijacking of the plant ethylene signaling pathway accelerates the plant cell death granting the access to *Fg* for nutrients [50]. The colonization of *Fg* begins when it starts to reproduce and increases its spore density. From the point of infection, *Fg* can spread to the adjacent florets either internally *via* vascular bundles or externally *via* stomata.

Plant responses to *Fusarium graminearum*

There are two components of plant FHB resistance: resistance to initial infection (Type I) and the resistance to dispersal (Type II) [51]. Type I resistance involves the basal resistance components in the plant. The first layer of defense line is the physical barrier of plant cuticle and cell wall. The waxy surface of plant cuticle limits the water retention and minimizes *Fg* spores germination [52]. Plants first recognize the *Fg* invasion by sensing of *Fg*'s cell wall features using an array of receptor proteins. The *Fg* recognition activates the expression of degradation enzymes (e.g. chitinases and glucanases) to degrade fungal cell wall and non-specific lipid transfer protein to disrupt fungal membrane integrity [53]. In addition, the fungal growth is halted by the plant action producing phenolic compounds which have suppressing effect on fungi. While breaking down the fungal cell wall, the plants release elicitors which induce the expression of several genes (e.g. polygalacturonase-inhibiting protein and xylanase inhibitor) in order to maintain its cell wall integrity and initiates the direct repair of damaged cuticles [52]. Due to this elicitor-

induced immune response, the plant cell wall gets thicker and becomes lignified to attempt to block the entry of *Fg*. In the case of successful penetration by *Fg*, plants regulate their cellular composition by detoxifying ROS and neutralizing DON toxin via *superoxide dismutase (SOD)* and *UDP-glucosyltransferase (UGT)* genes, respectively [54]. Following the induced immune response, systemic resistance is activated through salicylic acid (SA), jasmonic acid (JA) and ethylene (ET) to protect distant tissues prior to the spread of *Fg* by the activation of pathogenesis-related (PRs) protein gene expression and JA/ET responsive genes [55]. In all, the innate plant defense response provides broad-spectrum of resistance against the invasion of pathogens.

Transgenic approach for FHB resistance

A number of approaches have been used to generate transgenic wheat and barley plants which overexpress of pathogenesis-related (PR) or defense response genes to provide enhanced resistance to FHB [56]. For example, the overexpression of Arabidopsis *NPRI* (*nonexpressor pathogenesis-related protein*) gene in wheat induced rapid activation of plant defense response after initial infection [57]. Another transgenic strategy is to express antifungal or antimicrobial peptides from other species into wheat. Expression of radish defensin gene, an intraspecies antifungal gene, in wheat has managed to disrupt the fungal cell membrane and greatly slow down the fungal growth [58, 59]. Likewise, expression of mammal lactoferrin, an interspecies antibacterial peptide, in wheat can successfully alleviate disease symptoms through fungal growth retardation due to nutrient deprivation and cell membrane disruption [60]. Since DON is a key player in the onset of disease

symptom, there are three major tactics to block the disease progression and mycotoxin contamination. The first tactic is to prevent fungal penetration into host cell wall. For example, the expression of *PGIPs* (*polygalacturonase inhibiting proteins*) in wheat can prevent plant cell wall degradation by fungal polygalacturonase and avoid the onset of DON synthesis within the infected cells [61]. The second tactic is to modify the DON target site, namely, the ribosomal protein L3. Hence, expression of a truncated form of yeast ribosomal protein L3 in wheat has led to a reduction of DON levels in inoculated kernels [62]. The third tactic is to detoxify and neutralize DON by converting it to less toxic DON-3-glucoside (D3G). One such approach involved overexpressing the *UGT* (*UDP-glucosyltransferase*) gene, which functions to detoxify DON. In *Brachypodium* ectopic expression of UGT can establish resistance to FHB at the primary infection stage [63, 64]. Regardless of all these efforts in trying to deploy new resistance traits through conventional method in genetic engineering, the incorporating of foreign genes into the host results in genetically modified organisms (GMO) which are difficult to deploy in grain fields due to the regulatory law and general public concerns about GMOs. The emergence of CRISPR genome editing technology and ability to identify and manipulate host susceptibility gene provides a new approach to enhance resistance and produce plants that are not GMOs.

CRISPR (clustered regularly interspaced short palindromic repeats) is a microbial adaptive immune system [65]. It is a group of DNA sequences discovered within the genome of bacteria that act as a defense system against viruses. Cas9 (CRISPR-associated protein 9) enzyme recognizes and cleaves DNA strands that are complementary to CRISPR sequence [66]. This defense mechanism has provided the foundation for CRISPR-Cas9 gene editing

technology. The CRISPR-Cas9 system enables efficient and precise genome editing by inducing double-stranded breaks (DSBs) at the targeted genomic region [67]. These DSBs stimulate DNA repair by two distinct mechanisms which are NHEJ (non-homologous end joining) and HDR (homology-directed repair) [68]. NHEJ is error-prone and introduces random patterns of insertions and deletions (indels) which are sufficient for introducing unpredictable mutations at targeted genomic sites. Since HDR occurs at a relatively low rate, the precise genome editing by HDR-mediated insertional mutagenesis has a much lower efficiency [69]. Targeted genome editing can be achieved easily by customizing the guide RNA (gRNA) within the CRISPR-Cas9 system. Due to its versatility and specificity, it has been used intensively in mammalian cells and many organisms [70-74]. Application of CRISPR in plants has attained a great success in demonstrating a similar editing pattern as in other organisms and recovery of stable transgenic lines [75-82]. CRISPR, therefore, is a promising genetic engineering tool to be used in crop improvement.

Genistein – plant-based phytoestrogen

Genistein is one of the major isoflavones found in legumes, especially soybeans. Genistein and other isoflavones (daidzein and glycitein) are synthesized *via* the phenylpropanoid pathway [83]. Naringenin, the precursor for genistein biosynthesis, is an intermediate within the branch of phenylpropanoid pathway which leads to the synthesis of isoflavones, flavonols and anthocyanins. Naringenin is the product of chalcone synthase and chalcone isomerase which are commonly found in most plants. However, isoflavone production is unique to the legume family and dependent on the key enzyme, *isoflavone synthase (IFS)*

for synthesizing genistein [84]. Among the isoflavones, genistein is the most bioactive with potent antioxidant property. Studies showed that genistein can modulate various genes (e.g. protein tyrosine kinase) and proteins to strengthen the cell defense system under oxidative stress by scavenging reactive oxygen species (ROS) and preventing apoptosis [85]. In addition, genistein, a non-steroidal phytoestrogen, has a structural conformation that resembles to the estradiol-17 β , a form of estrogen, and confer ability for binding to estrogen receptors (ERs) [83], with higher affinity to ER- β than to ER- α [86]. Due to these phytoestrogenic features, it is capable of regulating mammalian metabolic diseases that are hormone-related such as cancer, neurodegenerative disorders, diabetes and obesity. Most of these diseases often cause an inflammatory response in affected tissues and genistein is known to inhibit the activation of nuclear factor κ B (NF- κ B), the inflammatory mediator, to protect tissues from cell death [87]. It is critical to point out that diseases such as osteoporosis and neurodegenerative disorders that rely on estrogen treatment are often accompanied with the unfavorable side effects. In contrast, while genistein can still act as an agonist to ER- β and influences cellular function without increasing other health risks [88, 89]. Genistein, therefore, is a promising medicinal compound that can contribute to anti-inflammatory, anticarcinogenic, anti-neurodegenerative, anti-osteoporosis and hypocholesterolemic effects [90].

Effect of genistein on Alzheimer's disease and other neurodegenerative disorders

Neurodegenerative diseases such as Alzheimer's disease (AD) and dementia are irreversible and result in progressive brain disorder for which there is no cure. Excessive

accumulation amyloid β ($A\beta$) peptide and the tangles of tau protein are the key indicators of Alzheimer's disease development [90]. Neurotoxic $A\beta$ peptide, is generated from sequential cleavage of the amyloid precursor protein (APP) by the α -secretase followed by γ -secretase [91]. $A\beta_{1-42}$ is known to be the most toxic form. The accumulation of $A\beta$ can induce neuronal inflammation and oxidative stress and eventually lead to neuron cell death [92]. Genistein has been studied for a long time for its protective effect in neurodegenerative disorders. Multiple pathways have been proposed to explain the mechanism of genistein on AD. Studies showed that genistein regulates the inflammatory pathway through nuclear factor $\text{NF}\kappa\text{B}$ by suppressing nuclear factor activation and preventing cell apoptosis leading to protection of neuron cell [93, 94]. In addition, estrogen receptor β , genistein's binding target, is abundantly expressed in brain tissue and it contributes to estrogen-induced protective effects such as modulating the calcium ion and antiapoptotic protein signaling pathways [92, 95] and up-regulating the expression of insulin-degrading enzyme (IDE) to drive the degradation of $A\beta$ [96, 97]. Apart from influencing cellular signaling cascades, a recent *in vitro* study indicated that genistein can inhibit or slow down the oligomerization of $A\beta$ in dose-dependently manner [98]. However, its *in vivo* effects and underlying mechanism(s) are not yet known. In all, genistein protects against AD mainly through its antiapoptotic effect.

Thesis objectives

In this doctoral study, two different aspects of plant biotechnology applications, disease resistance and nutrient enhancement, have been studied. As mentioned earlier, FHB is one

of the most important disease of cereal crops and most challenging to prevent. There are very limited effective strategies available for FHB control. The use of genetic engineering approach can be a promising solution to accelerate the production of resistance cultivars. Instead of introducing transgenes that enhance resistance in GMO plants, the availability of plant susceptibility genes allows us to deploy CRISPR gene editing technique to develop non-GMO plants that are potentially disease resistant. Apart from disease resistance, nutrient enhancement is another core interest for agricultural research. Genistein has been proved to have beneficial effects in preventing different chronic metabolic diseases such as cancer and Alzheimer's disease. However, consumption of soy-based products is uncommon in the western diet. Introduction of health-promoting plant compound into a more commonly consumed food would be an interesting approach to increase genistein intake.

The objectives of this thesis are to utilize biotechnology tools to engineer (i), *Arabidopsis* mutants lacking functional disease susceptibility gene in order to validate their gene involvement in FHB resistance and to confirm the corresponding function of barley orthologues and (ii), Moneymaker tomato which produces genistein and to study the synergistic effect of genistein and lycopene in Alzheimer's disease using the multicellular model animal *C. elegans*.

For the next two chapters, two susceptibility genes involved in FHB resistance are discussed. First, the FHB resistance effect of a CRISPR-edited *Arabidopsis 2-oxoglutarate Fe(II)-dependent oxygenase (At2OGO)* gene is assessed and the complementation test of

barley orthologue is described. Second, a CRISPR-edited *Arabidopsis ethylene insensitive 2 (EIN2)*, a key component in ethylene signaling pathway, is assessed for FHB resistance and the complementation test of barley orthologue is described. The last chapter discusses the generation of transgenic tomato with genistein expression and its therapeutic effect in Alzheimer's disease using *C.elegans*.

References

1. Nester, E.W., *Agrobacterium: nature's genetic engineer*. Front Plant Sci, 2014. **5**: p. 730.
2. Gelvin, S.B., *Agrobacterium-mediated plant transformation: the biology behind the "gene-jockeying" tool*. Microbiology and molecular biology reviews : MMBR, 2003. **67**(1): p. 16-37.
3. Harkess, A., *Smashing Barriers in Biolistic Plant Transformation*. Plant Cell, 2019. **31**(2): p. 273-274.
4. Li, L., et al., *An improved rice transformation system using the biolistic method*. Plant Cell Rep, 1993. **12**(5): p. 250-5.
5. Tian, B., et al., *Biolistic Transformation of Wheat*. Methods Mol Biol, 2019. **1864**: p. 117-130.
6. Baltés, N.J., J. Gil-Humanes, and D.F. Voytas, *Chapter One - Genome Engineering and Agriculture: Opportunities and Challenges*, in *Progress in Molecular Biology and Translational Science*, D.P. Weeks and B. Yang, Editors. 2017, Academic Press. p. 1-26.
7. Hanley, K., et al., *Development of a plant viral-vector-based gene expression assay for the screening of yeast cytochrome p450 monooxygenases*. Assay Drug Dev Technol, 2003. **1**(1 Pt 2): p. 147-60.
8. Zaidi, S.S.-E.A. and S. Mansoor, *Viral Vectors for Plant Genome Engineering*. Frontiers in plant science, 2017. **8**: p. 539-539.
9. Crane, Y.M. and S.B. Gelvin, *RNAi-mediated gene silencing reveals involvement of Arabidopsis chromatin-related genes in Agrobacterium-mediated root transformation*. Proceedings of the National Academy of Sciences of the United States of America, 2007. **104**(38): p. 15156-15161.
10. Davies, K.M., et al., *Biolistics-based gene silencing in plants using a modified particle inflow gun*. Methods Mol Biol, 2013. **940**: p. 63-74.
11. Couto, L.B. and K.A. High, *Viral vector-mediated RNA interference*. Curr Opin Pharmacol, 2010. **10**(5): p. 534-42.
12. Sardesai, N. and S. Subramanyam, *Agrobacterium: A Genome-Editing Tool-Delivery System*. Curr Top Microbiol Immunol, 2018. **418**: p. 509.

13. Yadava, P., et al., *Advances in Maize Transformation Technologies and Development of Transgenic Maize*. *Frontiers in plant science*, 2017. **7**: p. 1949-1949.
14. Liang, Z., et al., *Genome editing of bread wheat using biolistic delivery of CRISPR/Cas9 in vitro transcripts or ribonucleoproteins*. *Nature Protocols*, 2018. **13**: p. 413.
15. Zhang, S., et al., *Highly Efficient and Heritable Targeted Mutagenesis in Wheat via the Agrobacterium tumefaciens-Mediated CRISPR/Cas9 System*. *Int J Mol Sci*, 2019. **20**(17).
16. Brewer, H.C. and K.E. Hammond-Kosack, *Host to a Stranger: Arabidopsis and Fusarium Ear Blight*. *Trends Plant Sci*, 2015. **20**(10): p. 651-663.
17. Parry, D.W., P. Jenkinson, and L. McLeod, *Fusarium ear blight (scab) in small grain cereals—a review*. *Plant Pathology*, 1995. **44**(2): p. 207-238.
18. Kelly, A.C. and T.J. Ward, *Population genomics of Fusarium graminearum reveals signatures of divergent evolution within a major cereal pathogen*. *PLOS ONE*, 2018. **13**(3): p. e0194616.
19. McMullen, M., et al., *A Unified Effort to Fight an Enemy of Wheat and Barley: Fusarium Head Blight*. *Plant Dis*, 2012. **96**(12): p. 1712-1728.
20. Manstretta, V. and V. Rossi, *Effects of Temperature and Moisture on Development of Fusarium graminearum Perithecia in Maize Stalk Residues*. *Appl Environ Microbiol*, 2016. **82**(1): p. 184-91.
21. Linkmeyer, A., et al., *Influence of inoculum and climatic factors on the severity of Fusarium head blight in German spring and winter barley*. *Food Addit Contam Part A Chem Anal Control Expo Risk Assess*, 2016. **33**(3): p. 489-99.
22. Njanje, W.E., et al., *Regional Economic Impacts of Fusarium Head Blight in Wheat and Barley*. *Applied Economic Perspectives and Policy*, 2004. **26**(3): p. 332-347.
23. Windels, C.E., *Economic and Social Impacts of Fusarium Head Blight: Changing Farms and Rural Communities in the Northern Great Plains*. *Phytopathology*, 2000. **90**(1): p. 17-21.
24. Pestka, J.J. and A.T. Smolinski, *Deoxynivalenol: toxicology and potential effects on humans*. *J Toxicol Environ Health B Crit Rev*, 2005. **8**(1): p. 39-69.
25. Sobrova, P., et al., *Deoxynivalenol and its toxicity*. *Interdiscip Toxicol*, 2010. **3**(3): p. 94-9.
26. Dean, R., et al., *The Top 10 fungal pathogens in molecular plant pathology*. *Mol Plant Pathol*, 2012. **13**(4): p. 414-30.
27. Rocha, O., K. Ansari, and F.M. Doohan, *Effects of trichothecene mycotoxins on eukaryotic cells: a review*. *Food Addit Contam*, 2005. **22**(4): p. 369-78.
28. Sobrova, P., et al., *Deoxynivalenol and its toxicity*. *Interdisciplinary toxicology*, 2010. **3**(3): p. 94-99.
29. (FDA), U.S.F.a.D.A. *Advisory Levels for Deoxynivalenol (DON) in Finished Wheat Products for Human Consumption and Grains and Grain By-Products used for Animal Feed*. 2010; Available from: <https://www.fda.gov/regulatory-information/search-fda-guidance-documents/guidance-industry-and-fda-advisory-levels-deoxynivalenol-don-finished-wheat-products-human>.

30. Torres, A.M., et al., *Fusarium head blight and mycotoxins in wheat: prevention and control strategies across the food chain*. World Mycotoxin Journal, 2019: p. 1-24.
31. Abou Ammar, G., et al., *Identification of ABC Transporter Genes of Fusarium graminearum with Roles in Azole Tolerance and/or Virulence*. PLOS ONE, 2013. **8**(11): p. e79042.
32. Becher, R., et al., *Adaptation of Fusarium graminearum to Tebuconazole Yielded Descendants Diverging for Levels of Fitness, Fungicide Resistance, Virulence, and Mycotoxin Production*. Phytopathology, 2010. **100**(5): p. 444-453.
33. Buerstmayr, H., T. Ban, and J.A. Anderson, *QTL mapping and marker-assisted selection for Fusarium head blight resistance in wheat: a review*. Plant Breeding, 2009. **128**(1): p. 1-26.
34. Jayatilake, D.V., G.H. Bai, and Y.H. Dong, *A novel quantitative trait locus for Fusarium head blight resistance in chromosome 7A of wheat*. Theor Appl Genet, 2011. **122**(6): p. 1189-98.
35. Zhao, M., et al., *Molecular mapping of QTL for Fusarium head blight resistance introgressed into durum wheat*. Theor Appl Genet, 2018. **131**(9): p. 1939-1951.
36. Prat, N., et al., *QTL mapping of Fusarium head blight resistance in three related durum wheat populations*. TAG. Theoretical and applied genetics. Theoretische und angewandte Genetik, 2017. **130**(1): p. 13-27.
37. Sutton, J.C., *Epidemiology of wheat head blight and maize ear rot caused by Fusarium graminearum*. Canadian Journal of Plant Pathology, 1982. **4**(2): p. 195-209.
38. Wagacha, J.M. and J.W. Muthomi, *Mycotoxin problem in Africa: current status, implications to food safety and health and possible management strategies*. Int J Food Microbiol, 2008. **124**(1): p. 1-12.
39. Trail, F., *For Blighted Waves of Grain: Fusarium graminearum in the Postgenomics Era*. Plant Physiology, 2009. **149**(1): p. 103.
40. Ding, S., et al., *Transducin Beta-Like Gene FTL1 Is Essential for Pathogenesis in Fusarium graminearum*. Eukaryotic Cell, 2009. **8**(6): p. 867.
41. Jiang, C., et al., *An expanded subfamily of G-protein-coupled receptor genes in Fusarium graminearum required for wheat infection*. Nature Microbiology, 2019. **4**(9): p. 1582-1591.
42. Leonard, K.J. and W.R. Bushnell, *Fusarium head blight of wheat and barley*. 2003, St. Paul, Minn.: APS Press. x, 512 pages.
43. Bluhm, B.H., et al., *RAS2 Regulates Growth and Pathogenesis in Fusarium graminearum*. Molecular Plant-Microbe Interactions, 2007. **20**(6): p. 627-636.
44. Fernandes, T.R., et al., *How alkalization drives fungal pathogenicity*. PLoS pathogens, 2017. **13**(11): p. e1006621-e1006621.
45. Hussain, A., et al., *Comprehensive analysis of plant rapid alkalization factor (RALF) genes*. Plant Physiology and Biochemistry, 2016. **106**.
46. Audenaert, K., et al., *Deoxynivalenol: a major player in the multifaceted response of Fusarium to its environment*. Toxins, 2013. **6**(1): p. 1-19.
47. Gardiner, D.M., et al., *Early activation of wheat polyamine biosynthesis during Fusarium head blight implicates putrescine as an inducer of trichothecene mycotoxin production*. BMC plant biology, 2010. **10**: p. 289-289.

48. Mary Wanjiru, W., K. Zhensheng, and H. Buchenauer, *Importance of Cell Wall Degrading Enzymes Produced by Fusarium graminearum during Infection of Wheat Heads*. European Journal of Plant Pathology, 2002. **108**(8): p. 803-810.
49. Paccanaro, M.C., et al., *Synergistic Effect of Different Plant Cell Wall–Degrading Enzymes Is Important for Virulence of Fusarium graminearum*. Molecular Plant-Microbe Interactions, 2017. **30**(11): p. 886-895.
50. Chen, X., et al., *Fusarium graminearum exploits ethylene signalling to colonize dicotyledonous and monocotyledonous plants*. New Phytol, 2009. **182**(4): p. 975-83.
51. Brar, G.S., et al., *Genetic factors affecting Fusarium head blight resistance improvement from introgression of exotic Sumai 3 alleles (including Fhb1, Fhb2, and Fhb5) in hard red spring wheat*. BMC Plant Biology, 2019. **19**(1): p. 179.
52. Walter, S., P. Nicholson, and F.M. Doohan, *Action and reaction of host and pathogen during Fusarium head blight disease*. New Phytol, 2010. **185**(1): p. 54-66.
53. Kong, L., J.M. Anderson, and H.W. Ohm, *Induction of wheat defense and stress-related genes in response to Fusarium graminearum*. Genome, 2005. **48**(1): p. 29-40.
54. He, Y., et al., *Genome-wide analysis of family-1 UDP glycosyltransferases (UGT) and identification of UGT genes for FHB resistance in wheat (Triticum aestivum L.)*. BMC plant biology, 2018. **18**(1): p. 67-67.
55. Li, N., et al., *Signaling Crosstalk between Salicylic Acid and Ethylene/Jasmonate in Plant Defense: Do We Understand What They Are Whispering?* International journal of molecular sciences, 2019. **20**(3): p. 671.
56. Mackintosh, C.A., et al., *Overexpression of defense response genes in transgenic wheat enhances resistance to Fusarium head blight*. Plant cell reports, 2007. **26**(4): p. 479-488.
57. Makandar, R., et al., *Genetically engineered resistance to Fusarium head blight in wheat by expression of Arabidopsis NPR1*. Mol Plant Microbe Interact, 2006. **19**(2): p. 123-9.
58. Lacerda, A.F., et al., *Antifungal defensins and their role in plant defense*. Frontiers in microbiology, 2014. **5**: p. 116-116.
59. Li, Z., et al., *Expression of a radish defensin in transgenic wheat confers increased resistance to Fusarium graminearum and Rhizoctonia cerealis*. Functional & Integrative Genomics, 2011. **11**(1): p. 63-70.
60. Han, J., et al., *Transgenic expression of lactoferrin imparts enhanced resistance to head blight of wheat caused by Fusarium graminearum*. BMC plant biology, 2012. **12**: p. 33-33.
61. Kalunke, R.M., et al., *An update on polygalacturonase-inhibiting protein (PGIP), a leucine-rich repeat protein that protects crop plants against pathogens*. Frontiers in plant science, 2015. **6**: p. 146-146.
62. Di, R. and N.E. Tumer, *Expression of a Truncated Form of Ribosomal Protein L3 Confers Resistance to Pokeweed Antiviral Protein and the Fusarium Mycotoxin Deoxynivalenol*. Molecular Plant-Microbe Interactions, 2005. **18**(8): p. 762-770.

63. Gatti, M., et al., *The Brachypodium distachyon UGT Bradi5gUGT03300 confers type II fusarium head blight resistance in wheat*. Plant Pathology, 2019. **68**(2): p. 334-343.
64. Pasquet, J.-C., et al., *A Brachypodium UDP-Glycosyltransferase Confers Root Tolerance to Deoxynivalenol and Resistance to Fusarium Infection*. Plant Physiology, 2016. **172**(1): p. 559.
65. Barrangou, R., *The roles of CRISPR–Cas systems in adaptive immunity and beyond*. Current Opinion in Immunology, 2015. **32**: p. 36-41.
66. Anders, C., O. Niewoehner, and M. Jinek, *Chapter Seventeen - In Vitro Reconstitution and Crystallization of Cas9 Endonuclease Bound to a Guide RNA and a DNA Target*, in *Methods in Enzymology*, S.A. Woodson and F.H.T. Allain, Editors. 2015, Academic Press. p. 515-537.
67. Jiang, W., et al., *RNA-guided editing of bacterial genomes using CRISPR-Cas systems*. Nature Biotechnology, 2013. **31**: p. 233.
68. Sander, J.D. and J.K. Joung, *CRISPR-Cas systems for editing, regulating and targeting genomes*. Nature Biotechnology, 2014. **32**: p. 347.
69. Mali, P., et al., *RNA-Guided Human Genome Engineering via Cas9*. Science, 2013. **339**(6121): p. 823.
70. Fogarty, N.M.E., et al., *Erratum: Genome editing reveals a role for OCT4 in human embryogenesis*. Nature, 2017. **551**(7679): p. 256.
71. Friedland, A.E., et al., *Heritable genome editing in C. elegans via a CRISPR-Cas9 system*. Nat Methods, 2013. **10**(8): p. 741-3.
72. Hwang, W.Y., et al., *Efficient genome editing in zebrafish using a CRISPR-Cas system*. Nat Biotechnol, 2013. **31**(3): p. 227-9.
73. Sanchez, J.C., et al., *Phenotypic and Genotypic Consequences of CRISPR/Cas9 Editing of the Replication Origins in the rDNA of *Saccharomyces cerevisiae**. Genetics, 2019.
74. Xue, W., et al., *CRISPR-mediated direct mutation of cancer genes in the mouse liver*. Nature, 2014. **514**: p. 380.
75. Chen, K., et al., *CRISPR/Cas Genome Editing and Precision Plant Breeding in Agriculture*. Annu Rev Plant Biol, 2019. **70**: p. 667-697.
76. Endo, M., M. Mikami, and S. Toki, *Multigene Knockout Utilizing Off-Target Mutations of the CRISPR/Cas9 System in Rice*. Plant and Cell Physiology, 2014. **56**(1): p. 41-47.
77. Feng, C., et al., *Efficient Targeted Genome Modification in Maize Using CRISPR/Cas9 System*. J Genet Genomics, 2016. **43**(1): p. 37-43.
78. Feng, Z., et al., *Efficient genome editing in plants using a CRISPR/Cas system*. Cell Res, 2013. **23**(10): p. 1229-32.
79. Jiang, W., et al., *Demonstration of CRISPR/Cas9/sgRNA-mediated targeted gene modification in Arabidopsis, tobacco, sorghum and rice*. Nucleic Acids Res, 2013. **41**(20): p. e188.
80. Li, Z., et al., *Cas9-Guide RNA Directed Genome Editing in Soybean*. Plant physiology, 2015. **169**(2): p. 960-970.
81. Sanchez-Leon, S., et al., *Low-gluten, nontransgenic wheat engineered with CRISPR/Cas9*. Plant Biotechnol J, 2018. **16**(4): p. 902-910.

82. Zhang, Z., et al., *A multiplex CRISPR/Cas9 platform for fast and efficient editing of multiple genes in Arabidopsis*. Plant cell reports, 2016. **35**(7): p. 1519-1533.
83. Dixon, R.A. and D. Ferreira, *Genistein*. Phytochemistry, 2002. **60**(3): p. 205-11.
84. Barnes, S., *The Biochemistry, Chemistry and Physiology of the Isoflavones in Soybeans and their Food Products*. Lymphatic Research and Biology, 2010. **8**(1): p. 89-98.
85. Ganai, A.A., et al., *Genistein modulates the expression of NF- κ B and MAPK (p-38 and ERK1/2), thereby attenuating d-Galactosamine induced fulminant hepatic failure in Wistar rats*. Toxicology and Applied Pharmacology, 2015. **283**(2): p. 139-146.
86. Kuiper, G.G., et al., *Interaction of estrogenic chemicals and phytoestrogens with estrogen receptor beta*. Endocrinology, 1998. **139**(10): p. 4252-63.
87. Gupta, S.C., et al., *Role of nuclear factor kappaB-mediated inflammatory pathways in cancer-related symptoms and their regulation by nutritional agents*. Exp Biol Med (Maywood), 2011. **236**(6): p. 658-71.
88. McDowell, M.L., et al., *Neuroprotective effects of genistein in VSC4.1 motoneurons exposed to activated microglial cytokines*. Neurochemistry international, 2011. **59**(2): p. 175-184.
89. Zheng, X., S.-K. Lee, and O.K. Chun, *Soy Isoflavones and Osteoporotic Bone Loss: A Review with an Emphasis on Modulation of Bone Remodeling*. Journal of medicinal food, 2016. **19**(1): p. 1-14.
90. Matsuda, S., et al., *Chapter 93 - Neuroprotection of Genistein in Alzheimer's Disease*, in *Diet and Nutrition in Dementia and Cognitive Decline*, C.R. Martin and V.R. Preedy, Editors. 2015, Academic Press: San Diego. p. 1003-1010.
91. Chen, G.-f., et al., *Amyloid beta: structure, biology and structure-based therapeutic development*. Acta Pharmacologica Sinica, 2017. **38**(9): p. 1205-1235.
92. Devi, K.P., et al., *Molecular and Therapeutic Targets of Genistein in Alzheimer's Disease*. Mol Neurobiol, 2017. **54**(9): p. 7028-7041.
93. Wang, Y., et al., *Genistein suppresses the mitochondrial apoptotic pathway in hippocampal neurons in rats with Alzheimer's disease*. Neural Regen Res, 2016. **11**(7): p. 1153-8.
94. Mirahmadi, S.M., et al., *Soy isoflavone genistein attenuates lipopolysaccharide-induced cognitive impairments in the rat via exerting anti-oxidative and anti-inflammatory effects*. Cytokine, 2018. **104**: p. 151-159.
95. Zhao, L. and R.D. Brinton, *Estrogen receptor alpha and beta differentially regulate intracellular Ca(2+) dynamics leading to ERK phosphorylation and estrogen neuroprotection in hippocampal neurons*. Brain Res, 2007. **1172**: p. 48-59.
96. Zhao, L., et al., *17beta-Estradiol regulates insulin-degrading enzyme expression via an ERbeta/PI3-K pathway in hippocampus: relevance to Alzheimer's prevention*. Neurobiol Aging, 2011. **32**(11): p. 1949-63.
97. Zhao, L., S.K. Woody, and A. Chhibber, *Estrogen receptor beta in Alzheimer's disease: From mechanisms to therapeutics*. Ageing Res Rev, 2015. **24**(Pt B): p. 178-90.
98. Ren, B., et al., *Genistein: A Dual Inhibitor of Both Amyloid β and Human Islet Amylin Peptides*. ACS Chemical Neuroscience, 2018. **9**(5): p. 1215-1224.

Chapter **2**

The *DMR6*-edited Arabidopsis expressing a barley *2-oxoglutarate Fe(II)-dependent oxygenase* orthologue validates the gene's involvement in *Fusarium* head blight susceptibility

Chapter 2

The *DMR6*-edited *Arabidopsis* expressing a barley *2-oxoglutarate Fe(II)*-dependent oxygenase orthologue validates the gene's involvement in *Fusarium* head blight susceptibility

Introduction

Fusarium head blight (FHB) or scab is primarily caused by *Fusarium graminearum* (*Fg*) (teleomorph *Gibberella zeae*), is a devastating disease of cereal crops [1]. *Fg* grows rapidly under warm and high humidity conditions [2] and the key symptoms are the bleaching of spikelet and the production of non-viable seeds [3]. FHB infection causes severe economic loss [4, 5] and mycotoxin contamination, mainly deoxynivalenol (DON) [6, 7], within infected grains which is toxic to humans and animals. Deployment of resistant cultivars is important to guarantee food safety and promote human health.

Genetic engineering stands out as a promising solution to generate resistant cultivars. There are different attempts on generating resistant transgenic wheat and barley plants such as overexpression of pathogenesis-related (PR) or defense response genes [8-10], overexpression of antifungal [11] or antimicrobial peptide [12] from other species, inhibition of DON synthesis [13-16], modifying DON target site within the host system [17] and detoxifying DON into less toxic compound [18, 19]. However, these transgenic cultivars are considered as GMO. The emergence of CRISPR technology allows precise

and efficient genome editing by introducing random mutation at target site [20]. CRISPR has been used intensively in mammalian cells and many organisms [21-25] as well as in model and crop plants [26-33].

Identification of host susceptibility genes paves the way to develop disease resistant plants through genome editing. A susceptibility gene called *DMR6* (downy mildew resistance 6) was discovered and characterized while screening for Arabidopsis mutants (ethyl methane sulfonate and T-DNA insertion mutants) for a loss-of-susceptibility to downy mildew disease caused by *Hyaloperonospora arabidopsidis* pathogen [34, 35]. Map-based gene cloning revealed that *DMR6* encodes a putative *2-oxoglutarate Fe(II)-dependent oxygenase (2OGO)* that belongs to the *2-oxoglutarate-dependent dioxygenase* superfamily. The *dmr6-1* null mutant and *dmr6-2* T-DNA mutant (caused incorrect intron splicing event) demonstrated decreased susceptibility to downy mildew. The *2OGO* gene was shown to be a negative regulator of defense-associated genes. It was later shown that *DMR6* and its paralog *DLO1 (DMR6-like oxygenase 1)* were co-expressed during pathogen infection and redundantly suppressed plant immunity which is closely associated with the salicylic acid (SA) homeostasis [36]. It was verified that mutations in *DMR6* and *DLO1* resulted in an increase of SA levels and the upregulation of *pathogenesis related (PR)-1, PR-2* and *PR-5* genes. Interestingly, the *dlo1* mutant showed a lower level of resistance to *H. arabidopsidis* compared to the *dmr6* mutant, whereas, the *dmr6dlo1* double mutants showed complete resistance to downy mildew, albeit with an accompanying dwarf phenotype. It was concluded that *dmr6* mutant alone provides broad spectrum disease resistance to *H. parasitica*, and also to *Pseudomonas syringae* and *Phytophthora capsici*

[36]. The biochemical mechanism of *DMR6* was further elucidated by a report in 2017 [37] that showed that *DMR6* encodes a salicylic acid 5-hydroxylase (S5H) that can catalyze the conversion of SA to 2,5-dihydroxybenzoates (2,5-DHBA) by hydroxylating SA at the C5 position of its phenyl ring. It was shown that the *DMR6/S5H* expression is induced by SA and that conversion of SA to 2,5-DHBA represents a feedback mechanism which maintains SA homeostasis in Arabidopsis cells. Considering the broad spectrum resistance to different pathogens induced by *DMR6/S5H/2OGO* mutation, generating CRISPR-edited *dmr6* mutants represents promising solution to restrict diseases in crop plants.

In this study, we generated *dmr6*-knock out (KO) mutant Arabidopsis plants using the CRISPR/Cas9 system. The CRISPR-edited Arabidopsis *dmr6* mutants carry the frameshift mutations and show enhanced resistance to *Fg* on the inflorescence while remaining normal with respect to plant growth and development. We have identified the *DMR6* orthologue of barley (cv. Conlon) and transformed the *Hv2OGO* cDNA into Arabidopsis *dmr6*-KO mutant line and restored the susceptibility of Arabidopsis to *Fg*, indicating that *Hv2OGO* is involved in barley's susceptibility to FHB. The outcome of this study provides a foundation to generate *Hv2OGO* mutants for barley resistance to FHB.

Methods and materials

***Arabidopsis thaliana* plant growth**

Arabidopsis thaliana Columbia ecotype (Col-0) seeds were sterilized with 30% bleach for 30 minutes and washed with sterile water for five times. Sterilized seeds were stratified at 4 °C for two days and plated on growth medium [Murashige and Skoog (MS) medium containing 1% (w/v) sucrose and 0.3% (w/v) Gelzan™ agar]. The plated seeds grew at 22 °C under 16h/8h light-dark photoperiod. Germinated seedlings were transferred to Pro-Mix soil in an environmental-controlled chamber with a 16h/8h light-dark photoperiod at 22 °C and 40%-60% relative humidity.

Construction of *At2OGO* CRISPR-editing vector

The *Arabidopsis thaliana* genomic and mRNA sequence of 2-oxoglutarate and Fe(II)-dependent oxygenase (*At2OGO*) was obtained from TAIR (<https://www.arabidopsis.org/>) and NCBI (<https://www.ncbi.nlm.nih.gov/>) databases with accession number of AT5G24530 and NM_122361.4 respectively. The gRNA target sequence for *At2OGO* gene (5'-GGTCTCCAGATCTTGATCGACCGG-3') was identified according to selection guidelines with 20 nucleotides upstream of a proto-spacer adjacent motif (PAM) sequence (5'-N₂₀-NGG-3') and a target sequence beginning with the G nucleotide base. The *At2OGO*-editing vector was constructed following the protocol as published previously [29]. The gRNA sense and anti-sense oligos (forward: 5'-GATTGGTCTCCAGATCTTGATCGA-3'; reverse: 5'-AAACTCGATCAAGATCTGGAGACC-3') were phosphorylated and annealed under the following condition: 37 °C for 30 minutes, 95 °C for 5 minutes and then ramping down to 25 °C at the rate of 5 °C/minute, in a 10 µl reaction (1 µl of 10x T4 ligation buffer, 0.5 µl

of T4 PNK, 1 μ l of each oligo at 100 μ M). The annealed gRNA oligos were cloned into psgR-Cas9-At vector (kindly provided by Dr. J. Zhu, [29]). The resulting plasmid was sequenced and confirmed followed by subcloning into plant expression vector pCAMBIA1300 (<https://www.addgene.org/vector-database/5930/>), resulting in pRD207, and transformed into *Agrobacterium tumefaciens* EHA105 strain.

***Arabidopsis thaliana* plant transformation and mutant selection**

Arabidopsis thaliana Col-0 plants were grown for 3-4 weeks until flowering. *Agrobacterium tumefaciens* EHA105 strain harboring pRD207 (*At2OGO* gRNA/Cas9) was grown in 2 mL of LB liquid medium containing 50 μ g/ml kanamycin and 50 μ g/ml chloramphenicol. The 2 ml overnight culture was inoculated into 200 mL LB liquid medium containing the same antibiotics and was shaken at 30 °C for approximately 5 hours until the OD₆₀₀ reached to 0.6. *Agrobacterium* cells were spun down and rinsed twice with 5% sucrose before resuspending into 300 mL of 5% sucrose solution with 0.05% Silwet L-77. Floral buds were dipped into *Agrobacterium* solution for 1-2 s [38]. The inoculated plants were covered with a clear plastic dome for 24 hours before returning to controlled growth chamber. The transformed plants were grown for another 3-4 weeks for seed harvesting. The collected T₀ seeds were sterilized by 30% bleach and selected on growth medium containing 50 μ g/L hygromycin. The selected mutant plants were transferred to soil for acclimated growth.

Genomic DNA (gDNA) isolation of *Arabidopsis* mutant plants

200 mg leaf tissues from each putative mutant plant was collected for gDNA isolation using CTAB extraction buffer (2% cetyl trimethylammonium bromide, 1% polyvinyl pyrrolidone, 100 mM Tris-HCl, 1.4 M NaCl, 20 mM EDTA). The CTAB-leaf tissue mix was vortexed vigorously for 30s and then incubated at 65 °C for an hour followed by phenol-chloroform isolation. The supernatant was then mixed with 100% ethanol to precipitate the DNA followed by clean-up step with 70% ethanol. The DNA pellets were air-dried and resuspended with sterile deionized water. The concentration of DNA was measured with a Nanodrop spectrophotometer (Thermo Fisher, Waltham, MA, United States).

Mutant analysis: mutant confirmation, restriction fragment length polymorphism (RFLP) and T7 endonuclease I (T7E1) assays

The presence of the Cas9 gene in putative mutant plants was first confirmed by PCR-amplification using Cas9 primers (forward: 5'- GAAGCGGAAGGTCGGTATCCACGG -3'; reverse: 5'- GGCCAGATAGATCAGCCGCAGGTC -3') to confirm the integration of Cas9 transgene. The gDNA samples were used to amplify a 420 bp fragment flanking the target sequence (forward: 5'- GTGCTTGGTGAACAAGGTCAACAC -3'; reverse: 5'- GTGCTTGGTGAACAAGGTCAACAC -3'). The amplified fragments were purified using phenol/chloroform clean-up method and resuspended in sterile deionized water prior to analysis. RFLP assay was carried out by incubating *Bgl*II restriction enzyme with the purified 420 bp PCR fragment from each putative mutant line and the WT plant. Digested

samples were electrophoresed on 1% agarose gel and the gel images were captured. T7E1 assay was performed as well to serve as another analysis method using the formation of heteroduplex between PCR products with and without mutation followed by the digestion of T7 endonuclease I enzyme. The purified 420 bp PCR fragments were denatured and annealed in a thermocycler using the following program: 95 °C for 5 minutes, ramping down to 85 °C at the rate of 2 °C/second, 25 °C at the rate of 0.1 °C/second. The mixture was then digested with 0.5 µl of T7E1 enzyme (10 U/µl) at 37 °C for 60 minutes [39]. Samples were electrophoresed on 1% agarose gel immediately after incubation.

Complementation of *At2OGO*-KO line with *Hv2OGO*

In order to clone the *Hv2OGO* cDNA from barley cv. Conlon, we isolated the total RNA from cv. Conlon four weeks old leaf tissues and conducted RNAseq analysis by Novogen Co., Ltd.. The RNAseq data has been deposited in NCBI SRA database (accession number SRR10059574) under BioProject PRJNA563590. The RNAseq data from Conlon were aligned to cv. Morex *2OGO* gene sequence (mRNA: MLOC_59596.1; gDNA: HORVU4Hr1G084810.2) using the NCBI BLAST tool (<https://blast.ncbi.nlm.nih.gov/Blast.cgi>). Conlon *2OGO* cDNA was amplified by PCR with gene specific primers (forward: 5'-GGTCTAGAATGGCGGAGCAGCTCATCTC-3'; reverse: 5'-GGGAGCTCCTAGGTTCTGAAGAGCTCCAGGC-3') and cloned into plant expression vector pEL103 (kindly provided by Dr. E. Lam, [40]), resulting in pRD331, which was then transformed into *Agrobacterium tumefaciens* EHA105 strain. The homozygous *At2OGO*-KO line (RD207-15-5) was complementarily transformed with

pRD331 *via* the floral dip method. Seeds from T₀ plants were selected on 70 µg/L kanamycin. Confirmed T₁ complemented plants were segregated on 70 µg/L kanamycin. Homozygous T₂ generation was confirmed by antibiotic screening.

***Fg* inoculation on detached Arabidopsis inflorescences and quantitative assays for disease development**

Fg tagged with sGFP (superfolder green fluorescent protein) [41] was cultured on PDA agar for 7 days at 22 °C under UV light for 24/7. Fungal plug was extracted from PDA plate and cultured in 50 mL of mung bean soup for another 7 days to generate macroconidia [42]. The macroconidia were filtered out from mung bean soup using Miracloth (Millipore Sigma, Burlington, MA, United States) and washed twice with sterile deionize water before resuspension in sterile water. The concentration of macroconidia was measured using hemocytometer. The macroconidia solution was diluted to 1x10⁶ spores/mL for inflorescence inoculation. Bolting floral buds were detached from plants and laid perpendicularly onto 0.7% water agar in petri dishes. Each inflorescence was inoculated with 2 µl of 1x10⁶ spores/mL macroconidia solution along with a duplicate set of mock sample that was inoculated with sterile water. The inoculated detached inflorescences were maintained in a 100% humidity condition by spraying water on the inner side of the petri dish lids prior to plate sealing. The plates were left in environmentally controlled chamber with a 16h/8h light/dark photoperiod at 22 °C. Images were taken using the Dino-eye eyepiece camera (Dino-Lite, Hsinchu, Taiwan) on Nikon SMZ 645 stereomicroscope (Nikon corp., Minato, Japan) and samples were collected every 24 hours by pooling four

inflorescences in a tube per time point until reaching 144 hours. After each collection, the pooled samples were rinsed with 1 mL of sterile water and mild shaking to remove *Fg* spores from the surface of inflorescence. The first 1 mL of rinsed water was collected to quantitate the spore production at each time point using hemocytometer. The pooled samples were rinsed for another two times with 1 mL of water to get rid of as many surface-attached spores as possible. Total DNAs of pooled samples were then isolated using the CTAB method and quantitation on spores penetrated the floral tissues was performed using Applied Biosystems StepOne Plus thermocycler (Applied Biosystems, Thermo Fisher, Foster City, CA, United States) by amplifying the sGFP (forward: 5'-GTCCGCCCTGAGCAAAGA -3'; reverse: 5'-TCCAGCAGGACCATGTGATC-3') in the pooled samples. Both quantitative assays were repeated thrice and the data obtained from quantitative assays was averaged with standard deviations (SD), followed by the Student's *t*-test analysis on WT vs. *At2OGO*-KO and WT vs. *At2OGO*-KO/*Hv2OGO* groups using GraphPad software. Statistical significance determined using the Holm-Sidak method, with alpha = 0.05. Each time point was analyzed individually, without assuming a consistent SD.

Relative gene expression profiling on plant defense mechanism

In order to understand the molecular mechanisms underlining the defense signaling in *At2OGO*-KO and *At2OGO*-KO/*Hv2OGO* plants infected with *Fg*, some of the key downstream targets in the SA, JA, ET and ROS signaling pathways were chosen for quantitation by RT-qPCR analysis. Arabidopsis *Actin-2* (*ACT2*) gene was used as the

reference housekeeping gene in these studies. Primers for each selected gene were designed using the Primer Express software (Applied Biosystems, Thermo Fisher, Foster City, CA, United States). The primer sets for each gene were first validated to have similar amplification efficiency as the *ACT2* gene. Detached inflorescences were each inoculated with 2 μ l of *Fg* macroconidia solution as described above and collected at 3, 6, 12, 24, 48 hr time point. Four inflorescences were pooled into a tube and rinsed three times with 1 mL of sterile water. Total RNA of pooled samples were isolated using the TRIZOL method (Ambion Life Technologies, Thermo Fisher, Carlsbad, CA, United States) and the concentration was measured using the Nanodrop spectrophotometer (Thermo Fisher, Waltham, MA, United States). Reverse transcription (RT) reaction was carried out with the High Fidelity cDNA Synthesis Kit (Applied Biosystems, Thermo Fisher, Foster City, CA, United States) using approximately 2 μ g RNA. The RT products were used in RT-qPCR reactions with the SYBR 2X Master Mix (Applied Biosystems, Thermo Fisher, Foster City, CA, United States). The RT-qPCR assay was run on the default setting at 95 °C for 3 minutes for initial denaturation and 40 cycles at 95 °C for 30 s followed by 60 °C for 30 s. The fold change of gene expression was calculated by the $2^{-\Delta\Delta C_t}$ method [43]. The RT-qPCR analysis was repeated three times with different batches of samples, and the gene expression levels were averaged. Primers used in the RT-qPCR gene expression assay were listed in Table 2.1.

RT-qPCR primers	Forward	Reverse
<i>NPR1</i>	GCCGCCGAACAAGTACTCA	GCTGTTGGAGAGCAATTGCA
<i>PR1</i>	GTCTCCGCCGTGAACATGT	CGTGTTTCGCAGCGTAGTTGT
<i>PR2</i>	GCTGGACAAATCGGAGTATGC	CCGATGGACTTGGCAAGGTA
<i>PR5</i>	AACGGCGGGCGGAGTTC	CGCCATCGCCTACTAGAGTGA
<i>PDF1.2</i>	TTTGCTTCCATCATCACCTTA	GCGTCGAAAGCAGCAAAGA
<i>AOS</i>	CCACCGGTTACGGCTCAA	GCGTCGTGGCTTTCGATAA
<i>ERF1</i>	CCCTTCAACGAGAACGACTCA	TTGCGTGGACTGCTCGATT
<i>EIN3</i>	CCGACTCCTCATACTTGCAA	CGCAGACAAAAGCGATCCA
<i>PR3</i>	ACGCAGTGATCGCTTTCAA	TGGGAGGCTGAGCAGTCATC
<i>RBOHD</i>	CATGCGGGTGCCATT	ATCCGCGGCAATTAACG
<i>Actin2</i>	GATTCAGATGCCCAGAAGTCTT	TGGATTCCAGCAGCTTCCAT

Table 2.1. List of primers used in the RT-qPCR gene expression assay.

Results

Generating *DMR6* mutants in Arabidopsis using CRISPR/Cas9 system

The *DMR6* genomic (*At5g24530*) and mRNA (NM_122361.4) sequences were obtained from TAIR and NCBI databases respectively. We identified the active site of DMR6 (oxoglutarate/iron-dependent dioxygenase domain) at the C-terminal of its protein sequence (from a.a.188 to a.a.288) or exon 3 in genomic sequence which is responsible for DMR6-dependent susceptibility phenotype in *A. thaliana*. The gRNA guidelines (www.addgene.org/crispr/guide) were followed while choosing a 20-nucleotides genomic target which is unique within the Arabidopsis genome and is also adjacent to a PAM sequence. We designed a gRNA that specifically targets exon 3 (target region: 5'-

GGTCTCCCAGATCTTGATCGA -3') and that also flanks a *Bgl*III restriction site (underlined) for mutant screening. The gRNA target was cloned into the vector kindly provided by Dr. J. Zhu [29] containing Arabidopsis U6 promoter and a Cas9 gene that is driven by the 2x 35S promoter and terminated by the NOS terminator. For *Agrobacterium* transformation, the gRNA/Cas9 cassettes were subcloned into the *Eco*RI and *Hind*III region of pCAMBIA1300 vector, resulting in the plant expression vector pRD207. Flowering Arabidopsis Col-0 plants were transformed *via* EHA105 strain of *Agrobacterium* using the floral-dip method. The collected T₀ seeds were screened on 50 µg/L hygromycin. A total of 14 putative T₁ mutant plants were recovered from antibiotic selection.

Molecular characterization of *At2OGO*-KO (*dmr6*) mutants and identification of homozygous progeny

The *At2OGO* (pRD207) CRISPR-editing transformants were first confirmed by performing PCR with Cas9 specific primers using extracted genomic DNA from each T₁ line which later were genotyped using restriction fragment length polymorphism (RFLP) assay followed by Sanger sequencing to discover the mutations in T₁ progeny. A 420 base pairs (bp) genomic DNA (gDNA) flanking the target region was PCR-amplified and analyzed by RFLP with *Bgl*III restriction digestion (Figure 2.1a) and T7E1 assay (Figure 2.1b). The gel picture (Figure 2.1a) demonstrated that all putative mutant lines had three DNA bands after the RFLP assay. The bottom two bands (276 bp and 144bp) represented the digestion fragments for WT plant while the top band (420 bp) was the undigested

fragment, indicating that one allele of the gDNA was mutated at the restriction site in the target region (monoallelic mutation). By T7E1 assay, the formation of three DNA fragments indicates a monoallelic mutant since the heteroduplex formed with mutation on one allele results in the T7E1 digestion of the PCR fragments. Hence, Figure 2.1b further demonstrated that all T₁ mutant lines carried monoallelic mutations. The undigested PCR fragments following RFLP assay were extracted and purified for Sanger sequencing to decipher the mutations induced by pRD207 CRISPR-editing vector. T₁ mutants were segregated and the T₂ generation was analyzed by RFLP assay to screen for homozygous mutants. The T₂ homozygous mutants which showed single undigested fragments were sequenced to confirm the mutation pattern (Figure 2.1c).

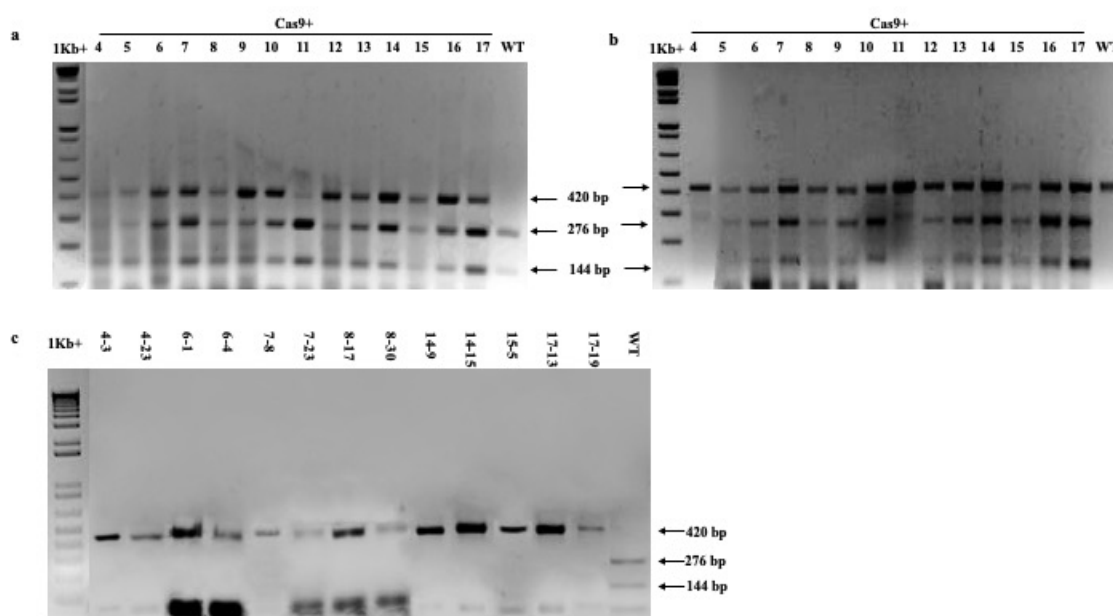


Figure 2.1. (a) RFLP assay and (b) T7E1 assay to confirm putative CRISPR-edited *At2OGO* (RD207) mutants. Total of 14 mutant lines were first confirmed to carry Cas9 gene which then followed by target region PCR and analyzed by *Bgl*III restriction digestion.

All T₁ mutants were heterozygous with single allele mutation. (c) RFLP assay to screen for homozygous T₂ mutants in which the target region was mutated in both alleles, hence resulting in the loss of the *Bgl*III restriction site.

Figure 2.2 showed the mutation profiles of RD207 (*At2OGO*-KO) mutants at T₁ generation as well as the segregated homozygous T₂ generation. There were 9 different mutation patterns observed in the T₁ generation. 13 out of 14 T₁ mutants had the deletion around the target region while one of them had the insertion within the target region. 57% (8 out of 14) of the T₁ mutants were confirmed to have frameshift (f.s.) mutations that truncated the protein product and disrupted the active site of *At2OGO*. Most of the mutation patterns from T₁ generation were retained in T₂ homozygous mutants. 31% (4 out of 13) of the identified homozygous mutants carried the stable frameshifting deletions around the target region. The frameshifted homozygous mutants were segregated to remove the gRNA and the Cas9 cassettes and the loss of these cassettes was confirmed by PCR with gRNA- and Cas9-specific primers. We had chosen the homozygous *At2OGO*-KO mutant line RD207-15-5 for subsequent disease assessment and barley gene complementation experiments. RD207-15-5 mutant carried an 8 bp frameshifting deletion in exon 3 of the *DMR6* gene resulting in the premature termination of the gene product as illustrated in Figure 2.3. It was expected that the truncated gene product would have disrupted the oxoglutarate/iron-dependent dioxygenase domain at the C-terminal resulting in the loss of susceptibility to *Fg* infection.

Wildtype	TACTGTTTGC <u>GGTCTCCAGATCT</u> <u>TGATCGA</u> CGGTCAGTGG	
	<i>Bgl</i> III	PAM
T₁ generation		
207-4	TACTGTTTG-----CGGTCAGTGG	-21
207-5	TACTGTTTGC <u>GGTCTCCA</u> ----- <u>GATCGA</u> CGGTCAGTGG	-6
207-6	TACTGTTTGC <u>GGTCTCCAGATC</u> ----- <u>CGA</u> CGGTCAGTGG	-5 (f.s.)
207-7	TACTGTTTGC <u>GGTCTCCAG</u> ----- <u>TCGA</u> CGGTCAGTGG	-7 (f.s.)
207-8	TACTGT----- <u>CTCCAGA</u> - <u>CACCA</u> <u>CGA</u> CGGTCAGTGG	-8 (f.s.)
207-9	TACTGTTTGC <u>GGTCTCCA</u> ----- <u>GATCGA</u> CGGTCAGTGG	-6
207-10	TACTGTTTGC <u>GGTCTCCAG</u> <u>TCTTGAT</u> <u>CGA</u> CGGTCAGTGG	+1 (f.s.)
207-12	TACTGTTTGC <u>GGTCTCCAGATC</u> ----- <u>CGA</u> CGGTCAGTGG	-5 (f.s.)
207-13	TACTGTTTGC <u>GGTCTCCAGATC</u> ----- <u>TCGA</u> CGGTCAGTGG	-4 (f.s.)
207-14	TACTGTTTGC <u>GGTCTCCAGA</u> -----CGGTCAGTGG	-10 (f.s.)
207-15	TACTGTTTGC <u>GGTCTCCAG</u> ----- <u>CGA</u> CGGTCAGTGG	-8 (f.s.)
207-16	TACTGTTTGC <u>GGTCTCCAGATC</u> ----- <u>GA</u> CGGTCAGTGG	-6
207-17	TACTGTTTGC <u>GGTCTCCAGATC</u> ----- <u>GA</u> CGGTCAGTGG	-6
T₂ generation		
207-4-3	TACTGTTTGC <u>GGTCTCCAGATC</u> ----- <u>CGA</u> CGGTCAGTGG	-5 (f.s.)
207-4-23	TACTGTTTG-----CGGTCAGTGG	-21
207-6-1	TACTGTTTGC <u>GGTCTCCAGA</u> -----CGGTCAGTGG	-10 (f.s.)
207-6-4	TACTGTTTGC <u>GGTCTCCA</u> ----- <u>GATCGA</u> CGGTCAGTGG	-6
207-7-8	TACTGTTTGC <u>GGTCTCCA</u> ----- <u>GATCGA</u> CGGTCAGTGG	-6
207-7-23	TACTGTTTGC <u>GGTCTCCA</u> ----- <u>GATCGA</u> CGGTCAGTGG	-6
207-8-17	TACTGTTTGC <u>GGTCTCCA</u> ----- <u>GATCGA</u> CGGTCAGTGG	-6
207-8-30	TACTGTTTGC <u>GGTCTCCA</u> <u>CATC</u> ----- <u>TGG</u>	-14 (f.s.)
207-14-9	TACTGTTTGC <u>GGTCTCCAGATC</u> ----- <u>G-T-G</u> --GGTCAGTGG	-6
207-14-15	TACTGTTTGC <u>GGTCTCCA</u> ----- <u>GATCGA</u> CGGTCAGTGG	-6
207-15-5	TACTGTTTGC <u>GGTCTCCAG</u> ----- <u>CGA</u> CGGTCAGTGG	-8 (f.s.)
207-17-13	TACTGTTTGC <u>GGTCTCCA</u> ----- <u>GATCGA</u> CGGTCAGTGG	-6
207-17-19	TACTGTTTGC <u>GGTCTCCA</u> ----- <u>GATCGA</u> CGGTCAGTGG	-6
	Red – sgRNA target Blue – Restriction site Gold – Base substitution Green – Insertion	

Figure 2.2. Mutation profiles of *At2OGO*-KO (RD207) mutants at T₁ generation and segregated homozygous mutants at T₂ generation. Frameshift mutation (f.s.) was observed in 57% of the T₁ mutants and the mutation patterns were retained mostly in homozygous T₂ mutants.

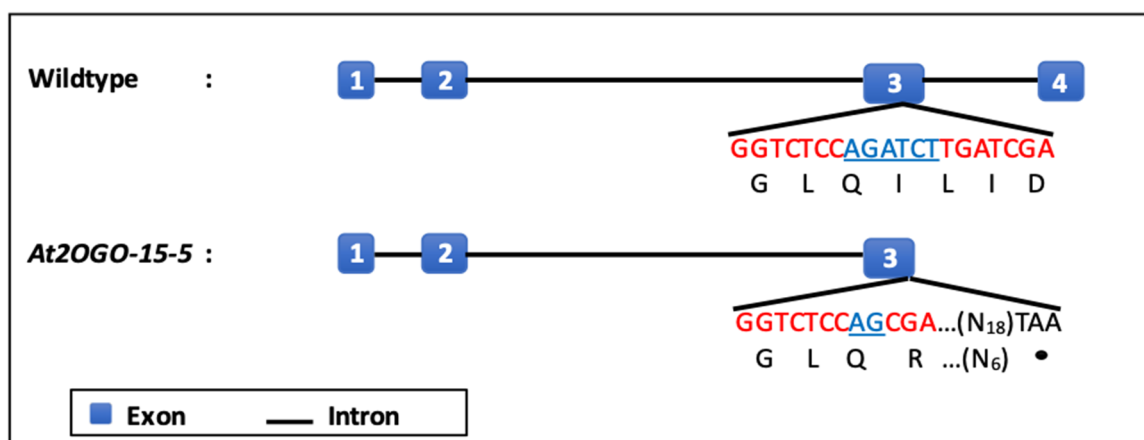


Figure 2.3. Schematic diagram of *At2OGO* gene in WT and homozygous mutant RD207-15-5. RD207-15-5 mutant carries an 8 bp frameshifting deletion in exon 3 of the *DMR6* gene resulting in the premature termination of the gene product.

Identification of *DMR6* (*2OGO*) orthologue from barley cultivar Conlon for complementation test

The *DMR6* orthologue of barley (*Hordeum vulgare*) was searched for in the PGSB barley genome database. Currently, high quality reference genome assembly and automated gene annotation have been done only on barley cv. Morex (Mascher et al. 2017). One copy of *Hv2OGO* gene in cv. Morex was identified from the database. The mRNA and gDNA sequences were tagged as MLOC_59596.1 and HORVU4Hr1G084810.2 respectively in the database. In order to confirm the *Hv2OGO* gene sequence in cv. Conlon as compared to cv. Morex, total RNA from cv. Conlon was extracted and sequenced by Novogene Co., Ltd. The RNAseq data was assembled and aligned against the cv. Morex *2OGO* gene sequence to identify the Conlon *2OGO* gene. The Conlon *2OGO* cDNA was cloned by RT-

PCR and sequenced *via* Sanger sequencing. The Conlon *Hv2OGO* nucleotide sequence was shown to be 99.9% identical to the Morex *Hv2OGO* nucleotide sequence except there was a mismatch at position 396 of the cDNA sequence, changing from cytosine (C) to thymine (T) base (Figure 2.4). This nucleotide change (highlighted in red) caused a change of amino acid from phenylalanine to leucine, which is conservative and which maintains hydrophobicity. The Conlon *Hv2OGO* was cloned into pEL103 (kindly provided by Dr. E. Lam, [40]) transformation vector, resulting in pRD331, which was then transformed into EHA105 strain of *Agrobacterium*. The homozygous *At2OGO*-KO (RD207-15-5) mutant was selected to be complementarily transformed with pRD331 *via* *Agrobacterium*-mediated floral dip method. The collected T₀ seeds were screened on 70 µg/L kanamycin-containing medium. A total of 7 putative T₁ *Hv2OGO*-complemented transformants were recovered from antibiotic selection and confirmed by PCR on *Hv2OGO* gene (Figure 2.5). Homozygous *At2OGO*-KO/*Hv2OGO* plants were obtained *via* segregation.

```

Conlon 1 ATGGCGGAGCAGCTCATCTCCACGGCCGTGCACCACACGCTGCCCCACAGCTACGTCCGC 60
Morex 1 ..... 60

Conlon 61 TCCGAGGCGGAGCGGCCGCGCCTCCACGAGGTGCTGCCCGACGCCGACATCCCCGTCGTC 120
Morex 61 ..... 120

Conlon 121 GACCTCGCCAACCCCGACCGCGCCGCGTCTCCAGATCGGCTCTGCCTGCAGCTCC 180
Morex 121 ..... 180

Conlon 181 CACGGCTTCTTCCAGGTGCTCAACCACGGGCTGCCGGTGGAGGCCATGCGGGCGGCGATG 240
Morex 181 ..... 240

Conlon 241 GCGGTGGCGCACGACTTCTTCCGCCTCTCGCCGGAGGAGAAGGCCAAGCTCTACTCCGAC 300
Morex 241 ..... 300

Conlon 301 GACCCGGCCAAGAAGATGCGGCTATCCACCAGCTTCAACGTGCGCAAGGAGACCGTCCAC 360
Morex 301 ..... 360

Conlon 361 AACTGGCGGACTACCTGCGGCTGCACTGCCACCCGCTCGACCAGTTCGTGCCGGAGTGG 420
Morex 361 .....T..... 420

Conlon 421 CCGGCCAATCCACCGCCCTCAGGGATGTATGAGCACATACTGCAAAGAGGTCCGGGAT 480
Morex 421 ..... 480

Conlon 481 CTTGGGTTCGGGCTTACGCGGCATCTCGGAGAGCCTAGGGCTGGAGCAGGACTATATC 540
Morex 481 ..... 540

Conlon 541 AAGAAGGTCCCTCGGTGAGCAGGAGCAGCACATGGCGGTGAACTTCTACCCCAAGTGCCCC 600
Morex 541 ..... 600

Conlon 601 TCGCCGGAGCTGACATATGGGCTCCCGGCCACACGGACCCCAACGCCCTCACCATCTTG 660
Morex 601 ..... 660

Conlon 661 ATGATGGACGAGCAGGTGCGCCGGCTACAGGTGCTCAAGGAAGGCCGGTGGATCGCCGTC 720
Morex 661 ..... 720

Conlon 721 AACC CGGCCCAACGCTCTCGTCATCAATCTTGGGGACCAGCTGCAGGCGCTGAGCAAC 780
Morex 721 ..... 780

Conlon 781 GGGAGATATAGGAGTGTGTGGCACC GCGTGTGTGAACTCAGACAGGCCAAGGATGTCC 840
Morex 781 ..... 840

Conlon 841 ATTGCCCTCGTTCCTGCCCCGCAATAGCGTCATGCTCGGCCCGCTGAGAAGCTCATC 900
Morex 841 ..... 900

Conlon 901 GGGGCCGAGACACCGCCGCTACAGAAATTACACCTACGATGAGTACTACAAGAAGTTC 960
Morex 901 ..... 960

Conlon 961 TGGAGTAGGAATTTGGACCAGGAGCACTGCCTGGAGCTCTTCAGAACCTAG 1011
Morex 961 ..... 1011

```

Figure 2.4. Pairwise alignment of Conlon and Morex *Hv2OGO* sequences. A . (period) indicates identical nucleotide bases and highlighted nucleotide base indicates the mismatch. Both sequences were 99.9% identical to each other with a mismatch at position 396, changing from cytosine (C) to thymine (T) base, resulting in the switching of amino acid from phenylalanine to leucine while still conserving its hydrophobic property.

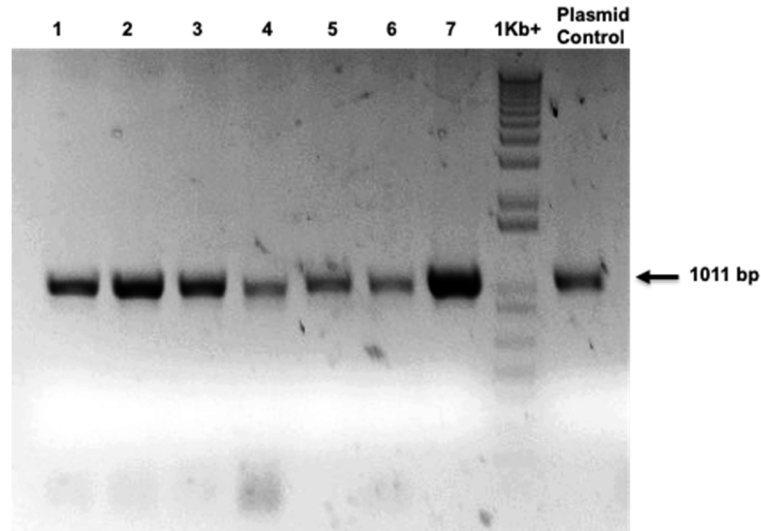


Figure 2.5. Gel image showed the PCR-confirmed *At2OGO*-KO/*Hv2OGO* lines (1-7) with a plasmid control (pRD331) carrying the *Hv2OGO* mRNA fragment of 1011 bp.

Characterization of disease phenotype on *At2OGO*-KO and *At2OGO*-KO/*Hv2OGO*-complemented homozygous plants

The homozygous *At2OGO*-KO mutant (RD207-15-5) with an 8 bp frameshifting deletion in exon 3 of the *DMR6* gene and homozygous *At2OGO*-KO/*Hv2OGO*-complemented plants (RD207-15-5/331-1) were used in the *Fg* infection assay together with the WT *Arabidopsis* as the control group. The *Fg* infection assay was performed by point inoculation of the sGFP-tagged *Fg* macroconidia on detached inflorescences and stereomicroscopic images were taken each day post inoculation (dpi) for 6 days (Figure 2.6). At 2 dpi, the fungal hyphae started to form on the inflorescence surface of WT and *At2OGO*-KO/*Hv2OGO* inflorescence while *At2OGO*-KO inflorescences remained free from fungal hyphae growth. The hyphae growth on WT and *At2OGO*-KO/*Hv2OGO*

inflorescences spread aggressively from one inflorescence to another starting from 3 to 4 dpi whereas *At2OGO*-KO inflorescences had minimal fungal hyphae growth on the inflorescence surface at 4 dpi. At 5 to 6 dpi, the *Fg* hyphae on WT and *At2OGO*-KO/*Hv2OGO* inflorescences became abundant and the colonization started to take over the inflorescence tissue by forming thick mycelium mat and the host tissue started to show wilting symptoms. The *At2OGO*-KO inflorescences remained in their initial infection condition at 6 dpi when a minimal amount of hyphae growth was observed. It was evident that the loss of susceptibility from the truncated *DMR6/2OGO* gene slowed down the infection progress of *Fg*. Our results showed that the *At2OGO*-KO inflorescences were more resistant to *Fg* infection than WT's, and the complementation of *At2OGO*-KO with *Hv2OGO* recovered the Arabidopsis susceptibility to *Fg*, indicating that *Hv2OGO* is an *Fg* susceptible factor for barley.

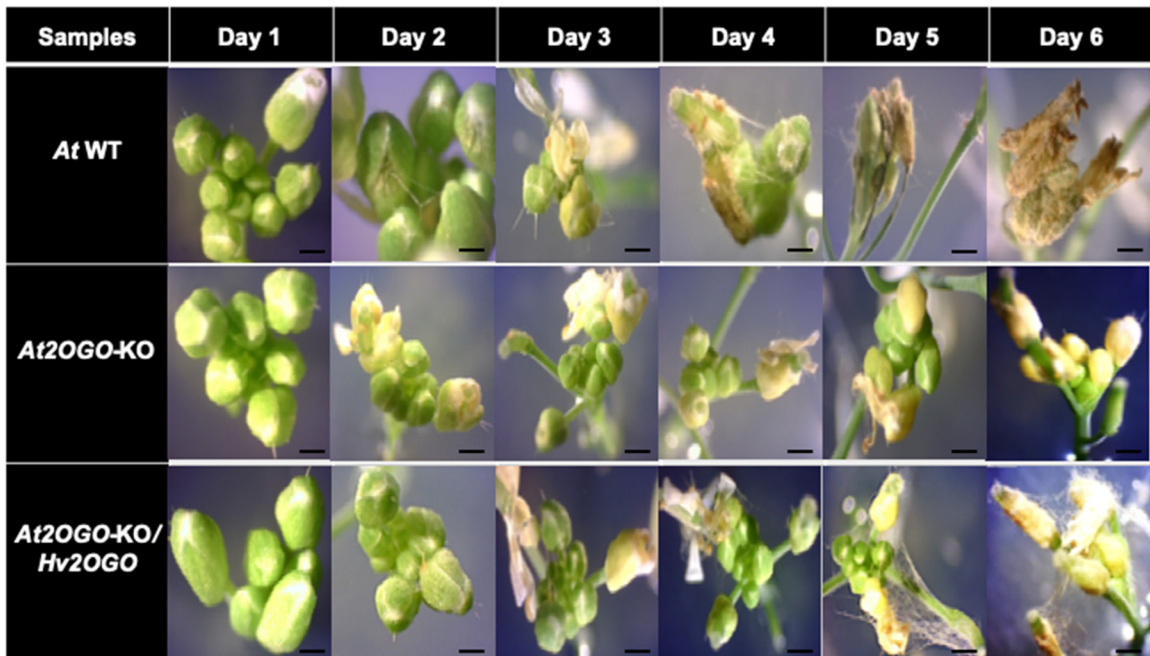


Figure 2.6. Illustration of FHB disease progression on detached *Arabidopsis* inflorescences. Fungal hyphae started to form on *At WT* and *At2OGO-KO/Hv2OGO* at 2 dpi while *At2OGO-KO* displayed a higher level of resistance with minimal fungal hyphae growth even on 4dpi. Pictures were taken using the Dino-eye eyepiece camera together with stereomicroscopes at 20x magnification. Scale bar (0.1 mm —).

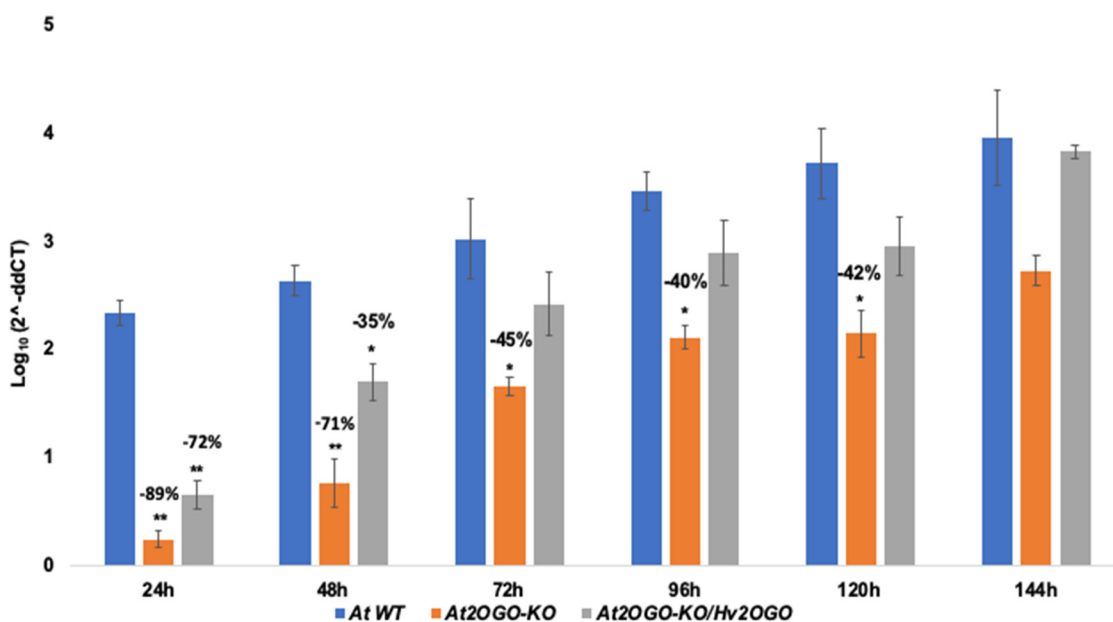


Figure 2.7. qPCR quantitative assay in measuring disease severity on *Fg* inoculated inflorescence. Experiment was repeated with three independent batches of samples. Statistical significance determined by *t*-test analysis followed by Holm-Sidak method, with alpha = 0.05. Each time point was analyzed individually, without assuming a consistent SD (p-value: * ≤ 0.05; ** ≤ 0.01; *** ≤ 0.001).

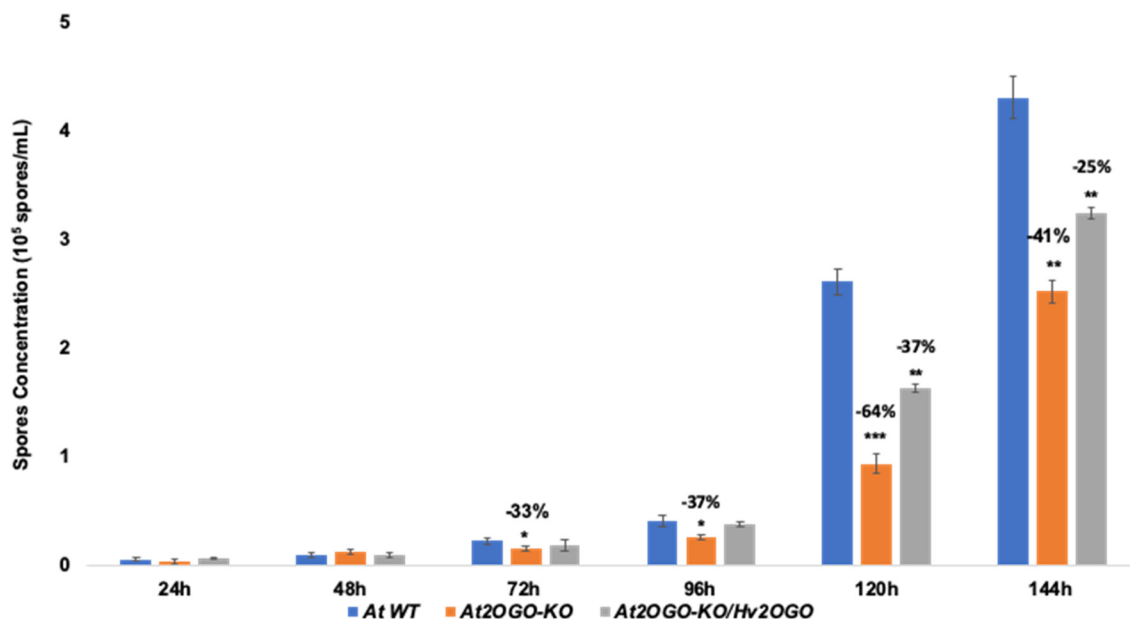


Figure 2.8. Quantitative assay of spore production on *Fg* inoculated inflorescence. The percentage of spore reduction was calculated for 72h, 96h, 120h and 144h. The experiment was repeated with three independent batches of samples. Statistical significance determined by t-test analysis followed by Holm-Sidak method, with alpha = 0.05. Each time point was analyzed individually, without assuming a consistent SD (p-value: * \leq 0.05; ** \leq 0.01; *** \leq 0.001).

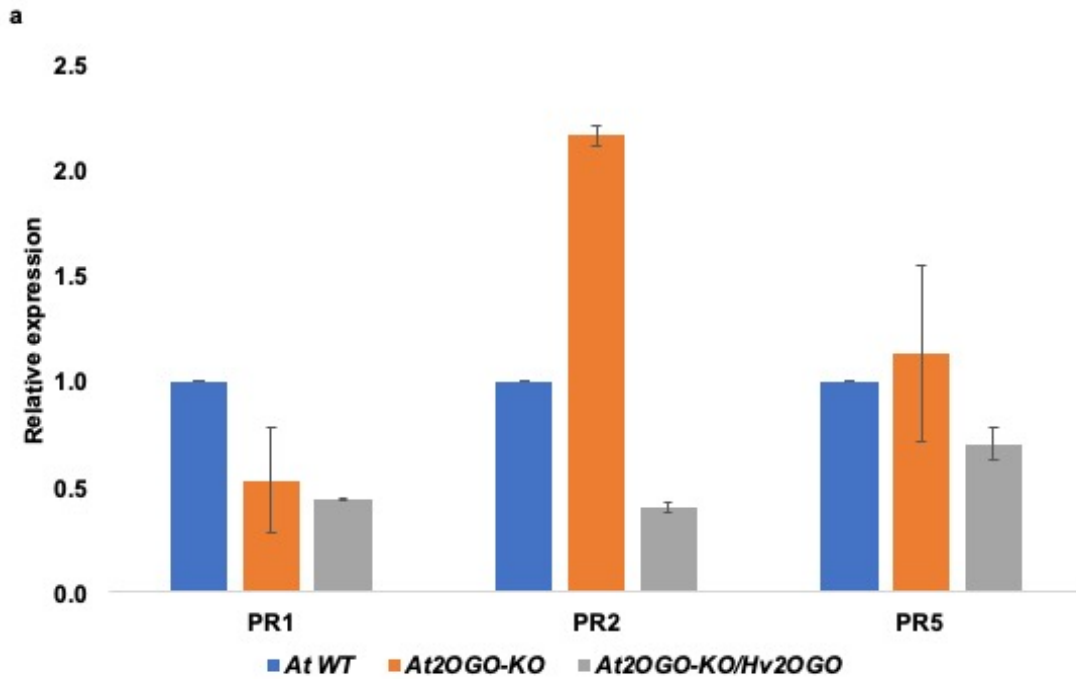
In order to assess the disease severity, we used the qPCR assay to quantitate the amount of *Fg* that had penetrated into the host tissue (Figure 2.7). The inoculated inflorescences were collected daily and rinsed off the surface *Fg* hyphae and macroconidia with sterile deionized water for three times with mild shaking. The rinsed and pat-dried inflorescences were analyzed in qPCR assay using the primers that amplified sGFP tagged to *Fg*. The WT and *At2OGO-KO/Hv2OGO* inflorescences showed similar infection pattern where the amount of *Fg* within the inflorescence tissues increased rapidly and consistently starting 2

dpi to 6 dpi while *At2OGO*-KO showed that the fungal penetration occurred at a much restricted rate, approximately 30% less than the other two test groups. Furthermore, the spore production on *Fg* inoculated inflorescences was quantitated using a hemocytometer (Figure 2.8). The result was similar to the qPCR assay in that the spore production increased rapidly in WT and *At2OGO*-KO/*Hv2OGO* inflorescences starting from 4 dpi when the fungal colonization defeated the plant defense. Spore production in *At2OGO*-KO inflorescences, however, had a more restricted pattern, indicating that the mutation suppressed *Fg* proliferation. At 6 dpi, the spore production in KO plants were 41% and 22% less than WT and complemented mutants, respectively. These results provided a solid evidence that *At2OGO* mutants are effective in restricting *Fg* growth and that barley *Hv2OGO* gene functions similarly as *At2OGO* during *Fg* infection.

Gene expression profiling on plant defense signaling pathway-related genes

The expression of several plant defense signaling pathways [salicylic acid (SA), jasmonic acid (JA) and ethylene (ET)]-related genes in *At2OGO*-KO, *At2OGO*-KO/*Hv2OGO* and WT was analyzed using RT-qPCR. *At2OGO* T-DNA-KO was known to accumulate SA due to the impairment in gene function [36]. Higher level of SA induced the defense-related genes and led to the heightened resistance in *At2OGO*-KO mutant upon pathogen infection. Previous studies showed that the gene expression level of PR genes in healthy KO plants was elevated to approximately 10-fold, especially for *PR1* gene [36] in the leaf tissues. We analyzed the floral and leaf samples from our *At2OGO* mutant. Figures 2.9a and 2.9b demonstrated that the relative gene expression of PR1, PR2 and PR5 in *At2OGO*-KO leaf

sample was similar to the assay mentioned in previous study except that PR2 was expressed at a much higher level (~20 folds) compared to PR1. The floral samples did not show the similar trend seen in leaf sample. PR2 gene was the only one expressed at one-fold higher than WT.



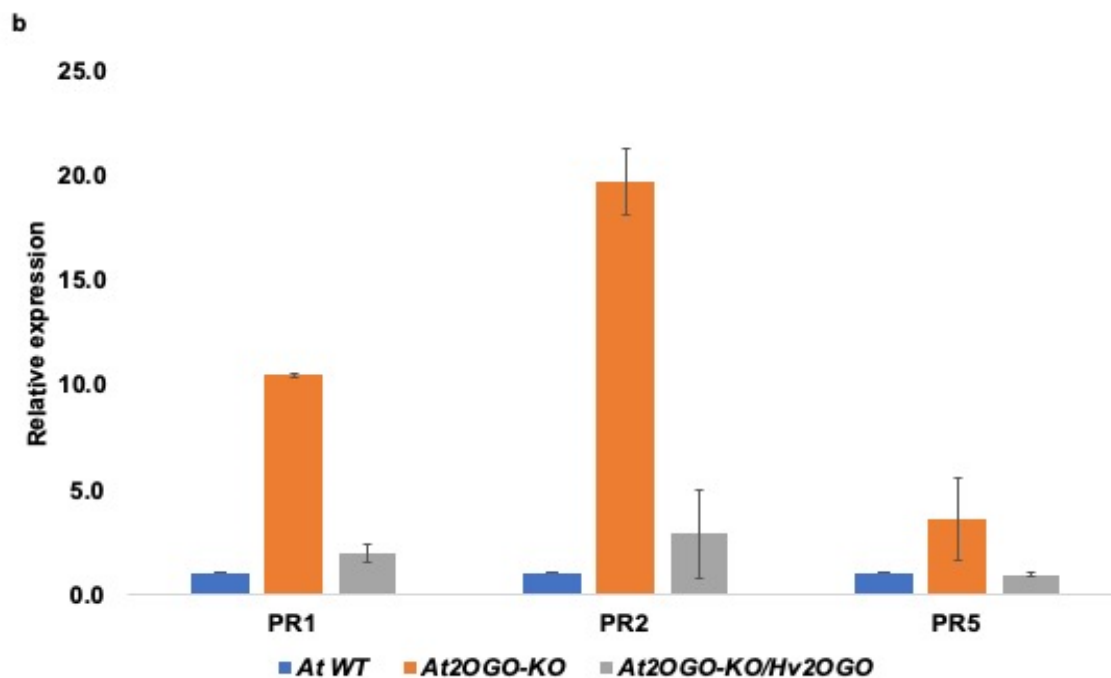
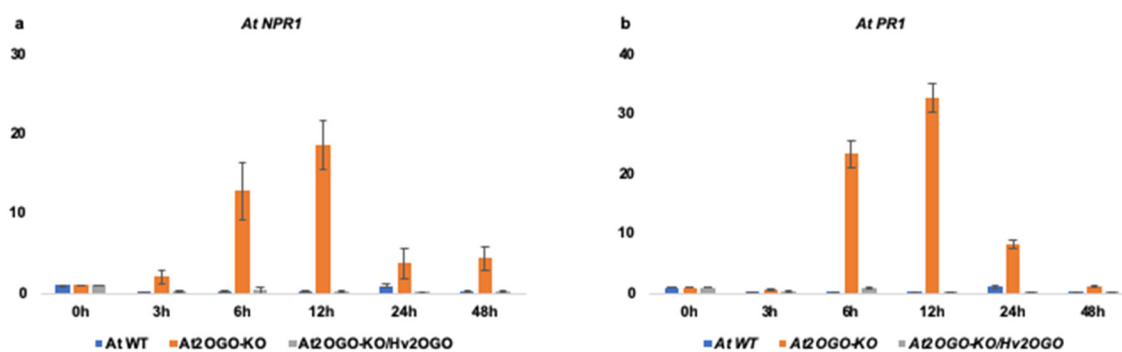


Figure 2.9. Relative gene expression of non-inoculated *At2OGO-KO* (a) floral and (b) leaf samples. The experiment was repeated three times with samples from three individual plants. The relative expression values were averaged.



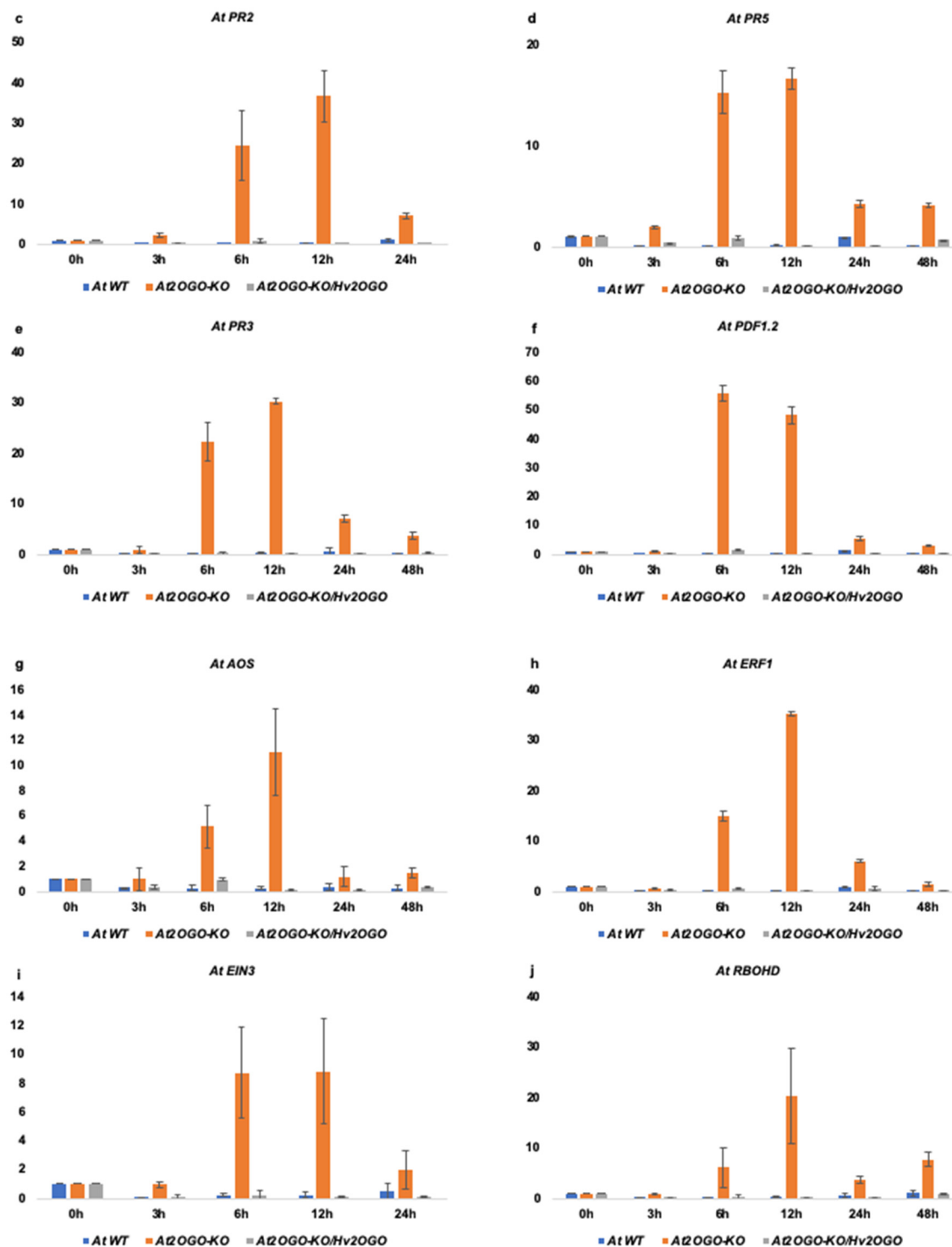


Figure 2.10. RT-qPCR analysis of plant defense-related genes relative expression.

Relative expression profile includes genes involved in SA signaling (a-d), JA/ET signaling

(e-i) and ROS activation (j). RT-qPCR assay was repeated three times with different batch of samples. The relative gene expression was calculated using the $2^{-\Delta\Delta Ct}$ formula.

Each sample group was point inoculated with sGFP-tagged *Fg* and collected at 3, 6, 12, 24, 48 hours after inoculation (hpi). All defense-related genes were expressed highly and visibly only in *At2OGO-KO* compared to WT and *At2OGO-KO/Hv2OGO* (Figure 2.10). SA accumulation activates the *NPR1* (Figure 2.10a) transcripts and hence the increase of its gene expression from 3 hpi to its peak at 12 hpi. The AOS gene (Figures 2.10g) were involved in the upstream of JA signaling pathway. Their gene expression started to increase at 6 hpi to its peak at 12 hpi and dropped sharply at 24-48 hpi back to basal level. The *EIN3* and *ERF1* genes (Figures 2.10h-i), which are activated by ET, displayed the similar gene expression pattern as JA-related genes in which the increment was observed only from 6-12 hpi and the expression levels decreased sharply from 24-48 hpi. *PR1*, *PR2*, *PR3* and *PR5* (Figures 2.10b-e) are pathogenesis-related genes which are the key components of plant innate immune system. These genes were upregulated from 6-12 hpi and decreased to a lower level of expression at 24-48 hpi except *PR1* gene returned to basal level at 48 hpi. On the other hand, *PDF1.2* (Figure 2.10f), a JA and ET responsive gene, expressed at extremely high level from 6 hpi and decreased after 12 hpi. The *RBOHD* gene (Figure 2.10j) was highly expressed from 6-12 hpi and maintained a much lower expression at 24-48 hpi. Overall, *At2OGO-KO* plants displayed an amplified the defense responses and hence resulting in a more resistant phenotype against pathogen attack.

Discussion

One of the major challenges for agribusiness and food security is to maintain a sustainable agriculture with higher quantity and quality of food sources. Pathogen attack, inevitably, is the leading cause of the yield loss and the falloff in crop quality globally. The plant immune system comprises two interconnected receptors which are the pattern recognition receptors located at the cell surface recognizing pathogen associated molecular patterns (PAMPs); and the resistance (R) genes that encode the intracellular nucleotide-binding and leucine-rich-repeat (NB-LRR) receptors which recognizing the pathogen effectors [44]. R genes have been widely studied and their introgression into susceptible cultivar *via* breeding method has led to substantial improvements in disease resistance. However, the pleiotropic effects of R genes, as well as linkage drag and competition drag in breeding approach have become significant limitations for breeders to generate resistant cultivars without compromising yield [45]. The discovery of susceptibility genes has made them an attractive target for loss-of-function mutations that may enhance plant resistance to infection. Likewise, impairment of Arabidopsis *DMR6* gene has been shown to confer broad-spectrum disease resistance [35, 36]. In this study, we utilized CRISPR/Cas9 technique to generate *At2OGO*-KO mutants and studied its disease phenotype by *Fg* infection on inflorescence. Our results showed *At2OGO*-KO mutants were resistant to *Fg* infection and proliferation. We have also shown that the *DRM6* orthologue of barley cv. Conlon (*Hv2OGO*) restored the WT disease phenotype in *At2OGO*-KO mutants, verifying its function as a susceptibility gene, paving the path for gene-editing to achieve barley resistance to FHB.

DMR6 belongs to 2-oxoglutarate Fe(II)-dependent oxygenase superfamily in which most of the members involve in biosynthesis of plant flavonoid and secondary metabolites [46]. The discovery of loss-of-function *dmr6* mutant in conferring broad spectrum resistance has stimulated our interest in identifying potential homologues or orthologues of *DMR6* in barley and studying its potential role in FHB disease resistance. In order to understand the role of *DMR6* in barley, the cv. Conlon orthologue was identified, cloned and transformed into the *At2OGO*-KO mutant in order to verify whether the barley orthologue carries the same function in facilitating *Fg* invasion. Based on our results on quantitative assays, *At2OGO*-KO plants were able to slow down the fungal invasion on their inflorescences and delay the onset of spore proliferation as compared to WT and to *Hv2OGO*-complemented plants. The impairment of *2OGO* gene on its genomic exon 3 or the truncated C-terminal gene product due to frameshift mutations has disrupted its function in Fe(II) 2OG dioxygenase domain. The disruption in this domain caused the loss of enzyme's catalytic function in the biosynthesis and catabolism of plant hormones, such as salicylic acid, ethylene, gibberellins and flavonoids production [46]. From previous reports, biochemical analysis of the *2OGO* gene indicates its specific function in fine-tuning SA homeostasis[37]. These findings provide an insightful view on *2OGO* potential role as plant immunity suppressor in *Fg* invasion. Our qPCR quantitative assay result has shown that *At2OGO*-KO plants were able to restrict the fungal invasion by 30% compared to WT and to complemented plants. Even though the resistant plants might not completely block the entry of *Fg* into host tissue, the fungal progression and proliferation was impeded and infection proceeded at a much slower rate. This observation provides a solid evidence for

an efficient defense mechanism within the resistant plants. We quantitated the spore production to measure the *Fg* disease progression and to determine the onset of *Fg* colonization and host wilting. Based on our results, *At2OGO*-KO plants were able to delay the fungal progression for at least 48 hours and restrict spore production by about 30-60% compared to the WT and complemented plants which demonstrating its heightened level of resistance in combating fungal invasion. This observation indicates that WT and complemented plants were compromised at the end of 2 dpi when *Fg* started to exterminate host defense system and exploit host nutrients for spore proliferation. On the other hand, *At2OGO*-KO plants manage to strengthen their defense system and alleviate the disease symptoms. Our data showed that impairment of the *2OGO* gene leads to enhanced FHB disease resistance.

In order to understand the underlying molecular mechanism of the resistant plants, we performed RT-qPCR assay to examine the effect of *2OGO* mutation on plant defense signaling pathways. Remarkably, the floral tissues of *At2OGO*-KO mutant showed much higher levels of gene expression in all the selected defense-related genes primarily after 3 hpi. Both the WT and complemented plants, nonetheless, had much lower and almost undetectable level of gene expression upon fungal infection in the floral tissues. It was known that *DMR6* encodes salicylate 5-hydrolase [37] and its impairment results in the loss of hydrolase activity and hence high levels of SA accumulation which stimulates systemic acquired resistance (SAR) [47]. SA is the central player in SAR and known to be a critical defense against biotroph infection. The accumulation of SA can enhance the SAR responsiveness and therefore pathogen resistance. Hence, during infection of

hemibiotrophic *Fg*, the early defense responses of *At2OGO*-KO mutants were expected to respond in a biphasic strategy by having higher levels of expression for SA-related genes, such as *NPR1*, and other SAR-associated markers (*PR1*, *PR2*, *PR3*, and *PR5*) as well as triggering an oxidative burst with the production of reactive oxygen species (ROS). Our results support these predictions. Figures 2.10a to 2.10d showed that the expression of SA-related genes was induced strongly, starting from 3 hpi to its peak at 12 hpi followed by a decrease thereafter. The drop in transcripts may reflect their negative regulation by the *MPK4* gene. It is evident that the high levels of SA in *At2OGO*-KO mutants has greatly enhanced its resistance to restrict fungal invasion and proliferation. PR genes are primarily SA-dependent. We showed that their expression patterns were almost identical to those SA-related genes. Following SA-related gene induction, it has been established that the JA/ET signaling pathways are activated to mediate the resistance against necrotrophic pathogen [48]. Our results have shown the sequential pattern in the activation of defense pathways. The JA/ET signaling pathways-related genes (*AOS*, *EIN3*, *ERF1*, *PR3* and *PDF1.2*) were induced rapidly starting from 6 hpi and their expression decreased after 12 hpi (Figures 2.10e to 2.10j). The upregulation of JA/ET-related genes and the marked induction of *PDF1.2* (approximately 56-fold, compared to the WT and to *At2OGO*-KO/*Hv2OGO* plants) indicate that these genes may well play a key role in the enhanced resistance displayed by *At2OGO*-KO plants and that, in return, maybe responsible for slowing down *Fg* infection and colonization. The *MYC2* is a negative regulator of the JA signaling pathway, mediating the JA defense response antagonistically [49]. *RBOHD* gene was highly expressed during 6-12 hpi implicating its involvement in regulating ROS production in order to protect plants from pathogen invasion [50-52]. Based on the qPCR

analysis, JA signaling was activated in parallel with the SA signaling to attenuate damage caused by fungal infection which was similar to the report by Makandar group [53]. Overall, the much higher level of defense genes expression may be the underlying mechanism responsible for enhanced *Fg* resistance of *At2OGO*-KO plants. In summary, SA signaling pathway is first initiated at the early stage of *Fg* infection followed by the activation of JA signaling pathway that contributes to resistance at later stage of infection. The impairment of *dmr6* gene in *At2OGO*-KO mutant may be responsible for increasing SA accumulation which then directly amplifies the effects in defense gene response through SA/JA/ET signaling pathways upon *Fg* infection leading to greater degree of disease resistance. The barley orthologue-complemented plants had the *Fg* susceptibility restored proved that *Hv2OGO* is involved in FHB susceptibility in barley. CRISPR-editing the *Hv2OGO* gene in barley cultivars could be a very promising strategy to combat FHB.

References

1. Munkvold, G.P., *Cultural and genetic approaches to managing mycotoxins in maize*. Annu Rev Phytopathol, 2003. **41**: p. 99-116.
2. Manstretta, V. and V. Rossi, *Effects of Temperature and Moisture on Development of Fusarium graminearum Perithecia in Maize Stalk Residues*. Appl Environ Microbiol, 2016. **82**(1): p. 184-91.
3. McMullen, M., et al., *A Unified Effort to Fight an Enemy of Wheat and Barley: Fusarium Head Blight*. Plant Dis, 2012. **96**(12): p. 1712-1728.
4. Nganje, W.E., et al., *Regional Economic Impacts of Fusarium Head Blight in Wheat and Barley*. Applied Economic Perspectives and Policy, 2004. **26**(3): p. 332-347.
5. W., W., B. Dahl, and W. Nganje, *Economic costs of Fusarium Head Blight, scab and deoxynivalenol*. World mycotoxin journal, 2018. **2011 v.4 no.1**(no. 2): p. pp. 291-302.

6. Pestka, J.J. and A.T. Smolinski, *Deoxynivalenol: toxicology and potential effects on humans*. J Toxicol Environ Health B Crit Rev, 2005. **8**(1): p. 39-69.
7. Sobrova, P., et al., *Deoxynivalenol and its toxicity*. Interdiscip Toxicol, 2010. **3**(3): p. 94-9.
8. Dahleen, L.S., P.A. Okubara, and A.E. Blechl, *Transgenic approaches to combat Fusarium head blight in wheat and barley*. Crop science, 2001. **2001 v.41 no.3**(no. 3): p. pp. 628-0.
9. Mackintosh, C.A., et al., *Overexpression of defense response genes in transgenic wheat enhances resistance to Fusarium head blight*. Plant Cell Reports, 2007. **26**(4): p. 479-488.
10. Makandar, R., et al., *Genetically engineered resistance to Fusarium head blight in wheat by expression of Arabidopsis NPR1*. Mol Plant Microbe Interact, 2006. **19**(2): p. 123-9.
11. Li, Z., et al., *Expression of a radish defensin in transgenic wheat confers increased resistance to Fusarium graminearum and Rhizoctonia cerealis*. Funct Integr Genomics, 2011. **11**(1): p. 63-70.
12. Han, J., et al., *Transgenic expression of lactoferrin imparts enhanced resistance to head blight of wheat caused by Fusarium graminearum*. BMC Plant Biol, 2012. **12**: p. 33.
13. Hallen-Adams, H.E., et al., *Deoxynivalenol biosynthesis-related gene expression during wheat kernel colonization by Fusarium graminearum*. Phytopathology, 2011. **101**(9): p. 1091-6.
14. Kimura, M., et al., *Molecular and genetic studies of fusarium trichothecene biosynthesis: pathways, genes, and evolution*. Biosci Biotechnol Biochem, 2007. **71**(9): p. 2105-23.
15. Seong, K.Y., et al., *Global gene regulation by Fusarium transcription factors Tri6 and Tri10 reveals adaptations for toxin biosynthesis*. Mol Microbiol, 2009. **72**(2): p. 354-67.
16. Ferrari, S., et al., *Transgenic expression of polygalacturonase-inhibiting proteins in Arabidopsis and wheat increases resistance to the flower pathogen Fusarium graminearum*. Plant Biol (Stuttg), 2012. **14 Suppl 1**: p. 31-8.
17. Di, R. and N.E. Tumer, *Expression of a truncated form of ribosomal protein L3 confers resistance to pokeweed antiviral protein and the Fusarium mycotoxin deoxynivalenol*. Mol Plant Microbe Interact, 2005. **18**(8): p. 762-70.
18. Shin, S., et al., *Transgenic Arabidopsis thaliana expressing a barley UDP-glucosyltransferase exhibit resistance to the mycotoxin deoxynivalenol*. J Exp Bot, 2012. **63**(13): p. 4731-40.
19. Pasquet, J.C., et al., *A Brachypodium UDP-Glycosyltransferase Confers Root Tolerance to Deoxynivalenol and Resistance to Fusarium Infection*. Plant Physiol, 2016. **172**(1): p. 559-74.
20. Liu, L. and X.D. Fan, *CRISPR-Cas system: a powerful tool for genome engineering*. Plant Mol Biol, 2014. **85**(3): p. 209-18.
21. Fogarty, N.M.E., et al., *Erratum: Genome editing reveals a role for OCT4 in human embryogenesis*. Nature, 2017. **551**(7679): p. 256.
22. Friedland, A.E., et al., *Heritable genome editing in C. elegans via a CRISPR-Cas9 system*. Nat Methods, 2013. **10**(8): p. 741-3.

23. Hwang, W.Y., et al., *Efficient genome editing in zebrafish using a CRISPR-Cas system*. Nat Biotechnol, 2013. **31**(3): p. 227-9.
24. Sanchez, J.C., et al., *Phenotypic and Genotypic Consequences of CRISPR/Cas9 Editing of the Replication Origins in the rDNA of *Saccharomyces cerevisiae**. Genetics, 2019.
25. Xue, W., et al., *CRISPR-mediated direct mutation of cancer genes in the mouse liver*. Nature, 2014. **514**: p. 380.
26. Chen, K., et al., *CRISPR/Cas Genome Editing and Precision Plant Breeding in Agriculture*. Annu Rev Plant Biol, 2019. **70**: p. 667-697.
27. Endo, M., M. Mikami, and S. Toki, *Multigene Knockout Utilizing Off-Target Mutations of the CRISPR/Cas9 System in Rice*. Plant and Cell Physiology, 2014. **56**(1): p. 41-47.
28. Feng, C., et al., *Efficient Targeted Genome Modification in Maize Using CRISPR/Cas9 System*. J Genet Genomics, 2016. **43**(1): p. 37-43.
29. Feng, Z., et al., *Efficient genome editing in plants using a CRISPR/Cas system*. Cell Res, 2013. **23**(10): p. 1229-32.
30. Jiang, W., et al., *Demonstration of CRISPR/Cas9/sgRNA-mediated targeted gene modification in Arabidopsis, tobacco, sorghum and rice*. Nucleic Acids Res, 2013. **41**(20): p. e188.
31. Li, Z., et al., *Cas9-Guide RNA Directed Genome Editing in Soybean*. Plant physiology, 2015. **169**(2): p. 960-970.
32. Sanchez-Leon, S., et al., *Low-gluten, nontransgenic wheat engineered with CRISPR/Cas9*. Plant Biotechnol J, 2018. **16**(4): p. 902-910.
33. Zhang, Z., et al., *A multiplex CRISPR/Cas9 platform for fast and efficient editing of multiple genes in Arabidopsis*. Plant cell reports, 2016. **35**(7): p. 1519-1533.
34. Van Damme, M., et al., *Identification of arabidopsis loci required for susceptibility to the downy mildew pathogen Hyaloperonospora parasitica*. Mol Plant Microbe Interact, 2005. **18**(6): p. 583-92.
35. van Damme, M., et al., *Arabidopsis DMR6 encodes a putative 2OG-Fe(II) oxygenase that is defense-associated but required for susceptibility to downy mildew*. Plant J, 2008. **54**(5): p. 785-93.
36. Zeilmaker, T., et al., *DOWNY MILDEW RESISTANT 6 and DMR6-LIKE OXYGENASE 1 are partially redundant but distinct suppressors of immunity in Arabidopsis*. Plant J, 2015. **81**(2): p. 210-22.
37. Zhang, Y., et al., *S5H/DMR6 Encodes a Salicylic Acid 5-Hydroxylase That Fine-Tunes Salicylic Acid Homeostasis*. Plant Physiol, 2017. **175**(3): p. 1082-1093.
38. Zhang, X., et al., *Agrobacterium-mediated transformation of Arabidopsis thaliana using the floral dip method*. Nat Protoc, 2006. **1**(2): p. 641-6.
39. Qiwei, S., et al., *Genome editing in rice and wheat using the CRISPR/Cas system*. Nature Protocols, 2014. **9**(10): p. 2395.
40. Mittler, R., V. Shulaev, and E. Lam, *Coordinated Activation of Programmed Cell Death and Defense Mechanisms in Transgenic Tobacco Plants Expressing a Bacterial Proton Pump*. The Plant Cell, 1995. **7**: p. 29-42.
41. Miller, S.S., et al., *Use of a Fusarium graminearum strain transformed with green fluorescent protein to study infection in wheat (Triticum aestivum)*. Canadian Journal of Plant Pathology, 2004. **26**(4): p. 453-463.

42. Nalam, V., S. Sarowar, and J. Shah, *Establishment of a Fusarium graminearum Infection Model in Arabidopsis thaliana Leaves and Floral Tissues*. Bio-protocol, 2016. **6**(14): p. e1877.
43. Livak, K.J. and T.D. Schmittgen, *Analysis of relative gene expression data using real-time quantitative PCR and the 2(-Delta Delta C(T)) Method*. Methods, 2001. **25**(4): p. 402-8.
44. Jones, J.D.G. and J.L. Dangl, *The plant immune system*. Nature, 2006. **444**(7117): p. 323-329.
45. Summers, R.W. and J.K.M. Brown, *Constraints on breeding for disease resistance in commercially competitive wheat cultivars*. Plant Pathology, 2013. **62**(S1): p. 115-121.
46. Farrow, S.C. and P.J. Facchini, *Functional diversity of 2-oxoglutarate/Fe(II)-dependent dioxygenases in plant metabolism*. Front Plant Sci, 2014. **5**: p. 524.
47. Gao, Q.M., et al., *Signal regulators of systemic acquired resistance*. Front Plant Sci, 2015. **6**: p. 228.
48. Yan, C. and D. Xie, *Jasmonate in plant defence: sentinel or double agent?* Plant Biotechnol J, 2015. **13**(9): p. 1233-40.
49. Kazan, K. and J.M. Manners, *MYC2: the master in action*. Mol Plant, 2013. **6**(3): p. 686-703.
50. Herrera-Vasquez, A., P. Salinas, and L. Holuigue, *Salicylic acid and reactive oxygen species interplay in the transcriptional control of defense genes expression*. Front Plant Sci, 2015. **6**: p. 171.
51. Kimura, M. and T. Kawano, *Salicylic acid-induced superoxide generation catalyzed by plant peroxidase in hydrogen peroxide-independent manner*. Plant Signal Behav, 2015. **10**(11): p. e1000145.
52. Lehmann, S., et al., *Reactive oxygen species and plant resistance to fungal pathogens*. Phytochemistry, 2015. **112**: p. 54-62.
53. Makandar, R., et al., *Involvement of salicylate and jasmonate signaling pathways in Arabidopsis interaction with Fusarium graminearum*. Mol Plant Microbe Interact, 2010. **23**(7): p. 861-70.

Chapter **3**

The *Ethylene Insensitive 2 (EIN2)*-edited *Arabidopsis* expressing a barley *EIN2* orthologue validates the gene's involvement in *Fusarium* head blight susceptibility

Chapter 3

The *Ethylene Insensitive 2 (EIN2)*-edited *Arabidopsis* expressing a barley *EIN2* orthologue validates the gene's involvement in *Fusarium* head blight susceptibility

Introduction

Ethylene (ET) is a gaseous hormone that influences and regulates diverse biological processes in plant growth, development and defensive responses [1]. It is best known for its effect on fruit ripening and its role in abscission signaling [2]. Apart from these features, it is one of the crucial components in modulating plant responses to various abiotic and biotic stresses. Pathogen perception induces the activation of ethylene biosynthesis genes and enzymes, and eventually leads to a cascade of ET-centered signaling transduction which acts synergistically with jasmonate (JA) in regulating defense genes against necrotrophic pathogens [3]. JA/ET signaling pathway usually acts sequentially after salicylic acid (SA) as a secondary defense modulator during pathogen infection. SA serves a critical role in restricting biotrophic pathogens through the activation of systemic acquired resistance (SAR) by which it transmits defense signals throughout the plant providing broad spectrum resistance to block further infections [4, 5]. Therefore, ethylene has a critical role in both local and systemic plant defense network. Based on genetic studies performed in *Arabidopsis thaliana*, ethylene is first perceived by a group of ER (endoplasmic reticulum)-bounded integral membrane receptors include *ETR1/2* (*ethylene insensitive 1* and *2*), *ERS1/2* (*ethylene response sensor 1* and *2*) and *EIN4* (*ethylene*

insensitive 4). The downstream ET signaling pathway is then regulated by a central component, *ethylene insensitive 2 (EIN2)* gene, located at the ER [6].

EIN2 is an essential positive regulator of ethylene signaling that links the ET perception to transcriptional regulation in the nucleus [7, 8]. The *EIN2* gene was first characterized two decades ago. *EIN2* encodes a protein with its hydrophobic N-terminal conserves a NRAMP transmembrane helices domain whereas its C-terminal (CEND) conserves a putative nuclear localization signal (NLS) [9]. Apart from serving as a transmembrane protein, its signaling mechanism to the nuclear-localized transcription factors was not clearly known until a recent study revealed the function of its CEND in ET signaling [7]. The CEND of *EIN2* is cleaved upon receiving ethylene induced signals [10]. This cleavage is essential for downstream activation of *EIN3* (ethylene insensitive 3) as it allows the signal to be translocated into the nucleus [11, 12]. A loss-of-function *ein2* mutant could cause ethylene insensitivity and possibly abolish or weaken the ET signaling output during pathogen attack. Losing the key regulator of ET signaling pathway could create a disastrous outcome upon biotic or abiotic stress. However, some contradictory observations of the *ein2* mutant show that disruption of this gene can confer resistance to pathogen infections. Reports showed that the *ein2* mutant displayed decreased disease symptoms and reduced fungal colonization on tomato plants infected by *Fusarium oxysporum* [13] and on wheat plants infected by *Fusarium graminearum*. The latter study showed the similar attenuation of disease symptoms in Arabidopsis *ein2* mutants and in RNAi knock-down *ein2* wheat plants; in both cases there was a significant reduction of *Fg* disease progression and in the levels of DON toxin present in plant tissues [14]. Hence, reduction in ET perception can, in some

cases, enhance host resistance to pathogen attack. It has long been speculated that the ET signaling pathway may be hijacked by some pathogens such as *Fusarium* species, in an effort to prolong infection while exploiting the host's resources [15]. Nonetheless, the exact hijacking mechanism remains unclear. Hence, *EIN2* gene is considered a host susceptibility factor in the study of *Fg*.

Identification of host susceptible genes to combat *Fusarium* head blight (FHB) disease has been challenging. There are some useful and promising susceptible genes for bioengineering of resistant plant [16-20]. Apart from *ZOGO* gene discussed in the previous chapter, *DMRI* is another susceptibility gene which holds great potential for FHB resistance in cereal crops [21]. The latest gene discovery is the wheat *HRC* gene, key factor for *Fhb1*-mediated resistance to *Fg*, that encodes a putative histidine-rich calcium-binding protein [22]. Deletion of this gene results in FHB resistance in wheat yet its mechanism and biological functions remains unknown. Likewise, mutation of *EIN2* gene was known to confer resistance to FHB but no further investigation has been carried out to elucidate the underlying mechanism of this protective phenotype. As was the case in the work described in the previous chapter, the aim of this study is to investigate the contribution of *ein2* to FHB disease and to utilize CRISPR technique to generate *ein2* mutants. The *Arabidopsis* mutants can then serve as a genetic platform to identify corresponding barley FHB susceptible genes using a gene complementation assay.

Methods and materials

***Arabidopsis thaliana* plant growth**

Arabidopsis thaliana Columbia ecotype (Col-0) seeds were sterilized with 30% bleach for 30 minutes and washed with sterile water for five times. Sterilized seeds were stratified at 4 °C for two days and plated on growth medium [Murashige and Skoog (MS) medium containing 1% (w/v) sucrose and 0.3% (w/v) Gelzan™ agar]. The plated seeds grew at 22 °C under 16h/8h light-dark photoperiod. Germinated seedlings were transferred to Pro-Mix soil in an environmental-controlled chamber with a 16h/8h light-dark photoperiod at 22 °C and 40%-60% relative humidity.

Construction of *AtEIN2* CRISPR-editing vector

The *Arabidopsis thaliana* genomic and mRNA sequence of *Ethylene insensitive 2 (AtEIN2)* was obtained from TAIR (<https://www.arabidopsis.org/>) and NCBI (<https://www.ncbi.nlm.nih.gov/>) databases with accession number of AT5G03280 and AF141203 respectively. The gRNA target sequence for *AtEIN2* gene (5'-GGAAGTATCGATTTCGTTGTATGG-3') was identified according to selection guidelines with 20 nucleotides upstream of a proto-spacer adjacent motif (PAM) sequence (5'-N₂₀-NGG-3') and a target sequence begins with the G nucleotide base. The *AtEIN2*-editing vector was constructed following the protocol as published previously [23]. The gRNA sense and anti-sense oligos (forward: 5'- GATTGGAAGTATCGATTTCGTTGTA -3'; reverse: 5'- AA ACTACAACGAATCGATACTTCC -3') were phosphorylated and

annealed under the following condition: 37 °C for 30 minutes, 95 °C for 5 minutes and then ramping down to 25 °C at the rate of 5 °C/minute, in a 10 µl reaction (1 µl of 10x T4 ligation buffer, 0.5 µl of T4 PNK, 1 µl of each oligo at 100 µM). The annealed gRNA oligos were cloned into psgR-Cas9-At vector (kindly provided by Dr. J. Zhu, [23]). The resulting plasmid was sequenced and confirmed followed by subcloning into plant expression vector pCAMBIA1300 (<https://www.addgene.org/vector-database/5930/>), resulting in pRD182, and transformed into *Agrobacterium tumefaciens* EHA105 strain.

***Arabidopsis thaliana* plant transformation and mutant selection**

Arabidopsis thaliana Col-0 plants were grown for 3-4 weeks until flowering. *Agrobacterium tumefaciens* EHA105 strain harboring pRD182 (*AtEIN2* gRNA/Cas9) was grown in 2 mL of LB liquid medium containing 50 µg/ml kanamycin and 50 µg/ml chloramphenicol. The 2 ml overnight culture was inoculated into 200 mL LB liquid medium containing the same antibiotics and was shaken at 30 °C for approximately 5 hours until the OD₆₀₀ reached to 0.6. *Agrobacterium* cells were spun down and rinsed twice with 5% sucrose before resuspending into 300mL of 5% sucrose solution with 0.05% Silwet L-77. Floral buds were dipped into *Agrobacterium* solution for 1-2 s [24]. The inoculated plants were covered with a clear plastic dome for 24 hours before returning to controlled growth chamber. The transformed plants were grown for another 3-4 weeks for seed harvesting. The collected T₀ seeds were sterilized by 30% bleach and selected on growth medium containing 50 µg/L hygromycin. The selected mutant plants were transferred to soil for acclimated growth.

Genomic DNA (gDNA) isolation of Arabidopsis mutant plants

200 mg leaf tissues from each putative mutant plant was collected for gDNA isolation using CTAB extraction buffer (2% cetyl trimethylammonium bromide, 1% polyvinyl pyrrolidone, 100 mM Tris-HCl, 1.4 M NaCl, 20 mM EDTA). The CTAB-leaf tissue mix was vortexed vigorously for 30s and then incubated at 65 °C for an hour followed by phenol-chloroform isolation. The supernatant was then mixed with 100% ethanol to precipitate the DNA followed by clean-up step with 70% ethanol. The DNA pellets were air-dried and resuspended with sterile deionized water. The concentration of DNA was measured with a Nanodrop spectrophotometer (Thermo Fisher, Waltham, MA, United States).

Mutant analysis: mutant confirmation, restriction fragment length polymorphism (RFLP) and TaqMan assays

The presence of the Cas9 gene in putative mutant plants was first confirmed by PCR-amplification using Cas9 primers (forward: 5'- GAAGCGGAAGGTCGGTATCCACGG -3'; reverse: 5'- GGCCAGATAGATCAGCCGCAGGTC -3'). The gDNA samples were used to amplify a 505 bp fragment flanking the target sequence (forward: 5'- GGGACTGGAAGCCTTTCACGGTTGC -3'; reverse: 5'- GGTATCCGTGAACTGTAGCTGGTTG -3') to confirm the integration of Cas9 transgene. The amplified fragments were purified using phenol chloroform clean-up

method and resuspended in sterile deionized water prior to analysis. RFLP assay was carried out by incubating *Cla*I restriction enzyme with the purified 505 bp PCR fragment from each putative mutant line and the WT plant. Digested samples were electrophoresed on 1% agarose gel and the gel images were captured. TaqMan gene expression assay was performed as well to serve as another analysis method. Two TaqMan probes (*EIN2* WT allele: TCGTTGTATGGATTAC; *ACT2*: TTGGTGCTGAGAGATT) and two qPCR primer pairs for *ACT2* (forward: 5'- CCGATGGGCAAGTCATCAC -3'; reverse: 5'- GGAACAAGACTTCTGGGCATCT -3') and *EIN2* (forward: 5'- GCAGCAGAGGACACCGGGAAG -3'; reverse: 5'- CGGTGACGGTGACGAACCTC -3') were designed for the qPCR assay. One of them hybridized to WT gRNA target site while the other hybridized to housekeeping gene, Arabidopsis *Actin-2* (*ACT2*) gene. Any indel mutation will prevent the probe from hybridizing to the target site due to the sequence mismatch. In such case, no fluorescence signal will be released from the FAM reporter. The gDNA sample from each mutant was used in the qPCR reaction with the TaqMan™ Universal PCR Master Mix (Applied Biosystems, Thermo Fisher, Foster City, CA, United States). The TaqMan qPCR assay was run on the default setting at 95 °C for 10 minutes for initial denaturation and 40 cycles at 95 °C for 15 s followed by 60 °C for 60 s. The fold-change of gene expression was calculated by the $2^{-\Delta\Delta C_t}$ method [25] and normalized by the *ACT2* gene expression.

Complementation of *AtEIN2*-KO line with *HvEIN2*

In order to clone the *HvEIN2* cDNA from barley cv. Conlon, we isolated the total RNA from cv. Conlon four weeks old leaf tissues and conducted RNAseq analysis by Novogen Co., Ltd.. This RNAseq data has been deposited in NCBI SRA database (accession number SRR10059574) under BioProject PRJNA563590. The RNAseq data from Conlon were aligned to cv. Morex *EIN2* gene sequence (mRNA: MLOC_74303; gDNA: HORVU5Hr1G050330) using the NCBI BLAST tool (<https://blast.ncbi.nlm.nih.gov/Blast.cgi>). Conlon *EIN2* cDNA was amplified by PCR with gene specific primers (forward: 5'- GGTCTAGAATGAACCAGATATTCATGA -3'; reverse: 5'- AGTGCTGCTAACTGCTTCCT -3') and cloned into plant expression vector pEL103 (kindly provided by Dr. E. Lam, [26]), resulting in pRD334, which was then transformed into *Agrobacterium tumefaciens* EHA105 strain. The homozygous *AtEIN2*-KO line (RD182-14-10-4-10) was complementarily transformed with pRD334 *via* the floral dip method. Seeds from T₀ plants were selected on 70 µg/L kanamycin. Confirmed T₁ complemented plants were segregated on 70 µg/L kanamycin. Homozygous T₂ generation was confirmed by antibiotic screening.

***Fg* inoculation on detached Arabidopsis inflorescences and quantitative assays for disease development**

Fg tagged with sGFP (superfolder green fluorescent protein) [27] was cultured on PDA agar for 7 days at 22 °C under UV light for 24/7. Fungal plug was extracted from PDA plate and cultured in 50 mL of mung bean soup for another 7 days to generate macroconidia [28]. The macroconidia were filtered out from mung bean soup using Miracloth (Millipore

Sigma, Burlington, MA, United States) and washed twice with sterile deionized water before resuspension in sterile water. The concentration of macroconidia was measured using hemocytometer. The macroconidia solution was diluted to 1×10^6 spores/mL for inflorescence inoculation. Bolting floral buds were detached from plants and laid perpendicularly onto 0.7% water agar in petri dishes. Each inflorescence was inoculated with 2 μ L of 1×10^6 spores/mL macroconidia solution along with a duplicate set of mock sample that was inoculated with sterile water. The inoculated detached inflorescences were maintained in a 100% humidity condition by spraying water on the inner side of the petri dish lids prior to plate sealing. The plates were left in environmentally controlled chamber with a 16h/8h light/dark photoperiod at 22 °C. Images were taken using the Dino-eye eyepiece camera (Dino-Lite, Hsinchu, Taiwan) on Nikon SMZ 645 stereomicroscope (Nikon corp., Minato, Japan) and samples were collected every 24 hours by pooling four inflorescences in a tube per time point until reaching 144 hours. After each collection, the pooled samples were rinsed with 1 mL of sterile water and mild shaking to remove *Fg* spores from the surface of inflorescence. The first 1 mL of rinsed water was collected to quantify the spore production at each time point using hemocytometer. The pooled samples were rinsed for another two times with 1 mL of water to get rid of as many surface-attached spores as possible. Total DNAs of pooled samples were then isolated using the CTAB method and quantitation on spores penetrated the floral tissues was performed using Applied Biosystems StepOne Plus thermocycler (Applied Biosystems, Thermo Fisher, Foster City, CA, United States) by amplifying the sGFP (forward: 5'-GTCCGCCCTGAGCAAAGA-3'; reverse: 5'-TCCAGCAGGACCATGTGATC-3') in the pooled samples. Both quantitative assays were repeated thrice and the data obtained

from quantitative assays was averaged with standard deviations (SD), followed by the Student's *t*-test analysis on WT vs. *AtEIN2*-KO and WT vs. *AtEIN2*-KO/*HvEIN2* groups using GraphPad software. Statistical significance determined using the Holm-Sidak method, with alpha = 0.05. Each time point was analyzed individually, without assuming a consistent SD.

Relative gene expression profiling on plant defense mechanism

In order to understand the molecular mechanisms underlining the defense signaling in *AtEIN2*-KO and *AtEIN2*-KO/*HvEIN2* plants infected with *Fg*, some of the key downstream targets in the SA, JA, ET and ROS signaling pathways were chosen for quantitation by RT-qPCR analysis. Arabidopsis *Actin-2* (*ACT2*) gene was used as the reference housekeeping gene in these studies. Primers for each selected gene were designed using the Primer Express software (Applied Biosystems, Thermo Fisher, Foster City, CA, United States). The primer sets for each gene were first validated to have similar amplification efficiency as the *ACT2* gene. Detached inflorescences were each inoculated with 2 μ l of *Fg* macroconidia solution as described above and collected at 3, 6, 12, 24, 48 hr time point. Four inflorescences were pooled into a tube and rinsed three times with 1 mL of sterile water. Total RNA of pooled samples were isolated using the TRIZOL method (Ambion Life Technologies, Thermo Fisher, Carlsbad, CA, United States) and the concentration was measured using the Nanodrop spectrophotometer (Thermo Fisher, Waltham, MA, United States). Reverse transcription (RT) reaction was carried out with the High Fidelity cDNA Synthesis Kit (Applied Biosystems, Thermo Fisher, Foster City, CA, United States) using

approximately 2 µg RNA. The RT products were used in qPCR reactions with the SYBR 2X Master Mix (Applied Biosystems, Thermo Fisher, Foster City, CA, United States). The RT-qPCR assay was run on the default setting at 95 °C for 3 minutes for initial denaturation and 40 cycles at 95 °C for 30 s followed by 60 °C for 30 s. The fold-change of gene expression was calculated by the $2^{-\Delta\Delta C_t}$ method [25]. The RT-qPCR analysis was repeated three times with different batches of samples, and the gene expression levels were averaged. Primers used in the RT-qPCR gene expression assay were listed in Table 3.1.

RT-qPCR primers	Forward	Reverse
<i>NPR1</i>	GCCGCCGAACAAGTACTCA	GCTGTTGGAGAGCAATTGCA
<i>PR1</i>	GTCTCCGCCGTGAACATGT	CGTGTTTCGCAGCGTAGTTGT
<i>PR2</i>	GCTGGACAAATCGGAGTATGC	CCGATGGACTTGGCAAGGTA
<i>PR5</i>	AACGGCGGCGGAGTTC	CGCCATCGCCTACTAGAGTGA
<i>PR3</i>	ACGCAGTGATCGCTTTCAA	TGGGAGGCTGAGCAGTCATC
<i>PDF1.2</i>	TTTGCTTCCATCATCACCTTA	GCGTCGAAAGCAGCAAAGA
<i>Actin2</i>	GATTCAGATGCCCAGAAGTCTTG	TGGATTCCAGCAGCTTCCAT

Table 3.1. List of primers used in the RT-qPCR gene expression assay.

Results

Generating *EIN2* mutants in Arabidopsis using CRISPR/Cas9 system

The *EIN2* genomic (AT5G03280) and mRNA (AF141203) sequences were obtained from TAIR and NCBI databases respectively. *EIN2* is encoded by a single gene copy in

Arabidopsis and its coding region, which comprises 3905 nucleotide bases, is interrupted by 7 introns. *EIN2* encodes a protein of 1294 amino acids (a.a.) conserved with a 12-transmembrane domain of the NRAMP family of metal ion transporters at extremely hydrophobic N-terminal (461 a.a.) while the exact function is not known [9]. Its C-terminal (833 a.a.), which is thought to involve in the ethylene signaling output, conserves a putative nuclear localization signal (NLS) from 1262-1269 a.a [10]. The gRNA guidelines (www.addgene.org/crispr/guide) were followed while choosing a 20-nucleotides genomic target which is unique within the Arabidopsis genome and is also adjacent to a PAM sequence. We designed a gRNA that specifically targets the C-terminal of the protein (target region: 5'- GGAAGTATCGATTCGTTGTA -3') and that also flanks a *ClaI* restriction site (underlined) for mutant screening. The gRNA target was cloned into the vector kindly provided by Dr. J. Zhu [23] containing Arabidopsis U6 promoter and a Cas9 gene that is driven by the 2x 35S promoter and terminated by the NOS terminator. For *Agrobacterium* transformation, this gRNA/Cas9 cassette was subcloned into the *EcoRI* and *HindIII* region of pCAMBIA1300 vector, resulting in the plant expression vector pRD182. Flowering Arabidopsis Col-0 plants were transformed *via* EHA105 strain of *Agrobacterium* using the floral-dip method. The collected T₀ seeds were screened on 50 µg/L hygromycin. A total of 15 putative T₁ mutant plants were recovered from antibiotic selection.

Molecular characterization of *AtEIN2*-KO mutants and identification of homozygous progeny

The *AtEIN2* (pRD182) CRISPR-editing transformants were first confirmed by performing PCR with Cas9 specific primers using extracted genomic DNA from each T₁ line which later were genotyped using restriction fragment length polymorphism (RFLP) assay followed by Sanger sequencing to discover the mutations in T₁ progeny. A 505 bp genomic DNA (gDNA) sequence that flanks the target region was PCR-amplified and analyzed by RFLP with *Cla*I restriction digestion (Figure 3.1) and by the highly sensitive TaqMan qPCR assay (Table 3.2). The gel picture (Figure 3.1) demonstrated that all putative mutant lines had three DNA bands after the RFLP assay. The bottom two bands (308 bp and 197 bp) represented the digestion fragments for WT plant while the top band (505 bp) was the undigested fragment, indicating that one allele of the gDNA was mutated at the restriction site in the target region (monoallelic mutation). In the TaqMan qPCR assay, the designed probe can anneal specifically to the WT EIN2 allele. A monoallelic mutation, either insertion or deletion at the gRNA target site, rendered the failure for probe to hybridize to half of the given gDNA sample and approximately 50% loss of the reporter dye signal [29]. In this regard, the normalized relative expression value of a heterozygous mutant should be at 0.5 or within the range of (0.1 < relative values < 1) whereas the relative expression values of a homozygous mutant should not be determined or within the range of 0-0.1. Table 3.2 showed that all T₁ mutant lines had their computed relative expression values fell within the range of 0.24 to 0.88. This result, in addition to RFLP assay, concluded that all the T₁ mutants were heterozygous with monoallelic mutations. The undigested PCR fragments (505 bp) following RFLP assay were extracted and purified for Sanger sequencing to decipher the mutations induced by pRD182 CRISPR-editing vector.

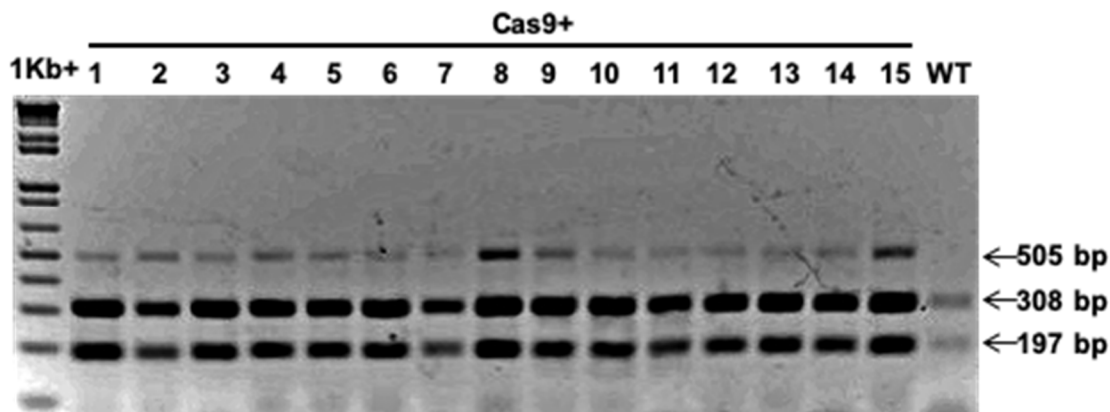


Figure 3.1. RFLP assay to confirm putative CRISPR-edited *AtEIN2* (RD182) mutants. Total of 15 mutant lines were first confirmed to carry Cas9 gene which then followed by target region PCR and analyzed by *ClaI* restriction digestion. The top band (505 bp) represented the mutated fragments which lose the restriction site while the bottom two bands result from digestion of WT fragments by *ClaI* restriction enzyme.

Lines	Relative values	Lines	Relative values
182-1	0.88	182-9	0.50
182-2	0.60	182-10	0.50
182-3	0.38	182-11	0.86
182-4	0.34	182-12	0.30
182-5	0.88	182-13	0.46
182-6	0.24	182-14	0.34
182-7	0.39	182-15	0.31
182-8	0.35	WT	1

Table 3.2. TaqMan qPCR assay to confirm putative CRISPR-edited *AtEIN2* (RD182) mutants. In addition to RFLP assay, this assay served as another method to identify zygosity of the mutants. The relative values of mutants were normalized by Arabidopsis *ACT2* gene expression and compared to the WT. The determination range for heterozygous mutant is $0.1 < \text{relative values} < 1$ and for homozygous mutant is either relative values ≤ 0.1 or relative values is undetermined.

Figure 3.2 shows the mutation profiles for RD182 (*AtEIN2-KO*) mutants. Among the 15 T₁ mutants, there were only 20% (3 out of 15) of them (*182-11*, *182-12* and *182-14*) with frameshift mutation while *182-15* carried a 3 bp deletion with one missing amino acid in the final protein. The other 11 mutants displayed point mutations with single base substitution without shifting the open reading frame. This phenomenon was very likely due to the low editing efficiency at this particular gRNA site. It could be because the *AtEIN2* gene is an essential gene so that any CRISPR-induced DNA breaks could be repaired by a homology-directed repair mechanism. These three frameshift mutants were selected for segregation.

Wildtype	GAGGACACCGGGAAGTATCGATTTCGTTGTA	TGGATTACAA	
	ClaI	PAM	
T₁ generation			
182-1	GAGGACACCGGGAAGTATGATTCGTTGTA	TGGATTACAA	
182-2	GAGGACACCGGGAAGTCTCGATTTCGTTGTA	TGGATTACAA	
182-3	GAGGACACCGGGAAGTACCGATTTCGTTGTA	TGGATTACAA	
182-4	GAGGACACCGGGAAGTATCGTTTCGTTGTA	TGGATTACAA	
182-5	GAGGACACCGGGAAGTATAGATTTCGTTGTA	TGGATTACAA	
182-6	GAGGACACCGGGAAGTATCAATTCGTTGTA	TGGATTACAA	
182-7	GAGGACACCGGGAAGTATCGACTCGTTGTA	TGGATTACAA	
182-8	GAGGACACCGGGAAGTTCGATTTCGTTGTA	TGGATTACAA	
182-9	GAGGACACCGGGAAGTCTCGATTTCGTTGTA	TGGATTACAA	
182-10	GAGGACACCGGGAAGTATCGACTCGTTGTA	TGGATTACAA	
182-11	GAGGACACCGGGA-----GTATGGATTACAA		-13 (f.s.)
182-12	GAGGACACCGGGAAG-----TACAA		-20 (f.s.)
182-13	GAGGACACCGGGAAGTCTCGATTTCGTTGTA	TGGATTACAA	
182-14	GAGGACACCGGGAAGTATCGA-ACG-AGTATGGATTACAA		-2 (f.s.)
182-15	GAGGACACCGGGAAGTCTCGAT---TTGTA	TGGATTACAA	-3
T₄ generation			
182-12-11-10-8	GAGGACACCGGGAAGTATCGATTTCGT-GTATGGATTACAA		-1 (f.s.)
182-14-10-4-10	GAGGACACCGGGAAGTATCGATTTCGTCAACCGTATGGATTACAA		-1 +20 (f.s.)
Red - sgRNA target Blue - Restriction site Gold - Base substitution Green - Insertion			

Figure 3.2. The mutation profiles of RD182 (*AtEIN2*-KO) mutants for the T₁ generation and the homozygous mutants for the T₄ generation. In the T₁ generation, only 20% of them (182-11, 182-12 and 182-14) carried frameshift mutation, and one with 3 bp deletion while the remaining mutants carried point mutations resulting in no shift of the open reading frame.

Lines	Relative values
182-12-11-10-8	0.02
182-14-10-4-10	Undetermined
WT	1

Table 3.3. TaqMan qPCR assay to confirm homozygous RD182 (*AtEIN2*-KO) mutants. The relative values of mutants were normalized by Arabidopsis *ACT2* gene expression and compared to the WT. The determination range for homozygous mutant is undetermined or

relative values of ≤ 0.1 . Only two homozygous mutants were identified after four generations of segregation.

Due to the difficulty of generating a frameshift mutant, as observed in the sequencing result, homozygous mutant screening was done solely by the TaqMan qPCR assay due to its capacity for large scale screening and its high sensitivity for mutant identification. We suspected that plants may attempt to correct the *EIN2* gene sequence during the process of DNA repair because no homozygous mutant could be identified in T₂ or T₃ generation which comprised 500-1000 of individual plants. It was not until the T₄ generation that two homozygous mutants were obtained from screening. Table 3.3 showed the TaqMan qPCR assay result for the two homozygous mutants. *182-12-11-10-8* had a relative value of 0.02 while *182-14-10-4-10* had an undetermined value which indicated both of them carried biallelic mutation. Their sequencing results (refer to Figure 3.2) revealed that *182-12-11-10-8* had a single base pair deletion which explained its results in the TaqMan assay that reporter dye can possibly hybridize with the target region even with one mismatch. On the other hand, *182-14-10-4-10* carried a 20 bp insertion at 3 bp upstream of PAM sequence but 4 bp downstream of *ClaI* restriction site which is one of the main reason that the RFLP assay might not be suitable for screening this gRNA target site. Since *182-14-10-4-10* was the only one with large insertion, its shifted nucleotide sequence resulting in a premature protein termination with 801 a.a. compared to a fully functional protein of 1294 a.a.. In other words, the C-terminal of *EIN2* was truncated and ethylene signaling output may consequently be hindered as a result. Hence, *182-14-10-4-10* was selected for disease assessment and barley gene complementation. Prior to any downstream experiments, the

gRNA and the Cas9 cassettes were segregated out from the homozygous line. The loss of these cassettes was confirmed by PCR with gRNA- and Cas9-specific primers.

Identification of *EIN2* orthologue from barley cultivar Conlon for complementation test

We searched for *EIN2* orthologues of barley (*Hordeum vulgare*) in the PGSB barley genome database. Currently, high quality reference genome assembly and automated gene annotation have been done only on barley cv. Morex [30]. One copy of *HvEIN2* gene in cv. Morex was identified from the database. The mRNA and gDNA sequences were tagged as MLOC_74303 and HORVU5Hr1G050330 respectively in the database. In order to confirm the *HvEIN2* gene sequence in cv. Conlon as compared to cv. Morex, total RNA from cv. Conlon was extracted and sequenced by Novogene Co., Ltd. The RNAseq data was assembled and aligned against the cv. Morex *EIN2* gene sequence to identify the Conlon *EIN2* gene. The Conlon *EIN2* cDNA was cloned by RT-PCR and sequenced *via* Sanger sequencing. The Conlon *HvEIN2* nucleotide sequence was shown to be 99.93% identical to the Morex *HvEIN2* nucleotide sequence except there were two mismatches at position 552 and 2571 of the cDNA sequence without changing the protein sequence. The Conlon *HvEIN2* was cloned into pEL103 (kindly provided by Dr. E. Lam, [26]) transformation vector, resulting in pRD334, which was then transformed into EHA105 strain of *Agrobacterium*. The homozygous *AtEIN2*-KO (RD182-14-10-4-10) mutant was selected as the host for transformation with pRD334 *via* *Agrobacterium*-mediated floral dip method. Seeds collected from T₀ plants were screened on 70 µg/L kanamycin-containing medium.

A total of 2 putative T₁ *HvEIN2*-complemented transformants were recovered from antibiotic selection and confirmed by PCR on *HvEIN2* gene (Figure 3.3). The *AtEIN2*-KO/*HvEIN2-1* from T₁ generation was used for disease assessment while waiting for the segregation of homozygous lines.

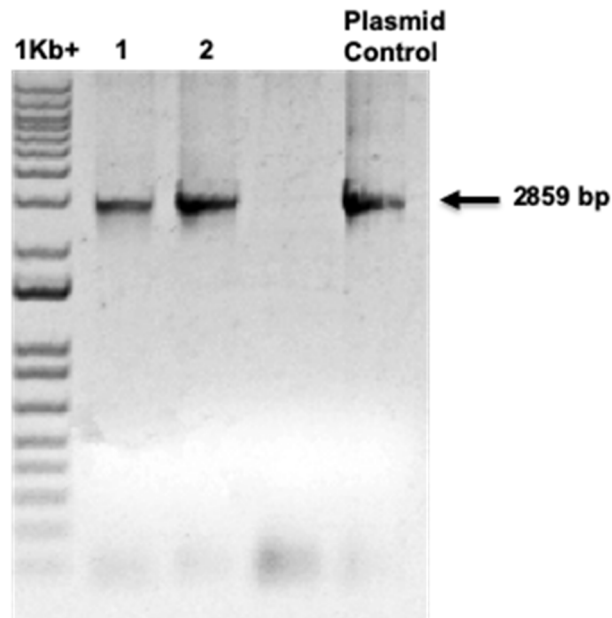


Figure 3.3. Gel image showed the PCR-confirmed *AtEIN2*-KO/*HvEIN2* lines (1-2) with a plasmid control (pRD334) carrying the *HvEIN2* mRNA fragment of 2859 bp.

Characterization of disease phenotype on *AtEIN2*-KO and *AtEIN2*-KO/*HvEIN2*-complemented homozygous plants

The homozygous *AtEIN2*-KO mutant (RD182-14-10-4-10) and heterozygous *At2OGO*-KO/*Hv2OGO*-complemented plants (RD182-14-10-4-10/334-1) were used in the *Fg*

infection assay together with the WT Arabidopsis as the control group. The *Fg* infection assay was performed by point inoculation of the sGFP-tagged *Fg* macroconidia on detached inflorescences and stereomicroscopic images were taken each day post inoculation (dpi) for 6 days (Figure 3.4).

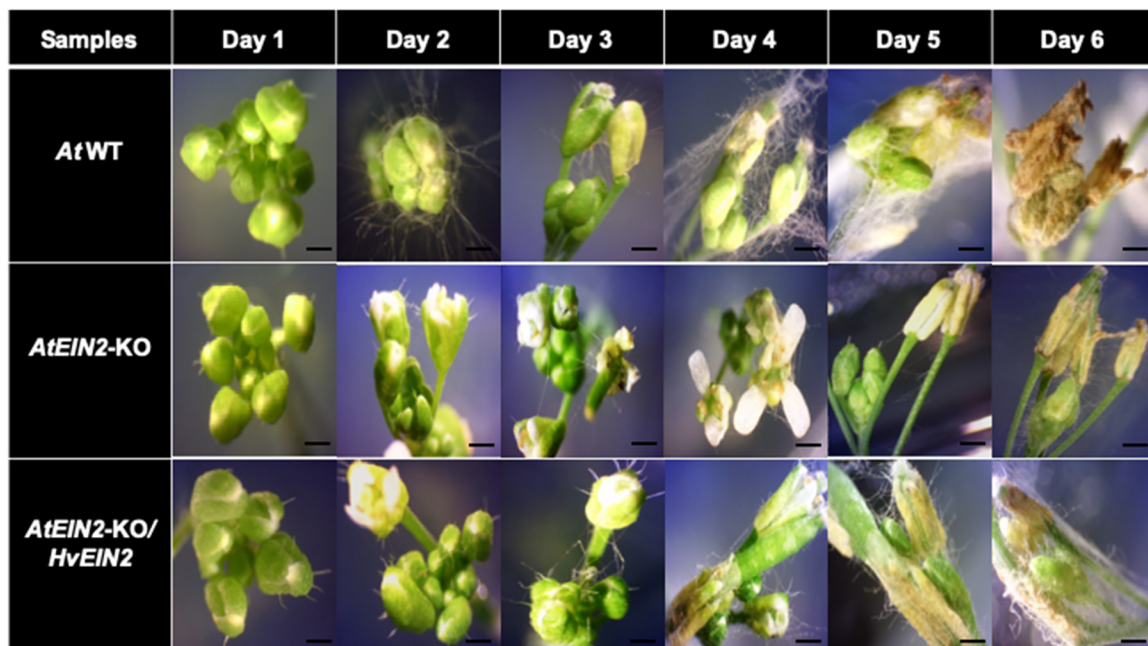


Figure 3.4. Illustration of FHB disease progression on detached Arabidopsis inflorescences. *AtEIN2-KO* inflorescences displayed a restricted rate of fungal hyphae growth from 4-6 dpi whereas WT and *AtEIN2-KO/HvEIN2* inflorescences spread aggressively from one inflorescence to another starting from 3 dpi onwards. Pictures were taken using the Dino-eye eyepiece camera together with stereomicroscopes at 20x magnification. Scale bar (0.1 mm —).

At 2 dpi, fungal hyphae started to form on the surface of WT, *AtEIN2*-KO and *AtEIN2*-KO/*HvEIN2* inflorescences. Nonetheless, *AtEIN2*-KO inflorescences displayed a restricted rate of fungal hyphae growth throughout the experimental period. KO inflorescences still appeared viable at day 6 with minimal hyphae growth as compared to WT and the complemented line. In contrast, hyphal growth on WT and *AtEIN2*-KO/*HvEIN2* inflorescences spread aggressively from one inflorescence to another starting from 3 dpi. At 5 to 6 dpi, the *Fg* hyphae on WT and *AtEIN2*-KO/*HvEIN2* inflorescences became abundant and the colonization started to take over the inflorescence tissue by forming thick mycelial mat. At the same time, the host tissue started to show wilting symptoms. It was evident that the loss of susceptibility from the truncated *EIN2* gene slowed down the infection progress of *Fg*. Our results showed that the *AtEIN2*-KO inflorescences were more resistant to *Fg* infection than WT's, and the complementation of *AtEIN2*-KO with *HvEIN2* recovered the Arabidopsis susceptibility to *Fg*, indicating that *HvEIN2* is an *Fg* susceptible factor for barley.

In order to assess the disease severity, we used the qPCR assay to quantitate the amount of *Fg* that had penetrated into the host tissue (Figure 3.5). The inoculated inflorescences were collected daily and rinsed off the surface *Fg* hyphae and macroconidia with sterile deionized water for three times with mild shaking. The rinsed and pat-dried inflorescences were analyzed in qPCR assay using the primers that amplified sGFP tagged to the *Fg*. The WT and *AtEIN2*-KO/*HvEIN2* inflorescences showed similar infection pattern where the amount of *Fg* within the inflorescence tissues increased rapidly and consistently starting from 1 dpi to 6 dpi while *AtEIN2*-KO had significantly lower *Fg* invasion compared to WT

at 1 dpi. Surprisingly, the fungal invasion increased sharply in KO plants by almost 45-54% at 2 dpi and remained consistently at the level of 11-20% lower than the WT and complemented line for the rest of the testing period. Despite the level of infection in *AtEIN2*-KO inflorescences was considerably high, the fungal invasion was still restricted starting 2-6 dpi. As expected, *AtEIN2*-KO/*HvEIN2* had a relatively similar trend compared to WT indicated the recovery of the gene function by *HvEIN2*.

Spore production on *Fg* inoculated inflorescences was quantitated by hemocytometer (Figure 3.6). The trend was relatively similar to that seen in the fungal quantitation assay by qPCR in that the spore production increased rapidly in WT and *AtEIN2*-KO/*HvEIN2* inflorescences starting from 3 dpi and 4 dpi respectively. Spores production was observed only when fungal colonization started to compromise plant defense (discussed below). Spore production in *AtEIN2*-KO inflorescences, however, showed an extreme restricted pattern. The spore count remained at a strikingly low level and spore production was completely inhibited despite the high level of fungal detection observed in Figure 3.5. These results, in summary, indicated that the mutation of *EIN2* gene suppressed *Fg* proliferation (i.e. reproduction or number of spores produced) but was ineffective for blocking *Fg* penetration. The complemented line, on the other hand, recovered the trend observed in WT for spore proliferation and that barley *HvEIN2* gene functions, showing similar behavior to *AtEIN2* (i.e. WT plants) during *Fg* infection.

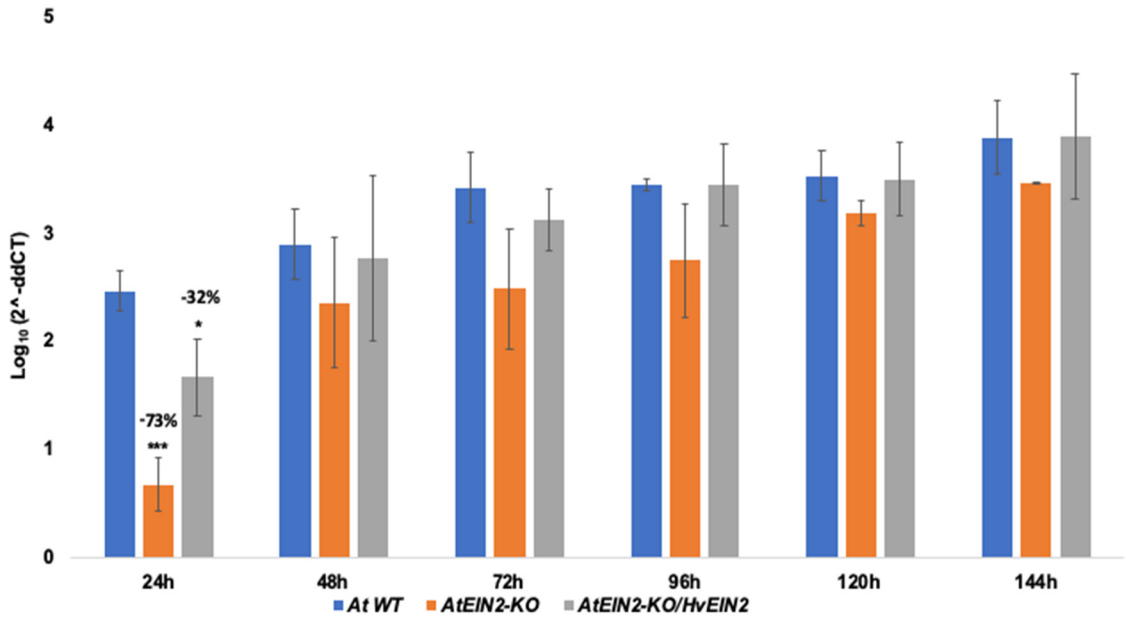


Figure 3.5. qPCR quantitative assay in measuring disease severity on *Fg* inoculated inflorescence. Experiment was repeated with three independent batch of samples. Statistical significance determined by *t*-test analysis followed by Holm-Sidak method, with alpha = 0.05. Each time point was analyzed individually, without assuming a consistent SD (p-value: * ≤ 0.05 ; ** ≤ 0.01 ; *** ≤ 0.001).

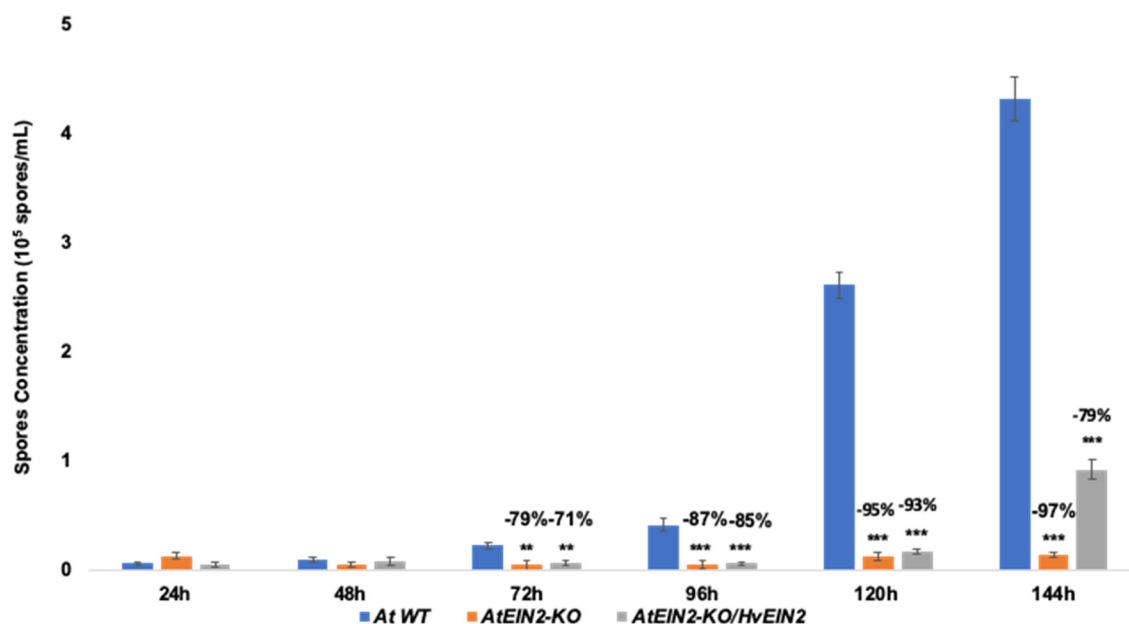


Figure 3.6. Quantitative assay of spore production on *Fg* inoculated inflorescence. The percentage of spore reduction was calculated for 72h, 96h, 120h and 144h. Experiment was repeated with three independent batch of samples. Statistical significance determined by *t*-test analysis followed by Holm-Sidak method, with alpha = 0.05. Each time point was analyzed individually, without assuming a consistent SD (p-value: * ≤ 0.05 ; ** ≤ 0.01 ; *** ≤ 0.001).

Gene expression profiling on plant defense signaling pathway-related genes

The expression of several plant defense signaling pathways [salicylic acid (SA), jasmonic acid (JA) and ethylene (ET)]-related genes in *AtEIN2-KO*, *AtEIN2-KO/HvEIN2* and WT was analyzed using RT-qPCR. Each sample group was point inoculated with sGFP-tagged *Fg* and collected at 3, 6, 12, 24, 48 hours after inoculation (hpi). Figure 3.7 illustrated the RT-qPCR analysis of plant defense-related genes relative expression involved in SA

signaling and JA/ET signaling. SA-related genes such as *NPR1*, *PR1*, *PR2* and *PR5* were upregulated in all three experimental groups except that *AtEIN2*-KO expressed in a much lower level compared to WT and the complemented line. All three groups displayed a similar trend at the initial stage of fungal invasion. SA-signaling pathway was first stimulated at 3 hpi and increase consistently at 24 hpi. The elevated level of SA-related genes expression in WT and complemented line can be related to the high amount of *Fg* detected in the host tissue at 24 hpi. The host system may have responded to the fungal invasion during the biotrophic stage by increasing the SA signal output to induce downstream regulator for resistance enhancement. Interestingly, *PR2* gene expression of *AtEIN2*-KO/*HvEIN2* and WT plants was induced during pathogen infection but no induction in KO plants. It was plausible that *ein2* mutation partially hindered or weakened its signaling with other defense genes. *AtEIN2*-KO plants displayed a suppressive pattern in the JA/ET related genes expression. Despite the lower level of expression on ET signaling-related genes, *AtEIN2*-KO showed resistance to fungal invasion and minimal hyphae growth was observed. Gene expression level of *PR3* and *PDF1.2* genes were recovered by the complemented line and gene induction was seen at 6 hpi after pathogen infection which indicating the activation JA/ET signaling pathway for stopping any further assaults from pathogen. The truncated C-terminal of *AtEIN2*-KO could have caused the failure to induce defense-related genes at appropriate timing. Its exact mechanism of gaining resistance to *Fg* by compromising ET signaling pathway still remains elusive.

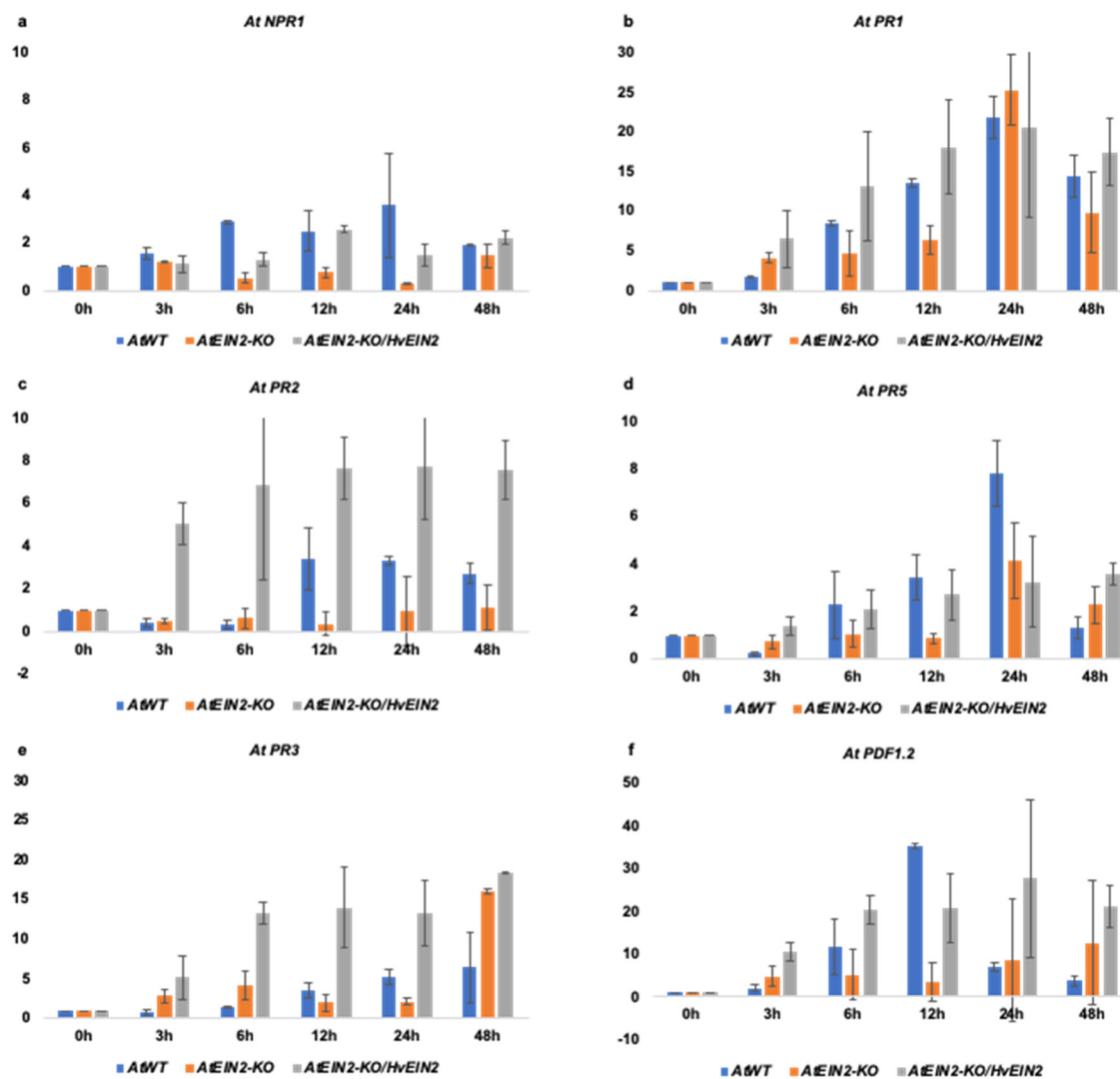


Figure 3.7. RT-qPCR analysis of plant defense-related genes relative expression. Relative expression profile includes genes involved in SA signaling (a-d) and JA/ET signaling (e-f). RT-qPCR assay was repeated three times with different batch of samples. The relative gene expression was calculated using the $2^{-\Delta\Delta Ct}$ formula.

Discussion

Fg infection has long been known to induce ET biosynthesis in monocot model plant, *Brachypodium* [31] and that manipulation of ET signaling in wheat, barley and *Arabidopsis* has shown enhanced resistance to *Fg* [14]. In this study, the CRISPR-edited *ein2* mutant carries a frameshift mutation at 3' end of the coding sequence which renders the premature termination of protein at the CEND. It is known that CEND which containing the NLS is essential for signal translocation to nuclear following to its proteolysis from the N-terminal upon ethylene perception [32]. Losing the CEND in the CRISPR-edited mutant implies the loss of this "cleave and shuttle" mode leading to the ethylene insensitivity and abolishment of ET signaling responses [7]. Even though the ET signaling pathway is crucial for halting necrotrophic attack, perception of *Fg* in the *ein2* mutant displayed enhanced resistance with very minimal disease symptoms. Interruption of ET signaling transduction blocks the disease progression as seen in Figure 3.4 in which KO inflorescences has little hyphae growth since 1 dpi as compared to WT and the complemented line. Both WT and the complemented line displayed a phenotype of severe colonization by *Fg* at 6 dpi. However, the qPCR quantitative assay for measuring the degree of disease severity in each sample group showed a rather puzzling yet interesting result. The fungal invasion (Figure 3.5) observed within the host floral tissue for KO plants was relatively lower (at least 50% less than the other two groups) by 1 dpi prior to a sharp increment in the amount of penetrated fungal pathogens. The *ein2* mutant was unable to block the entry of *Fg* into host tissue but it managed to inhibit the fungi from further spreading through spore proliferation. By observing the vigorous growth of *Fg* hyphae and wilting symptom in WT and complemented line, exploitation of ET signaling pathway by *Fg* is evident. Previous

studies also showed that the ethylene receptor *ETR1*, which is upstream of *EIN2* in ethylene perception, is required for *Fusarium oxysporum* pathogenicity [33]. Similarly, *Fg* requires the ET signaling for its pathogenesis and possibly suppresses host defense signal transduction to achieve effective colonization as seen in the spores quantitation assay in Figure 3.6. The *ein2* mutant had extremely low level of spores amount despite the elevated level of *Fg* detected within the host cell. ET signaling pathway must have serve as the shortcut for *Fg* to gain access to plant's resources for continuous grow and defeating the host defense. Some necrotrophic or hemibiotrophic pathogens produce toxins to gain access to host tissue and *Fg* is known to produce mycotoxin to kill host during its necrotrophic stage [34]. It is unclear that whether mycotoxin production could be induced by the presence of ethylene or another modulator is involved. A close relative of *Fg*, *Fusarium oxysporum* secretes necrosis and ethylene-inducing protein (NEP1) during its course of necrotrophic attack [35]. NEP1 is a member of the NEP1-like family of fungal proteins (NLPs) characterized as the elicitors of necrosis [36]. NLPs are a group of small conserved molecules that induce ROS and ET production as well as hypersensitive response (HR)-like cell death [37]. NEP1 protein, as observed in *Fusarium oxysporum* (*Fo*), elicits a cascade of plant response in transcript regulation related to cell death and promote the ethylene production [38, 39]. Since ethylene is one of the key components for modulating cell death and defense response in the plants, it is believed that the induction of ET biosynthesis could accelerate cell death upon pathogen attack and make the cell contents available for exploitation [40]. We were able to locate the potential *Fg* NEP1 domain in chromosome 2 and 3 after comparing *Fg* complete genome sequence against NEP1 gene sequence in *Fo* (GenBank accession number AF036580.1). Therefore, *Fg* is

very likely to have produced a molecule similar to NEP1 to control the ET production and elicit the HR-like cell death response. This speculation could explain the results in our study that WT and the complemented line which have a functional *EIN2* gene are more favorable for invasion and colonization as seen in intense hyphae growth and immersive spore production whereas KO plants deficit in ET signaling transduction are able to halt the further attack by *Fg*. Nonetheless, this speculation may need to be further investigated.

The gene expression profiling on plant defense-related genes (Figure 3.7) provides another perspective on understanding plant response during the fungal infection. Figures 3.7a to 3.7d depict pathogenesis-related genes (PRs) induced by SA and Figures 3.7e to 3.7f depict *PR3* and *PDF1.2* genes induced by JA/ET signaling. All three experimental groups (WT, *AtEIN2*-KO and *AtEIN2*-KO/*HvEIN2*) displayed a similar trend in SA signaling induction during the first contact with *Fg* except that KO plants expressed *PR2* and *PR5* in a much lower level. However, the downregulated gene expression of ET-related genes in *ein2* mutant is consistent with our analysis that interruption in CEND causes the loss of nuclear localized ET signal transduction and that phenotype is recovered in the complemented line with a functional barley *EIN2* gene. Interestingly, resistance to *Fg* is achieved with a underperforming ET signaling pathway. Apart from the possibility of ET induction by fungal elicitor, the loss-of-function *ein2* mutant could have influenced the production and accumulation of certain metabolites which pose inhibitory effect on *Fg* growth or perhaps lethal to *Fg*. A study on the role of barley flavonoids in conferring resistance to *Fg* showed that a nonsense mutation in the *DFR* gene (*dihydroflavonol reductase*), one of the flavonoid synthase genes, leads to the accumulation of a small amount of dihydroquercetin which is a

strong inhibitor of *Fg* growth [41]. However, *dfr* mutation results in developmental defects and makes it an unfavorable target for bioengineering of resistant cultivar. Similarly, *EIN2* is plausibly involved in some metabolic synthesis pathway and its dysfunction could result in metabolite accumulation [42]. A recent metabolomics study in maize discovered two maize metabolites, smilaside A and smiglaside C, that may contribute to improved disease resistance to *Fg* [43]. QTL mapping revealed that maize *EIN2* genes regulates the synthesis of these metabolites as ET production involves in fine-tuning the abundance of metabolites. Their *in vitro* assay revealed that diacetylated smilaside A caused greater inhibition in *Fg* growth than the triacetylated smiglaside C. Lower ET sensitivity inclines to drive the production ratio towards the smilaside A. In other words, *ein2* mutant can redirect the metabolite flux into synthesis of bioactive smilaside A and hence the increase of *Fg* resistance. Even though this study is done on maize, its striking discovery could shed light on *EIN2* gene function in regulating metabolite synthesis in some other important hosts.

The exact molecular mechanism used by *Fg* to hijack ET signaling transduction pathway remains largely unknown. Based on all the previous reports and our results, ET sensitivity is a key determinant in the progression of *Fg*. Additional investigations are needed to answer the exact mechanism on *Fg* infection *via* ET signaling cascade.

References

1. Hao, D., et al., *6 - Ethylene*, in *Hormone Metabolism and Signaling in Plants*, J. Li, C. Li, and S.M. Smith, Editors. 2017, Academic Press. p. 203-241.

2. Liu, M., et al., *Ethylene Control of Fruit Ripening: Revisiting the Complex Network of Transcriptional Regulation*. *Plant Physiol*, 2015. **169**(4): p. 2380-90.
3. van Loon, L.C., B.P. Geraats, and H.J. Linthorst, *Ethylene as a modulator of disease resistance in plants*. *Trends Plant Sci*, 2006. **11**(4): p. 184-91.
4. Gao, Q.M., et al., *Signal regulators of systemic acquired resistance*. *Front Plant Sci*, 2015. **6**: p. 228.
5. Ryals, J.A., et al., *Systemic Acquired Resistance*. *Plant Cell*, 1996. **8**(10): p. 1809-1819.
6. Bisson, M.M., et al., *EIN2, the central regulator of ethylene signalling, is localized at the ER membrane where it interacts with the ethylene receptor ETR1*. *Biochem J*, 2009. **424**(1): p. 1-6.
7. Li, W., et al., *EIN2-directed translational regulation of ethylene signaling in Arabidopsis*. *Cell*, 2015. **163**(3): p. 670-83.
8. Merchante, C., et al., *Gene-specific translation regulation mediated by the hormone-signaling molecule EIN2*. *Cell*, 2015. **163**(3): p. 684-97.
9. Alonso, J.M., et al., *EIN2, a bifunctional transducer of ethylene and stress responses in Arabidopsis*. *Science*, 1999. **284**(5423): p. 2148-52.
10. Wen, X., et al., *Activation of ethylene signaling is mediated by nuclear translocation of the cleaved EIN2 carboxyl terminus*. *Cell Research*, 2012. **22**: p. 1613.
11. An, F., et al., *Ethylene-induced stabilization of ETHYLENE INSENSITIVE3 and EIN3-LIKE1 is mediated by proteasomal degradation of EIN3 binding F-box 1 and 2 that requires EIN2 in Arabidopsis*. *Plant Cell*, 2010. **22**(7): p. 2384-401.
12. Ji, Y. and H. Guo, *From endoplasmic reticulum (ER) to nucleus: EIN2 bridges the gap in ethylene signaling*. *Mol Plant*, 2013. **6**(1): p. 11-4.
13. Di, X., J. Gomila, and F.L.W. Takken, *Involvement of salicylic acid, ethylene and jasmonic acid signalling pathways in the susceptibility of tomato to Fusarium oxysporum*. *Mol Plant Pathol*, 2017. **18**(7): p. 1024-1035.
14. Chen, X., et al., *Fusarium graminearum exploits ethylene signalling to colonize dicotyledonous and monocotyledonous plants*. *New Phytol*, 2009. **182**(4): p. 975-83.
15. Han, X. and R. Kahmann, *Manipulation of Phytohormone Pathways by Effectors of Filamentous Plant Pathogens*. *Front Plant Sci*, 2019. **10**: p. 822.
16. Fukuoka, S., et al., *Loss of function of a proline-containing protein confers durable disease resistance in rice*. *Science*, 2009. **325**(5943): p. 998-1001.
17. Shi, G., et al., *The hijacking of a receptor kinase-driven pathway by a wheat fungal pathogen leads to disease*. *Sci Adv*, 2016. **2**(10): p. e1600822.
18. Wang, Y., et al., *Simultaneous editing of three homoeoalleles in hexaploid bread wheat confers heritable resistance to powdery mildew*. *Nat Biotechnol*, 2014. **32**(9): p. 947-51.
19. Faris, J.D., et al., *A unique wheat disease resistance-like gene governs effector-triggered susceptibility to necrotrophic pathogens*. *Proc Natl Acad Sci U S A*, 2010. **107**(30): p. 13544-9.
20. Rawat, N., et al., *Wheat Fhb1 encodes a chimeric lectin with agglutinin domains and a pore-forming toxin-like domain conferring resistance to Fusarium head blight*. *Nat Genet*, 2016. **48**(12): p. 1576-1580.

21. Brewer, H.C., N.D. Hawkins, and K.E. Hammond-KOsack, *Mutations in the Arabidopsis homoserine kinase gene DMRI confer enhanced resistance to Fusarium culmorum and F. graminearum*. BMC Plant Biol, 2014. **14**: p. 317.
22. Su, Z., et al., *A deletion mutation in TaHRC confers Fhb1 resistance to Fusarium head blight in wheat*. Nat Genet, 2019. **51**(7): p. 1099-1105.
23. Feng, Z., et al., *Efficient genome editing in plants using a CRISPR/Cas system*. Cell Res, 2013. **23**(10): p. 1229-32.
24. Zhang, X., et al., *Agrobacterium-mediated transformation of Arabidopsis thaliana using the floral dip method*. Nat Protoc, 2006. **1**(2): p. 641-6.
25. Livak, K.J. and T.D. Schmittgen, *Analysis of relative gene expression data using real-time quantitative PCR and the 2(-Delta Delta C(T)) Method*. Methods, 2001. **25**(4): p. 402-8.
26. Mittler, R., V. Shulaev, and E. Lam, *Coordinated Activation of Programmed Cell Death and Defense Mechanisms in Transgenic Tobacco Plants Expressing a Bacterial Proton Pump*. The Plant Cell, 1995. **7**: p. 29-42.
27. Miller, S.S., et al., *Use of a Fusarium graminearum strain transformed with green fluorescent protein to study infection in wheat (Triticum aestivum)*. Canadian Journal of Plant Pathology, 2004. **26**(4): p. 453-463.
28. Nalam, V., S. Sarowar, and J. Shah, *Establishment of a Fusarium graminearum Infection Model in Arabidopsis thaliana Leaves and Floral Tissues*. Bio-protocol, 2016. **6**(14): p. e1877.
29. Peng, C., et al., *High-throughput detection and screening of plants modified by gene editing using quantitative real-time polymerase chain reaction*. The Plant Journal, 2018. **95**(3): p. 557-567.
30. Mascher, M., et al., *A chromosome conformation capture ordered sequence of the barley genome*. Nature, 2017. **544**(7651): p. 427-433.
31. Pasquet, J.C., et al., *Differential gene expression and metabolomic analyses of Brachypodium distachyon infected by deoxynivalenol producing and non-producing strains of Fusarium graminearum*. BMC Genomics, 2014. **15**: p. 629.
32. Qiao, H., et al., *Processing and subcellular trafficking of ER-tethered EIN2 control response to ethylene gas*. Science, 2012. **338**(6105): p. 390-3.
33. Pantelides, I.S., et al., *The ethylene receptor ETR1 is required for Fusarium oxysporum pathogenicity*. 2013. **62**(6): p. 1302-1309.
34. Laluk, K. and T. Mengiste, *Necrotroph attacks on plants: wanton destruction or covert extortion?* The arabidopsis book, 2010. **8**: p. e0136-e0136.
35. Pemberton, C.L. and G.P. Salmond, *The Nep1-like proteins-a growing family of microbial elicitors of plant necrosis*. Mol Plant Pathol, 2004. **5**(4): p. 353-9.
36. Gijzen, M. and T. Nurnberger, *Nep1-like proteins from plant pathogens: recruitment and diversification of the NPP1 domain across taxa*. Phytochemistry, 2006. **67**(16): p. 1800-7.
37. Oome, S. and G. Van den Ackerveken, *Comparative and functional analysis of the widely occurring family of Nep1-like proteins*. Mol Plant Microbe Interact, 2014. **27**(10): p. 1081-94.
38. Bae, H., et al., *Necrosis- and Ethylene-Inducing Peptide from Fusarium oxysporum & Induces a Complex Cascade of Transcripts Associated with Signal Transduction and Cell Death in Arabidopsis*. Plant Physiology, 2006. **141**(3): p. 1056.

39. de Sain, M. and M. Rep, *The Role of Pathogen-Secreted Proteins in Fungal Vascular Wilt Diseases*. International journal of molecular sciences, 2015. **16**(10): p. 23970-23993.
40. Bouchez, O., et al., *Ethylene Is One of the Key Elements for Cell Death and Defense Response Control in the Arabidopsis Lesion Mimic Mutant vad1*. Plant physiology, 2007. **145**: p. 465-77.
41. Skadhauge, B., K.K. Thomsen, and D. Von Wettstein, *The Role of the Barley Testa Layer and its Flavonoid Content in Resistance to Fusarium Infections*. Hereditas, 1997. **126**(2): p. 147-160.
42. Kumar, D., et al., *Transcriptome analysis of Arabidopsis mutants suggests a crosstalk between ABA, ethylene and GSH against combined cold and osmotic stress*. Scientific Reports, 2016. **6**: p. 36867.
43. Zhou, S., et al., *Ethylene signaling regulates natural variation in the abundance of antifungal acetylated diferuloylsucroses and Fusarium graminearum resistance in maize seedling roots*. bioRxiv, 2018: p. 332056.

Chapter **4**

Overexpression of genistein in transgenic Moneymaker tomato and its anti-Alzheimer's effect on amyloid β -expressing *C. elegans*

Chapter 4

Overexpression of genistein in transgenic MoneyMaker tomato and its anti-Alzheimer's effect on amyloid β -expressing *C. elegans*

Introduction

Genistein is a major isoflavones in legumes, and especially abundant in soybeans. It is also called a phytoestrogen due to the resemblance of its chemical structure with the estrogen estradiol-17 β . This allows genistein to bind to estrogen receptors [1]. These phytoestrogenic features and antioxidant properties have made genistein a promising medicinal compound that can contribute to anti-inflammatory, anticarcinogenic, anti-neurodegenerative, anti-osteoporosis and hypocholesterolemic effects [2]. Genistein is well studied for its function in cancer and neurodegenerative diseases as well as women's health. Genistein is widely available as supplement besides being available in soy-based foods. Genistein has been shown to be beneficial in helping post-menopausal women who are deficient in estrogen to prevent osteoporosis and alleviate post-menopausal symptoms [3]. Apart from women health and wellness, genistein also serves as a promising chemopreventive agent for different metabolic diseases especially cancer, diabetes and obesity. Studies have shown that genistein exerts its protective effects by interfering with the inflammatory system and in the endocrine signaling pathway [4].

Neurodegenerative diseases such as Alzheimer's disease and dementia are irreversible and progressive brain disorder that currently have no cure available. Two hallmark pathological factors for the Alzheimer's disease development are the production and accumulation of amyloid β ($A\beta$) peptide and the tangles of tau protein. Studies reveal that excessive accumulation of $A\beta$ aggregates can induce neuronal inflammation and oxidative stress which eventually leads to neuronal cell death [5]. Genistein has been studied for a long time for its protective effect in neurodegenerative disorders. It has been demonstrated that genistein regulates the inflammatory pathway through nuclear factor $NF\kappa B$ by suppressing nuclear factor activation and preventing cell apoptosis leading to protection of neuron cell [6, 7]. Moreover, estrogen receptor β , genistein's binding target, is abundantly expressed in brain tissue and it contributes to estrogen-induced protective effects such as modulating the calcium ion and antiapoptotic protein signaling pathway [5, 8] and up-regulating the expression of insulin-degrading enzyme (IDE) to drive the degradation process of $A\beta$ [9, 10]. The cognitive benefits of genistein have made it an attractive and promising medicinal compound in treating and preventing neurodegenerative diseases. These properties suggest that genistein may be a useful and health-promoting addition to our daily diet.

Soy products are not a major part of the western diet. To benefit from its health-promoting effects either soy or soy-derived products need to be incorporated into the diet. Even though the demand for soy-based foods has increased in Western countries due to the increasing number of people on vegan diet [11], it is still far from reaching the amount of soy that eastern society consumes daily. Metabolic engineering opens up the possibility to express different health-promoting compounds in other common plant hosts. The notion of

introducing genistein and other nutrients into more widely consumed crops, such as tomato [12, 13], brassica [14] and rice [15], has created interest among researchers. Tomato is rich in lycopene, β -carotene and other antioxidant compounds [16]. In 100 g of raw and ripening tomato, there are 2,573 mg of lycopene and 449 mg of β -carotene [17]. Lycopene contributes an inhibitory effect on neurodegenerative disorders by preventing oxidative stress-mediated neuron cell death [17]. Generating genistein in tomato would complement the properties of lycopene by providing additional anti-neurodegenerative phytonutrients in this commonly consumed fruit [18].

The aim of this study is to utilize biotechnology tools to engineer the tomato cultivar Moneymaker to produce genistein. Transgenic tomato has been engineered to express the isoflavone synthase gene, but the resulting genistein level was not highly expressed such that the highest expresser contained only 0.451 nM/g of genistein in tomato fruit peel [12]. In order to achieve a higher yield of genistein, more than one of the enzymes involved in isoflavone synthesis pathway have to be engineered into tomato genome. Two vectors were constructed to test this strategy.

Another objective of this project is to test the combinatory health-promoting effect of genistein with lycopene and other antioxidant compounds in neurodegenerative diseases using the *C. elegans* system. Based on the functions of genistein, we hypothesize that the combination of genistein and lycopene might have a greater potential for delaying Alzheimer's disease progression and reducing neuronal damage.

Methods and materials

Plasmid construction of *isoflavone synthase (IFS)* and *chalcone isomerase (CHI)* gene transformation vectors

The pIFS/CHI plasmid vector containing both the alfalfa (*Medicago sativa*) *IFS* and *CHI* genes under the control of separate constitutive 35S promoters of *Cauliflower mosaic virus (CaMV)* was kindly provided by Dr. Richard A. Dickson from University of North Texas. The pIFS vector was constructed with soybean *IFS* gene under the control of tomato fruit-specific tomato *E8* promoter. The soybean (*Glycine max*) *IFS* mRNA sequence was obtained from NCBI database with accession number of FJ770473.1. A fragment of 1566 bp *IFS* coding sequence was cloned from soybean cv. Jack with primers (forward: 5'-ATGCTGCTTGAAGTTGC -3'; reverse: 5'-AGAAAGGAGTTTAGATGC -3'). The *E8* promoter sequence was obtained from NCBI (accession number KJ561284.1) and its 2.2 kbp fragment was cloned from tomato fruit sample. Both *E8* promoter and *IFS* gene sequences were ligated into pBIN19 vector (GenBank ID: U09365.1) and recorded as pIFS. Both pIFS/CHI and pIFS vectors were transformed into *Agrobacterium* LBA4404 strain. Protein sequence alignment of *IFS* and *CHI* genes between alfalfa and soybean was performed using web-based pairwise global alignment tool (EMBOSS Needle program based on the Needleman-Wunsch algorithm).

Tomato seedling growth for *Agrobacterium tumefaciens* transformation

Tomato cv. Moneymaker WT seeds were purchased through NextHarvest.com. 30-50 seeds were sterilized with 30% bleach for 30 minutes and rinsed with sterile water for five times. Sterilized seeds were plated on growth medium [Murashige and Skoog (MS) medium containing 3% (w/v) sucrose and 0.3% (w/v) Gelzan™ agar adjusted to pH 5.8] contained in Magenta box and stratified at 4 °C for two days before switching to 22 °C under 16h/8h light-dark photoperiod. The seedlings were collected after 7-10 days post germination. A day prior to collection, *Agrobacterium* LBA4404 strain that harbored both pIFS/CHI and pIFS transformation vectors were grown separately in LB medium for 16 hours. Upon plant tissue collection, the cotyledons were sliced into two pieces along the main vein region and hypocotyls were cut immediately into 5 mm per piece and incubated with overnight grown *Agrobacterium* culture containing 50 µM of acetosyringone (Sigma-Aldrich, St. Louis, MO, USA) for 15 minutes. The hypocotyls and cotyledons were then transferred to co-cultivation medium [Murashige and Skoog (MS) medium containing 3% (w/v) sucrose, 50 µM/L acetosyringone and 0.3% (w/v) Gelzan™ agar adjusted to pH 5.8] for 2 days at 24 °C in the dark. Prior to antibiotic selection, hypocotyls and cotyledons were first transferred to recovery medium [Murashige and Skoog (MS) medium containing 3% (w/v) sucrose, 1 mg/L BAP, 0.1 mg/L NAA and 0.3% (w/v) Gelzan™ agar adjusted to pH 5.8. and 300 µg/L cefotaxime] for a week in order to kill *Agrobacterium*.

Generation of transgenic tomatoes *via* tissue culture selection

The recovered and cleaned hypocotyls and cotyledons tissues were transferred to shoot selection medium [Murashige and Skoog (MS) medium containing 3% (w/v) sucrose, 1 mg/L BAP, 0.5 mg/L Zeatin and 0.3% (w/v) Gelzan™ agar adjusted to pH 5.8, and 200 µg/L kanamycin] for 4-6 weeks. Regenerated shoots that were 1 cm tall were transferred to root induction medium [Murashige and Skoog (MS) medium containing 3% (w/v) sucrose, 2 mg/L IBA and 0.3% (w/v) Gelzan™ agar adjusted to pH 5.8, and 100 µg/L kanamycin] for 1-2 weeks until the root growth was observed. Shoots with substantial root growth were transferred to Pro-Mix soil and acclimated for 2 days in an environmental-controlled chamber with a 16h/8h light-dark photoperiod at 22 °C and 40%-60% relative humidity. The putative transgenic plants from antibiotic selection were grown for another 1-2 weeks prior to leaf sample collection.

Transgenic line confirmation and homozygous line segregation

100 mg samples of leaf tissue were collected from each regenerated tomato plantlets. Genomic DNA (gDNA) from each putative transgenic line was isolated using CTAB extraction buffer (2% cetyl trimethylammonium bromide, 1% polyvinyl pyrrolidone, 100 mM Tris-HCl, 1.4 M NaCl, 20 mM EDTA and 1% β-mercaptoethanol). The CTAB-leaf tissue mix was vortexed vigorously for 30s and then incubated at 65 °C for 1 hour followed by phenol/chloroform extraction. The supernatant was then mixed with 100% ethanol to precipitate the DNA followed by a clean-up step with 70% ethanol. The DNA pellets were air-dried and resuspended with sterile deionized water. The concentration of DNA was measured with a Nanodrop spectrophotometer (Thermo Fisher, Waltham, MA, United

States). 100 ng of gDNA from each putative transgenic line was used in PCR amplification for transgene integration confirmation. Primers amplifying alfalfa *IFS* gene (forward: 5'-ATGTTGCTTGAAGCTTGCACTTGG -3'; reverse: 5'-GGAGTTTAGATGCAACGCCG -3') were used to identify true pIFS/CHI T₀ transformants whereas the primers used for cloning soybean *IFS* gene was used to confirm pIFS T₀ transformants. Transformation efficiency was measured as percentage of explants in which transgenes were detected. Confirmed T₀ transformants for pIFS/CHI and pIFS were grown so that T₁ seeds could be harvested. T₁ plants from each transformant were segregated by germinating the T₁ seeds on growth medium containing 100 µg/L kanamycin antibiotic. Seeds from individual T₁ plants were harvested and screened by 100 µg/L kanamycin again to identify the homozygous T₂ lines. T₂ transgenic plants were grown for about 4 months until fruits were at the red ripe stage, at which time fruit flesh and peel samples were collected.

Quantitation of gene expression of *IFS* and *CHI* genes in homozygous tomato fruit peel and flesh

Fruit peel and flesh tissues from each homozygous transgenic line were separated using a scalpel. All the flesh tissues were scraped off from the peel layer prior to total RNA isolation. 100 mg of peel and flesh tissues from each transgenic line were collected separately in 1.5 mL tube. Total RNA from peel and flesh samples were isolated using TRIZOL method (Ambion Life Technologies, Thermo Fisher, Carlsbad, CA, United States) and the concentration was measured using the a Nanodrop spectrophotometer (Thermo Fisher, Waltham, MA, United States). Reverse transcription (RT) reaction was performed

using the High Fidelity cDNA Synthesis Kit (Applied Biosystems, Thermo Fisher, Foster City, CA, United States) with approximately 2 μ g of total RNA. The RT products were used in RT-qPCR reactions with the SYBR 2X Master Mix (Applied Biosystems, Thermo Fisher, Foster City, CA, United States). Three sets of 5 μ M RT-qPCR primers were used in this reaction: *IFS* (forward: 5'- CCGAGGAGCTTCTGAAATGG -3' and reverse: 5'- TCGCCGAGCATCATCATG -3'), *CHI* (forward: 5'- GCACGCTGTTTCCCCTGAT -3' and reverse: 5'-CGTTCAACAACGCAGGTAATCTT -3') and tomato β -tubulin as the housekeeping gene (forward: 5'- CCCACCAACTGGGCTGAA -3' and reverse: 5'- CCTGAATGGAGGTTGAATTTCC -3'). The RT-qPCR assay was run on the default setting at 95 °C for 3 minutes for initial denaturation and 40 cycles at 95 °C for 30 s followed by 60 °C for 30 s. The fold-change of gene expression was calculated by the $2^{-\Delta\Delta C_t}$ method [19]. The RT-qPCR analysis was repeated three times with independent set of samples, and the gene expression levels were averaged with standard deviation .

Lyophilization of transgenic fruit peel and flesh tissues

The remaining peel and flesh tissues were pooled into 50 mL tube and their wet weights were measured and recorded. Peel samples were grounded into powder with liquid nitrogen prior to freeze-drying procedure. All peel and flesh samples were then lyophilized using the Labconco Freezone 2.5L Freeze Dry System which was run on Automode with vacuum set point between 0.22 to 0.01. Samples were left overnight for freeze-drying and were collected the next day when the samples dried completely. The lyophilized flesh samples

were grounded into fine powder for extraction. Samples dry weights were measured and recorded.

Extraction and analysis of isoflavones in transgenic tomato

Approximately 0.2 g of each lyophilized sample was accurately weighed in a 15 mL centrifugal tube and 10 mL 70% methanol was added for extraction of isoflavones. Sample tubes were wrapped with aluminum foil and shaken for 2 hours. Samples were then centrifuged at 14,000 g for 10 minutes and loaded on to the UPLC-QqQ-MS/MS system for analysis. Analyses of isoflavones were carried out on an Agilent 1290 Infinity II UPLC system interfaced with an Agilent 6470 triple quadrupole mass spectrophotometer (QqQ-MS/MS) with an electrospray ionization (ESI) source (Agilent Technology, Palo Alto, CA, USA). Chromatographic separation was achieved with a Waters Acquity UPLC BEH C18 column (2.1 × 50 mm, 1.7 μm) (Milford, Massachusetts, USA) equipped with a Waters VanGuard Acquity C18 guard column (2.1 × 5 mm, 1.7 μm). The binary mobile phase system consisted of phase A (0.1% acetic acid in water) and phase B (0.1% acetic acid in ACN) and the flow rate was set at 0.45 mL/min. The LC gradient program for each run started at 12% (B%), followed by 25% at 3.5 min, 65% at 4.5 min, held for 0.5 min before returning to initial conditions. The column was equilibrated for 2.5 min before the next injection. Thermostats of the column and the autosampler were set at 30°C and 4°C, respectively. Injection volume was 5 μL for all standard solutions and sample extracts. Mass spectral data acquisition was achieved using dynamic multiple reaction monitoring (dMRM) with positive polarity. Two specific transitions for each analyte were monitored

over a period of 1 min centered around retention time. The ESI parameters were set as follows: dry gas at 300 °C with a flow rate of 12.0 L/min, sheath gas at 250 °C with a flow rate of 12.0 L/min, nebulizer at 30 psi, nozzle voltage at 1.5 kV and capillary voltage at 3.0 kV. Identification and confirmation of target compounds were achieved by comparing their MRM precursor-product ion pair transitions (daidzein, 255.1→199.0/137.0; daidzin, 417.1→255.0/199.0; genistein, 271.1→153.0/91.1; genistin, 433.1→271.0/152.9) and the retention time of authentic standards. Quantitation was achieved with calibration curves established using the peak area of quantifier ion of the analyte.

***C. elegans* strain and maintenance**

The CL2355 strain [*smg-1*^{ts} (*snb-1*:: A β ₁₋₄₂::3' UTR(long) + *mtl-2*::GFP)] was obtained from Caenorhabditis Genetics Center (CGC) (University of Minnesota, Minneapolis, MN). This strain employs the promoter of the *C. elegans* synaptobrevin ortholog (*snb-1*) to drive pan-neuronal expression of human A β ₁₋₄₂ peptide which is inducible by temperature upshift (16 °C to 23 °C) and marked with green fluorescent protein that expresses constitutively within the intestinal region. The worms were propagated at 16 °C on solid nematode growth medium (NGM) [0.25% (w/v) peptone, 0.3% (w/v) sodium chloride and 1.9% (w/v) agar with post-autoclaving addition of 5 mg/L cholesterol, 1 mL of 1 M CaCl₂, 1 mL of 1 M MgSO₄, and 25 mL of 1 M KPO₄, pH 6.0]. All 35 x 10 mm NGM plates were seeded with 50 μ l of *E.coli* OP50.

Serotonin (5-HT) sensitivity assay in transgenic *C. elegans*

Transgenic worms (CL2355) were egg-synchronized onto 35 x 10 mm petri dishes containing the crude extracts from selected transgenic tomato fruit peel (IFS/CHI 9-7, IFS/CHI 7-3, IFS 10-4 and WT) and pure genistein extract (Sigma-Aldrich, St. Louis, MO, USA) in different concentrations of 100 μ M, 10 μ M, 1 μ M, 0.1 μ M and 0.0355 μ M including two control sets (CK and CK+DMSO), one of which containing 0.6% of DMSO. The synchronized worms were fed on different treatment plates and allowed to grow at 16 °C until L3 stage (approximately 4-5 days after egg synchronization). After the synchronized worms reached the L3 stage, the temperature was upshifted to 23 °C to induce the A β ₁₋₄₂ expression for 36 hours. Worms were harvested at the end of 36 hours from different treatment plates and washed twice with M9 buffer to remove all the bacteria residual. Thirty worms from each treatment were transferred to 96-well assay plate and mixed with 10 mg/ml serotonin (creatinine sulfate salt) (Sigma-Aldrich, St. Louis, MO, USA). Worms were scored for paralysis phenotype every minute until all worms were completely paralyzed (non-motile for 5 s). Three independent experiments were performed. The mean and standard deviation of the data were calculated.

Quantitative fluorescence staining of A β aggregates with thioflavin-T

Synchronized CL2355 worms were collected from each treatment plate post temperature upshift from 16 °C to 23 °C for 36 hours. All collected worms were washed twice with 1 mL of 1x PBS (diluted from 10x PBS) (Fisher Scientific, Hampton, NH, USA) to remove any bacteria residual. The worms were spun down at 1000 rpm for 2 min and 100 μ l of 1x

PBS were added in each sample prior to sonification. Each worm sample was sonicated with Branson Sonifier 150 at setting 2 for 15 s and 45 s on ice for a total of 4 times. The sonicated worms were centrifuged at 14,000 rpm for 2 minutes and the supernatant was transferred to a new tube. The concentration of total soluble protein in each sample was measured using a Nanodrop spectrophotometer (Thermo Fisher, Waltham, MA, United States). Equal amount of total protein from each sample was mixed with 10 μ l of 10x PBS and 20 μ M of thioflavin-T (Sigma-Aldrich, St. Louis, MO, USA) in a final volume of 100 μ l. Fluorescence signal from the binding of thioflavin-T dye with A β aggregates was measured using Biotek Synergy 4 Plate Reader with excitation at 440 nm and emission at 482 nm. Three independent experiments were repeated, readings were averaged and standard deviations were calculated.

Results

Construction of pIFS/CHI and pIFS plasmid vectors for the expression of *IFS* and *CHI* genes

Two vectors were designed to express the *IFS* and *CHI* genes to produce a significant level of genistein in Moneymaker tomato. The pIFS/CHI vector was obtained from Dr. Richard A. Dixon (University of North Texas). It was tailored to co-express the alfalfa *IFS* and *CHI* genes under the control of the 35S promoter which were cloned into a single T-DNA cassette. A previous study has shown that tomato transformed with a vector expressing the

soybean *IFS* gene driven by 35S promoter was unable to generate a significant amount of genistein in fruit tissues [12]. Another strategy was to use the pIFS vector to express only the soybean *IFS* gene driven by the tomato fruit-specific *E8* promoter with the expectation that *IFS* gene can only be expressed in fruit tissues and the production of genistein can be concentrated in the fruit tissues. Figure 4.1 shows a schematic representation of transgenes and promoters used in this study.



Figure 4.1. Illustration of the plasmid vectors used for tomato transformation. pIFS/CHI vector was designed to co-express the alfalfa *IFS* and *CHI* gene under the control of 35S promoter whereas the pIFS vector was designed to only express the soybean *IFS* gene under the control of tomato fruit-specific *E8* promoter.

Both alfalfa and soybean belong to the legume family Fabaceae under the subfamily of Papilionoideae. They are predicted to be very closely related based on the molecular analyses of their phylogenetic relationships in the Fabaceae evolutionary study [20, 21]. In order to confirm the conservation of functional domain in *IFS* and *CHI* genes from both alfalfa and soybean, their protein sequences were compared to determine their sequence similarity. Both the cloned alfalfa *IFS* and *CHI* genes were sequenced from pIFS/CHI vector and compared to soybean reference sequences. In Figure 4.2a, the *IFS* gene

sequence alignment showed that both sequences were highly conserved with 96% identity and 98% similarity while *CHI* gene (Figure 4.2b) sequence alignment showed that the sequences were conserved with 79% identity and 88% in similarity. Despite the 2% and 12% dissimilarity in *IFS* and *CHI* sequences respectively, the cytochrome p450 domain (accession number COG2124) within the p450 superfamily (accession number cl12078) was conserved in both alfalfa and soybean *IFS* gene sequences with the interval of 33 to 477 a.a and chalcone-flavanone isomerase domain (accession number pfam02431) within the chalcone_3 superfamily (accession number cl03589) was conserved in both alfalfa and soybean *CHI* gene sequences with the interval of 10 to 212 a.a. The presence of conserved domains within alfalfa and soybean *IFS* and *CHI* genes indicated that their biochemical properties were conserved.

a

		IFS gene		
Medicago	1	MLELALGLLVLALFLHLRPTPTAKSKALRHLNPPSPKRLPFIHGLHL	50	
Glycine	1	MLELALGLFVLALFLHLRPTPSAKSKALRHLNPPSPKRLPFIHGLHL	50	
Medicago	51	LKDKLLHYALIDLKSKHGPLFSLYFGSMPTVVASTPELFLQTHEATS	100	
Glycine	51	LKDKLLHYALIDLKSKHGPLFSLSFGSMPTVVASTPELFLQTHEATS	100	
Medicago	101	FNTRFQTSAIRRLTYDSSVAMVPPGYPWKFVRKLIIMNDLLNATTVNKLRP	150	
Glycine	101	FNTRFQTSAIRRLTYDNSVAMVPPGYPWKFVRKLIIMNDLLNATTVNKLRP	150	
Medicago	151	LRTQIRKFLRVMAQGAEAQKPLDLTEELLKWTNSTISMMLGEAEIIRD	200	
Glycine	151	LRTQIRKFLRVMAQSAEAQKPLDVTTEELLKWTNSTISMMLGEAEIIRD	200	
Medicago	201	IAREVLKIFGEYSLTDFIWPLKHLKVGKYEKRIDDILNKFPVVERVIK	250	
Glycine	201	IAREVLKIFGEYSLTDFIWPLKYLKVGKYEKRIDDILNKFPVVERVIK	250	
Medicago	251	RREIVRRRNKGEVVEGEVSGVFLDTLLEFAEDETMEIKITKDHIKGLVVD	300	
Glycine	251	RREIVRRRNKGEVVEGEASGVFLDTLLEFAEDETMEIKITKEQIKGLVVD	300	
Medicago	301	FFSAGTDSSTAVATEWALAEELNNPKVLEKAREEVYSVVGKDRLVDEVDTQ	350	
Glycine	301	FFSAGTDSSTAVATEWALAEELNNPRVLQKAREEVYSVVGKDRLVDEVDTQ	350	
Medicago	351	NLPYIRAIKGTFRMHPPLPVVRRKCTEECEINGYVIPEGALIFNVWQV	400	
Glycine	351	NLPYIRAIKGTFRMHPPLPVVRRKCTEECEINGYVIPEGALVLFNVWQV	400	
Medicago	401	GRDPKYWRPSEFRFRERFLETGAEGEAGPLDIRGQHFQLLPNGSGRRMCP	450	
Glycine	401	GRDPKYWRPSEFRPERFLETGAEGEAGPLDLRGQHFQLLPFGSGRRMCP	450	
Medicago	451	GVNGATSGMATLLASLIQWFDVQVLGPOQQILKGGDAKVSMEERAGLTVP	500	
Glycine	451	GVNLATSGMATLLASLIQCPDLQVLGPOQQILKGGDAKVSMEERAGLTVP	500	
Medicago	501	RAHSLVCVPLARIGVASKLLS	521	
Glycine	501	RAHSLVCVPLARIGVASKLLS	521	

b

		CHI gene		
Medicago	1	MAASITAITVENLEYPAVVTSPVTGKSYFLGGAGERGLTIEGNFIKFTAI	50	
Glycine	1	-MATISAVQVEFLEFPVVTSPASGKTYFLGGAGERGLTIEGKFIKFTGI	49	
Medicago	51	GVYLEDIAVASLAAKWKGSSEELLETDFYRDIISGPPEKLIRGSKIRE	100	
Glycine	50	GVYLEDKAVPSLAAKWKGTSEELVHTLHFYRDIISGPPEKLIRGSKILP	99	
Medicago	101	LSGPEYSRKVMENCVAHLKSVGTYGDAEAEAMQKFAEAFKPNVFPFGASV	150	
Glycine	100	LGAEYSKVMENCVAHMKS VGTYGDAEAAAIEKFAEAFKPNVFPFGASV	149	
Medicago	151	FYRQSPDGILGLSFPDTSIPEKEAALIENKAVSSAVLETMIGEHAVSPD	200	
Glycine	150	FYRQSPDGILGLSFPSEDAT IPEKEAAVIENKAVSAVLETMIGEHAVSPD	199	
Medicago	201	LKRCLAARLPALLNEGAFKIGN	222	
Glycine	200	LKRSLASRLPAVLSHGIIV---	218	

Figure 4.2. (a) *IFS* and (b) *CHI* protein sequence alignment between alfalfa (*Medicago sativa*) and soybean (*Glycine max*). A | (vertical bar) indicates fully conserved residue. A : (colon) indicates conservation between residues of strongly similar properties with scoring > 0.5 in the Gonnet PAM 250 matrix. A . (period) indicates conservation between residues of weakly similar properties with scoring ≤ 0.5 in the Gonnet PAM 250 matrix.

Generation of homozygous transgenic tomato plants expressing both the pIFS/CHI and pIFS vectors

Organogenesis from explants is the common route used to generate transgenic plants due to there being a well-established protocol applied in a number of different plant systems such as tobacco, squash, potato, and tomato. This method is highly favored for its ease, high efficiency of transgene integration and lower risk of chimerism [22]. Genetic modification of tomato, especially for cultivar Micro-Tom, using this method has been reported to have a transformation efficiency ranging between 6 to 40%, yet some researchers still find it difficult to obtain sufficient true transformants for functional studies [23]. In order to maximize the transformation efficiency of tomato cultivar MoneyMaker in this study, multiple protocols were researched and few of them with higher transformation efficiency (30-40%) were referenced for adapting optimum conditions to transform the explants with the designed vectors [22-25]. Figure 4.3a-e showed the tissue culture stages of transformed tomato explants. Clipped hypocotyls produced calli at the cut region 20 days after *Agrobacterium* transformation (Figure 4.3a). The calli formed at the end of the hypocotyls were excised and transferred to shoot selection medium containing

kanamycin. At the shoot selection stage, calli were placed on a relatively high concentration of kanamycin (200 $\mu\text{g/L}$) to select for true transformants that maintained green and viable looking throughout the selection period (Figure 4.3b-c). Selected shoots were further selected at the rooting stage using root selection medium with 100 $\mu\text{g/L}$ kanamycin. The kanamycin-resistant transformants formed a dense root mat after 2 weeks (Figure 4.3d-e). Regenerated putative transgenic plants were transplanted to Pro-Mix soil and were confirmed by PCR. A total of 17 transgenic tomato plants carrying pIFS/CHI vector were regenerated from a total of 50 explants which account for about 34% of the transformation efficiency while 11 transgenic tomato plants carrying pIFS vector were regenerated from a total of 30 explants which account for approximately 37% of the transformation efficiency.

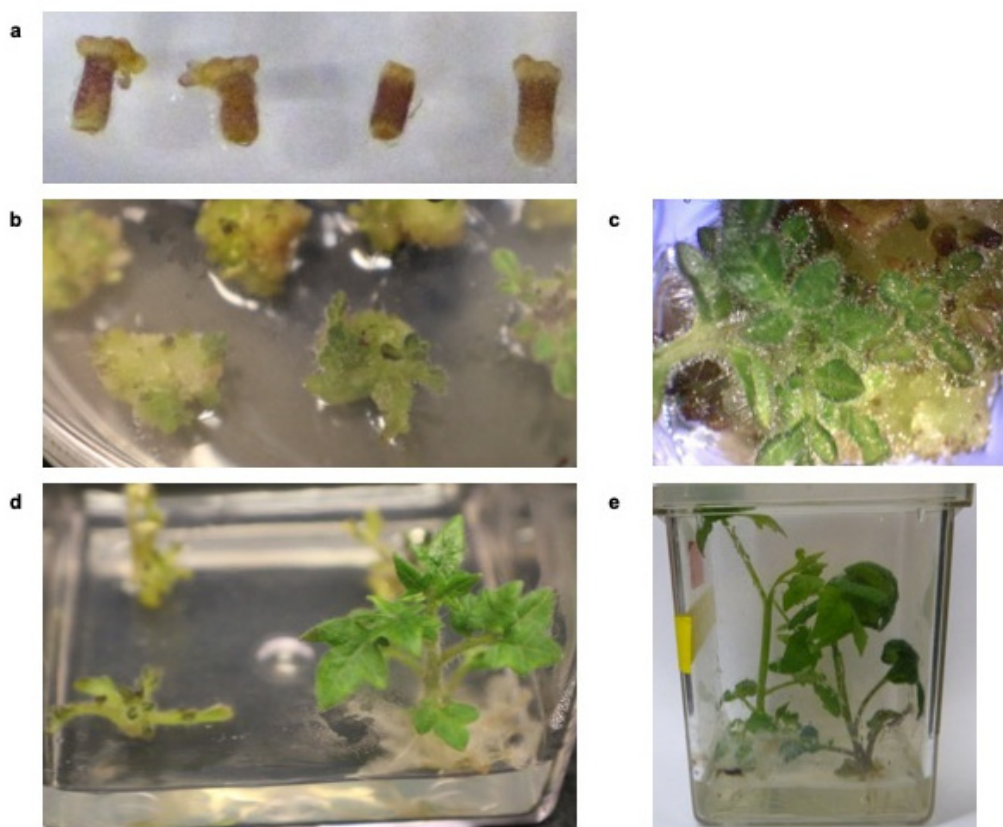


Figure 4.3. (a) Transformed hypocotyls with *Agrobacterium* after 20 days. Callus started to form at the end of the hypocotyls. (b) Transformed tomato calli with regenerated shoot on shoot selection medium containing 200 µg/L kanamycin after 6 weeks and (c) close up image on a single callus with regenerated shoot. (d) Regenerated shoots on root selection medium containing 100 µg/L kanamycin after 2 weeks and only the true transformants showed robust root growth. (e) True transformants on root selection medium was ready for transplanting to Pro-Mix soil.

Out of all the regenerated transgenic plants, five transgenic T₁ lines each from both pIFS/CHI and pIFS transformed lines were maintained in the greenhouse for segregation. Table 4.1 shows the record of all the transgenic tomato lines from T₁ to T₂ generation. Homozygous T₂ plants were confirmed by antibiotic selection and PCR amplification of the transgenes. A total of 18 homozygous T₂ IFS/CHI and 10 homozygous T₂ IFS transgenic plants were segregated from their respective T₁ transgenic plants and confirmed as homozygous lines.

T ₁ transgenic tomato	T ₂ transgenic tomato	Homozygous T ₂ transgenic tomato	T ₁ transgenic tomato	T ₂ transgenic tomato	Homozygous T ₂ transgenic tomato
IFS/CHI			IFS		
3	3-1 to 3-11	3-1 3-5 3-6 3-11	6	6-1 to 6-8	6-2
5	5-5 to 5-16	5-5 5-7 5-16	7	7-1 to 7-8	7-3 7-4 7-5
6	6-4 to 6-15	6-8 6-9 6-12 6-13 6-14	8	8-1 to 8-9	8-1
7	7-3 to 7-12	7-3 7-8 7-12	9	9-1 to 9-8	9-4 9-6
9	9-1 to 9-7	9-1 9-4 9-7	10	10-1 to 10-7	10-4 10-5 10-6

Table 4.1. The record of transgenic tomato lines from T₁ to T₂ generation. Total of 18 homozygous T₂ IFS/CHI and 10 homozygous T₂ IFS transgenic plants were confirmed.

Quantitation of transgene expression in homozygous transgenic tomato plants

Peel and flesh tissues from each homozygous line in both IFS/CHI and IFS groups were isolated and quantitated for transgene expression. Figure 4.4a shows the transgene expression in peel samples for IFS/CHI group normalized with the tomato β -tubulin (housekeeping gene) gene expression. All homozygous lines except those segregated from

T₁ generation of IFS/CHI-3 displayed a relatively high transgene expression profile in peel samples with IFS/CHI 9-7 as the highest expresser among all. However, the transgene expression trend in flesh samples (Figure 4.4b) was very different from the trend seen in peel samples. In flesh samples, the transgene expression in flesh samples of IFS/CHI-6-(8, 9, 12, 13, 14) and IFS/CHI-9-(1, 4, 7) were reduced for about 10-20%, relative to levels determined in peel samples. On the other hand, the *IFS* gene expression in IFS/CHI-3-(1, 5, 6, 11) was relatively similar to the expression level in its peel sample group. IFS/CHI-5-(5, 7, 16) and IFS/CHI-7-(3, 8, 12) group displayed a rather interesting trend for their *IFS* gene expression which increased by 5-20% while their *CHI* gene expression was declined. In IFS transgenic lines, *IFS* gene is the only transgene involved for quantitation. Figure 4.5 shows the *IFS* gene expression in both peel and flesh samples from the IFS group. The *IFS* gene expression was relatively similar for both peel and flesh samples except for lines IFS 7-4 and IFS 9-4. IFS line 10-4 displayed the highest levels of *IFS* gene expression among all the other homozygous lines within its group. The differences in transgene expression trend could be an indication of the amount of genistein that each line produces in fruit tissues. In order to assess the effect of transgene expression in controlling the isoflavone production, a total of 7 homozygous lines in IFS/CHI group (IFS/CHI 3-11, 5-16, 6-8, 6-12, 7-3, 7-12, 9-7) and all 10 homozygous line in IFS group were selected for chemical quantitation analysis.

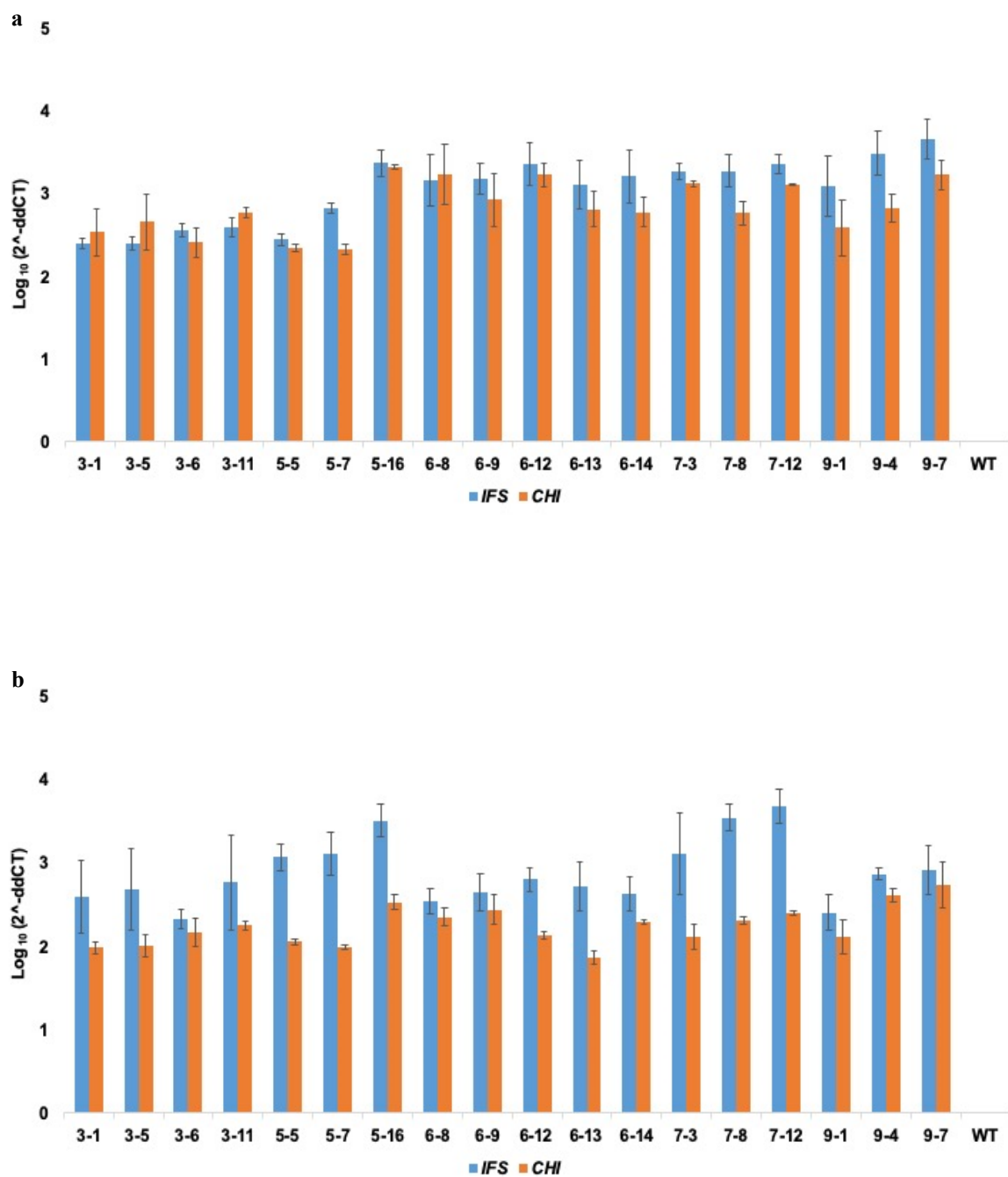


Figure 4.4. Transgene expression of *IFS* and *CHI* in (a) peel and (b) flesh tissue of *IFS/CHI* homozygous lines. Relative expression of each transgenic line was normalized with β -*tubulin* gene expression and expressed in \log_{10} scale. Experiments were repeated three times with independent batches of fresh samples.

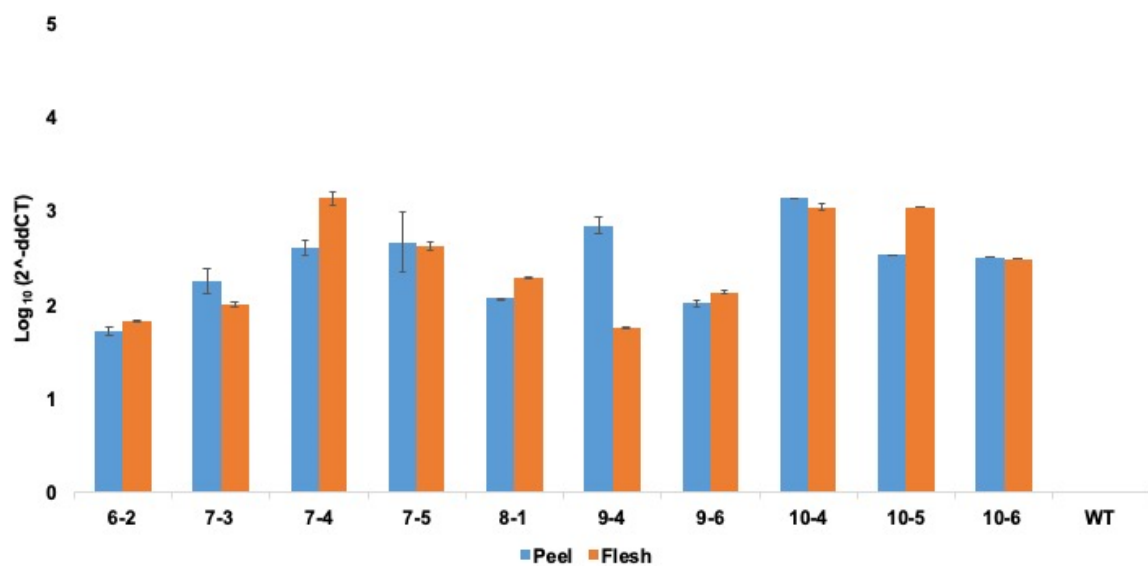


Figure 4.5. Transgenes expression of *IFS* in peel and flesh tissue of *IFS* homozygous lines. Relative expression of each transgenic line was normalized with β -*tubulin* gene expression and expressed in \log_{10} scale. Experiments were repeated three times with independent batches of fresh samples.

Chemical quantitation analysis of isoflavones in homozygous transgenic tomato lines

Crude extracts from all selected homozygous lines were analyzed by Agilent 1290 Infinity II UPLC system. A preliminary experiment was run using WT tomato and a couple of the *IFS*/*CHI* transgenic samples along with the isoflavone standards. Glycitein and glycitin were excluded from the standard set due to their undetectable levels in all the transgenic samples used in the preliminary experiment. Hence, only 4 isoflavone standards (genistein,

genistin, daidzein and daidzin) were used for the sample run. The summary of the chemical quantitation analysis in dry weight and fresh weight basis are illustrated in Table 4.2 and 4.3 respectively. IFS/IFS 9-7 transgenic line, as expected from the gene expression result, was the one that had the highest genistein content with 95935 ng in 1 g of dried tomato peel and 19578 ng in 1 g of dried tomato flesh. For 1 g of fresh tomato peel and flesh, it contained 21201 ng and 1390 ng of genistein respectively whereas WT tomato barely contained any significant amount of genistein. In addition to this striking finding, the levels of genistein present in dried and fresh tomato peel and flesh tissues were approximately 250-fold higher than those found in WT tomato. Besides the IFS/CHI 9-7 transgenic line, IFS/CHI 6-12 was the second transgenic line with a relatively high genistein content, in this case, approximately 180-fold higher than WT tomato. The remaining homozygous lines in IFS/CHI group did not produce a significant amount of genistein as compared to WT tomato. Likewise, all homozygous lines in IFS groups did not produce genistein to a satisfactory level which the highest expresser (IFS 10-4) was only 2-fold higher than WT tomato. The highest amount of genistein produced was 844 ng per 1 g of dried tomato peel and 383 ng per 1 g dried of tomato flesh. Chromatograms of IFS/CHI 9-7 and WT (Figure 4.6) were generated to depict the responses of IFS/CHI 9-7 and WT peel and flesh sample analytes. The peak area of quantifier ion of the analyte, the highlighted region shown in the chromatogram, represents the amount of target compound that is present. The strong comparison between the peaks of IFS/CHI 9-7 and WT reinforced our idea that expression of both *IFS* and *CHI* gene synergistically drove the metabolic flux into genistein production in our transgenic tomato plants.

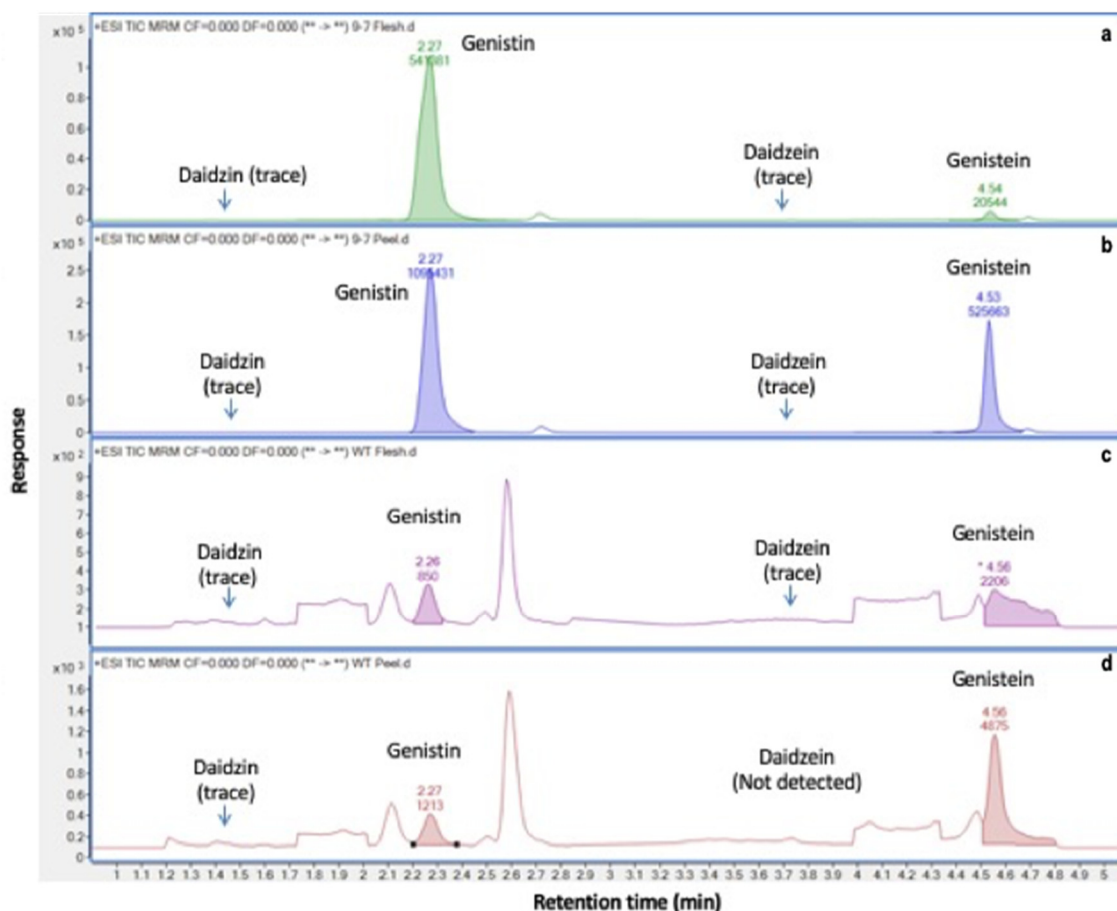


Figure 4.6. Extracted ion chromatogram of IFS/CHI 9-7 (a-flesh; b-peel) and WT (c-flesh; d-peel). Standard solution and peel and flesh sample extract (5 μ L) were analyzed by UPLC-QqQ-MS/MS system. Analytes from each sample were identified and confirmed by comparing to their respective MRM precursor-product ion pair transitions (daidzein, 255.1 \rightarrow 199.0/137.0; daidzin, 417.1 \rightarrow 255.0/199.0; genistein, 271.1 \rightarrow 153.0/91.1; genistin, 433.1 \rightarrow 271.0/152.9) and the retention time of standards. Highlighted peak area of quantifier ion for each analyte was calibrated and quantitated for its amount in each sample. Daidzein and daidzin were detected in only trace amounts or not detected at all for most of the transgenic samples besides the above listed samples. Genistin appeared to be the most abundant form in tomato fruit as its levels were much higher than genistein.

Sample Name	Daidzin (ng/g)	Daidzein (ng/g)	Genistin (ng/g)	Genistein (ng/g)	Total Genistein (ng/g)	Total Genistein (nM/g)
Tomato fruit peel						
IFS/CHI 9-7	6.778	24.342	61402.489	57557.000	95934.799	354.999
IFS/CHI 6-12	5.000	16.810	24780.398	57040.898	72529.148	268.388
IFS/CHI 7-3	Trace*	0.000	748.355	1194.397	1662.134	6.151
IFS/CHI 7-12	0.000	18.922	72.183	759.826	804.942	2.979
IFS/CHI 5-16	8.300	15.161	508.316	461.110	778.818	2.882
IFS/CHI 3-11	Trace*	14.698	241.345	472.679	623.525	2.307
IFS/CHI 6-8	Trace*	19.211	163.131	508.392	610.352	2.259
WT	0.000	Trace*	64.404	347.289	387.543	1.434
Tomato fruit flesh						
IFS/CHI 9-7	10.926	18.252	27879.976	2152.567	19578.116	72.447
IFS/CHI 6-12	9.967	54.368	19267.761	1078.768	13121.508	48.555
IFS/CHI 7-3	12.180	0.000	233.525	39.074	185.032	0.685
IFS/CHI 6-8	13.444	11.386	86.631	81.277	135.423	0.501
IFS/CHI 3-11	12.055	17.217	61.914	47.750	86.447	0.320
IFS/CHI 7-12	13.938	15.148	16.748	63.617	74.085	0.274
IFS/CHI 5-16	10.116	11.185	25.858	54.906	71.067	0.263
WT	0.000	0.000	49.098	47.763	78.450	0.290
IFS 10-5	0.000	8.097	370.152	151.845	383.198	1.418
IFS 7-4	0.000	4.923	303.289	78.281	267.842	0.991
IFS 6-2	0.000	12.617	75.416	154.793	201.930	0.747
IFS 8-1	0.000	15.411	34.794	172.660	194.407	0.719
IFS 7-5	15.026	13.386	29.834	121.944	140.590	0.520
IFS 9-6	0.000	22.162	53.731	97.188	130.771	0.484
IFS 10-6	0.000	0.000	65.856	88.117	129.279	0.478
IFS 7-3	0.000	0.000	18.213	106.788	118.172	0.437
IFS 10-4	0.000	Trace*	70.398	29.127	73.127	0.271
IFS 9-4	0.000	16.426	6.223	64.583	68.472	0.253

*compound detected but below the limit of quantification.

Table 4.2. Chemical quantification analysis of isoflavone content on the dry weight basis.

Experiment was repeated twice and the concentration of each isoflavone compound in peel and flesh tissues of selected homozygous transgenic lines in both IFS/CHI and IFS groups were averaged and listed in three decimal places. The total genistein was computed by summing the genistein and genistin levels, after correcting for molarity.

Sample Name	Daidzin (ng/g)	Daidzein (ng/g)	Genistin (ng/g)	Genistein (ng/g)	Total Genistein (ng/g)	Total Genistein (nM/g)
Tomato fruit peel						
IFS/CHI 9-7	1.498	5.380	13569.611	12719.779	21201.060	78.453
IFS/CHI 6-12	1.105	3.715	5476.331	12605.723	16028.541	59.312
IFS/CHI 7-3	Trace*	0.000	165.382	263.955	367.322	1.359
IFS/CHI 7-12	0.000	4.182	15.952	167.917	177.888	0.658
IFS/CHI 5-16	1.834	3.350	112.335	101.903	172.114	0.637
IFS/CHI 3-11	Trace*	3.248	53.336	104.459	137.796	0.510
IFS/CHI 6-8	Trace*	4.246	36.051	112.352	134.884	0.499
WT	0.000	Trace	14.233	76.749	85.645	0.317
IFS 10-4	0.000	0.000	210.431	54.938	186.462	0.690
IFS 6-2	0.000	4.990	105.312	88.403	154.225	0.571
IFS 7-4	0.000	3.392	22.705	138.577	152.767	0.565
IFS 10-5	Trace*	2.419	10.578	129.682	136.293	0.504
IFS 9-6	0.000	3.936	27.427	105.717	122.859	0.455
IFS 9-4	0.000	3.278	19.528	109.483	121.688	0.450
IFS 7-3	0.000	0.000	4.926	109.589	112.667	0.417
IFS 7-5	Trace*	8.036	23.982	88.403	103.392	0.383
IFS 8-1	0.000	3.991	26.708	81.064	97.757	0.362
IFS 10-6	0.000	0.000	39.299	60.079	84.642	0.313
Tomato fruit flesh						
IFS/CHI 9-7	0.776	1.296	1979.409	152.827	1389.998	5.144
IFS/CHI 6-12	0.708	3.860	1367.963	76.590	931.594	3.447
IFS/CHI 7-3	0.865	0.000	16.580	2.774	13.137	0.049
IFS/CHI 6-8	0.954	0.808	6.151	5.770	9.615	0.036
IFS/CHI 3-11	0.856	1.222	4.396	3.390	6.138	0.023
IFS/CHI 7-12	0.990	1.075	1.189	4.517	5.260	0.019
IFS/CHI 5-16	0.718	0.794	1.836	3.898	5.046	0.019
WT	0.000	0.000	3.486	3.391	5.570	0.021
IFS 10-5	0.000	0.575	26.280	10.781	27.206	0.101
IFS 7-4	0.000	0.350	21.533	5.558	19.016	0.070
IFS 6-2	0.000	0.896	5.354	10.990	14.337	0.053
IFS 8-1	0.000	1.094	2.470	12.258	13.802	0.051
IFS 7-5	1.067	0.950	2.118	8.658	9.982	0.037
IFS 9-6	0.000	1.573	3.815	6.900	9.284	0.034
IFS 10-6	0.000	0.000	4.676	6.256	9.178	0.034
IFS 7-3	0.000	0.000	1.293	7.582	8.390	0.031
IFS 10-4	0.000	Trace*	4.998	2.068	5.192	0.019
IFS 9-4	0.000	1.166	0.442	4.585	4.861	0.018

*compound detected but below the limit of quantification.

Table 4.3. Chemical quantification analysis of isoflavone content on the fresh weight basis.

Experiment was repeated twice and the concentration of each isoflavone compound in peel and flesh tissues of selected homozygous transgenic lines in both IFS/CHI and IFS groups were averaged and listed in three decimal places. The total genistein was computed by summing the genistein and genistin levels, after correcting for molarity.

Serotonin (5-HT) sensitivity assay in transgenic *C. elegans*

Genistein is well known for its ability to modulate inflammatory pathways through the inhibition of nuclear factor (NF)- κ B [26]. Inflammation and oxidative damage have been implicated in neurodegenerative diseases and one of the key inflammatory inducers is the accumulation of A β peptides [27]. Hence, genistein has the potential to reduce the pathological damage resulting from the formation of A β aggregates in neurodegenerative disease [28]. On the other hand, tomato is rich in lycopene which is well known for its antioxidant, anti-inflammatory and chemopreventive properties against different diseases, especially cancer. It has been reported that lycopene attenuates A β -induced cellular toxicity in cultured neuron cells [29]. It is plausible to speculate that both lycopene and genistein might work synergistically in reducing the pathological damage by neurodegenerative diseases.

Three transgenic lines (IFS/CHI 9-7, 7-3 and IFS 10-4) including WT and a set of genistein standards with different concentrations were used to test the effect they have on the neurodegenerative disease. Transgenic CL2355 *C. elegans* with pan-neuronal expression of human A β_{1-42} peptide under permissive temperature [30] was used in this study. Serotonin is known to be an important signaling molecule and neurotransmitter that regulates the response of worm to changing environmental cues. It does this by affecting behaviors in locomotion, egg-laying and olfactory learning [31, 32]. Expression of A β in transgenic worms' nerve system can cause them to be hypersensitive in exogenous

serotonin exposure eventually resulting in paralysis due to A β toxicity [33-35]. This paralysis phenotype was used as a scoring parameter to observe any possible therapeutic effects of feeding worms with the crude compounds prepared from selected transgenic lines. A dose-response assay of pure genistein compound was developed and established by feeding worms in various concentrations of genistein to worms. Figures 7a and 7b show the effect of the crude compound from different transgenic lines on neurodegenerative disease symptoms in transgenic *C. elegans*. The amount of IFS/CHI 9-7 crude compounds fed to transgenic worms in these experiments contained 35.5 nM of genistein. Consequently, we used the same amount of pure genistein as a standard positive control in the treatment sets for comparison. Worms fed with IFS/CHI 9-7 crude compounds and 100 μ M of genistein showed a delayed paralysis time of about 15 minutes, compared to non-treated groups (CK and CK+DMSO) that reached complete paralysis by an average of 5 minutes. This observation showed that our transgenic tomato sample (IFS/CHI 9-7) could generate the same level of inhibitory effect on A β toxicity with an amount of genistein that was 99.97% less than those present in the 100 μ M pure genistein compound. When comparing worms fed with WT to IFS/CHI 9-7 crude compounds, worms in the former group became paralyzed around 10 minutes while the latter group managed to delay onset of paralysis by 50%. This finding suggests a possible collaborative effect of lycopene and genistein in neutralizing the A β toxicity, possibly, through their interference in worms' inflammatory pathway. The group of worms fed with IFS/CHI 7-3 crude compounds and 10 μ M of genistein paralyzed at 13 and 14 minutes respectively whereas the remaining group of worms fed with WT and BINIFS 10-4 crude extracts as well as 1 μ M and 0.1 μ M of genistein paralyzed between 9-12 minutes. Overall, genistein dose-dependently reduced

the stress response caused by A β toxicity and transgenic tomato sample performed better in attenuating the neuronal damage than WT tomato extracts.

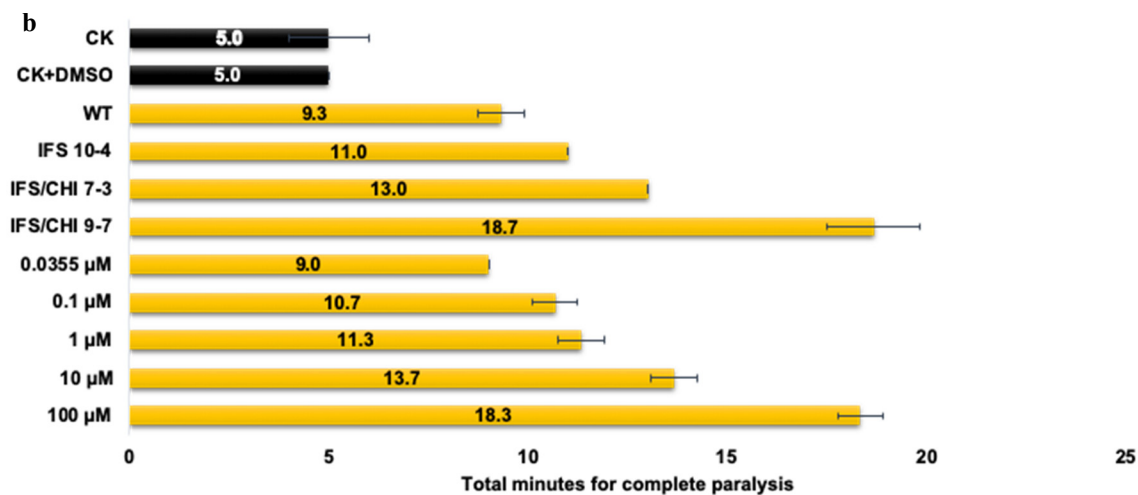
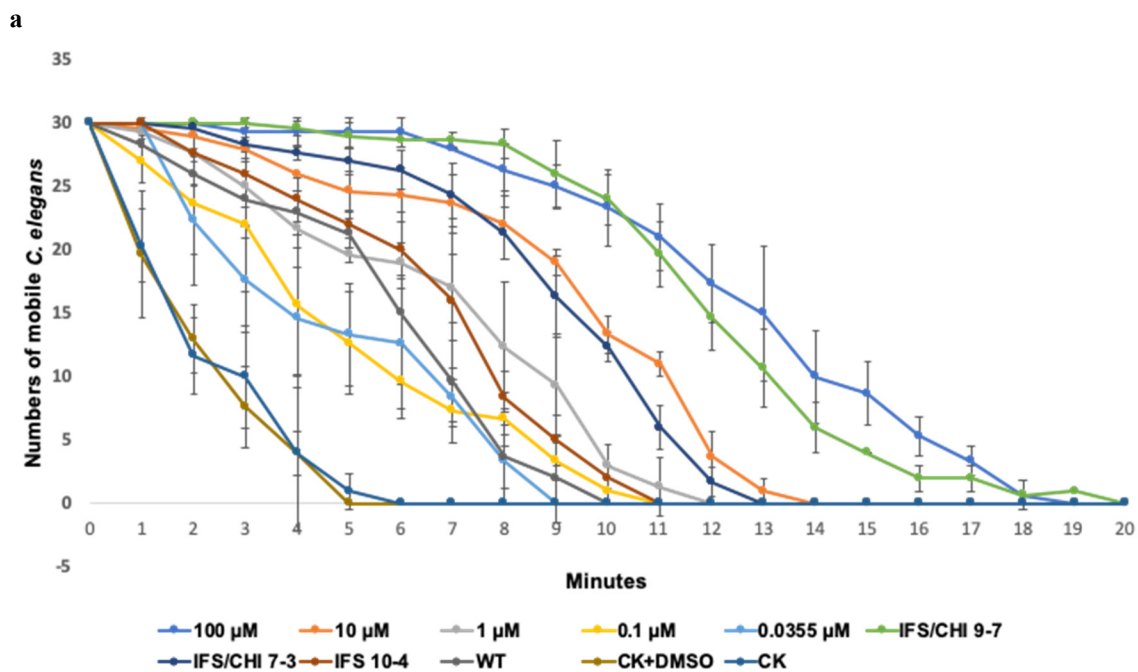


Figure 4.7. Serotonin sensitivity assay illustrates the effects of *C. elegans* fed with different crude extracts from transgenic samples and different concentrations of genistein standard. Assay was carried out post 36 hours of temperature upshift (16 °C to 23 °C) to induce the A β ₁₋₄₂ expression and deposition. **(a)** The number of mobile worms detected at minute intervals was recorded for each treatment group and **(b)** total time for worms in each treatment group to be completely paralyzed was summarized. The experiment was repeated with three independent sample sets and data were averaged with standard deviation.

Quantitative fluorescence staining of A β aggregates with thioflavin-T

Since the serotonin sensitivity assay result demonstrated a protective effect of transgenic crude compounds in reducing the A β toxicity, we further investigated if our transgenic crude compounds would have any direct effect on the A β expression or the A β aggregate formation. Thus, the A β aggregates were quantified using the fluorescence staining of thioflavin-T, which binds to A β aggregates [36, 37]. Similarly to the serotonin sensitivity assay, worms were fed with different crude compounds and genistein standards together with the untreated control with and without DMSO. The total protein was isolated from each treatment set after 36 hours of temperature upshift. Figure 4.8 shows the level of A β in CL2355 transgenic worm after treating with transgenic crude compounds and genistein standards. The readings generated by the 96-well plate reader were normalized to blank samples and the percentage of A β was calculated comparing to CK+DMSO group as a control. IFS/CHI 9-7 treatment set (containing 35.5 nM of genistein), demonstrated a

protective effect in that the formation of A β aggregates was 39% lower than the control set. The protective effect seen in IFS/CHI 9-7 was double the effect on worms fed with 100 μ M of genistein. For the genistein standard treatment set, the effect on A β formation was not significant as compared to the control set, ranging from 6-10%, except for the 100 μ M treatment set which was 19% lower than the control set. On the contrary, the crude compound treatment set performed better than the pure genistein compound treatment set alone. IFS/CHI 7-3, IFS 10-4 and WT crude compounds (containing 0.312 nM, 0.615 nM, 0.143 nM of genistein respectively) separately had achieved 6%, 12% and 17% reduction in A β formation. In summary, the inhibitory effect of pure genistein treatment alone in A β oligomerization is not that remarkable as compared to the crude compound treatment in this quantitation assay.

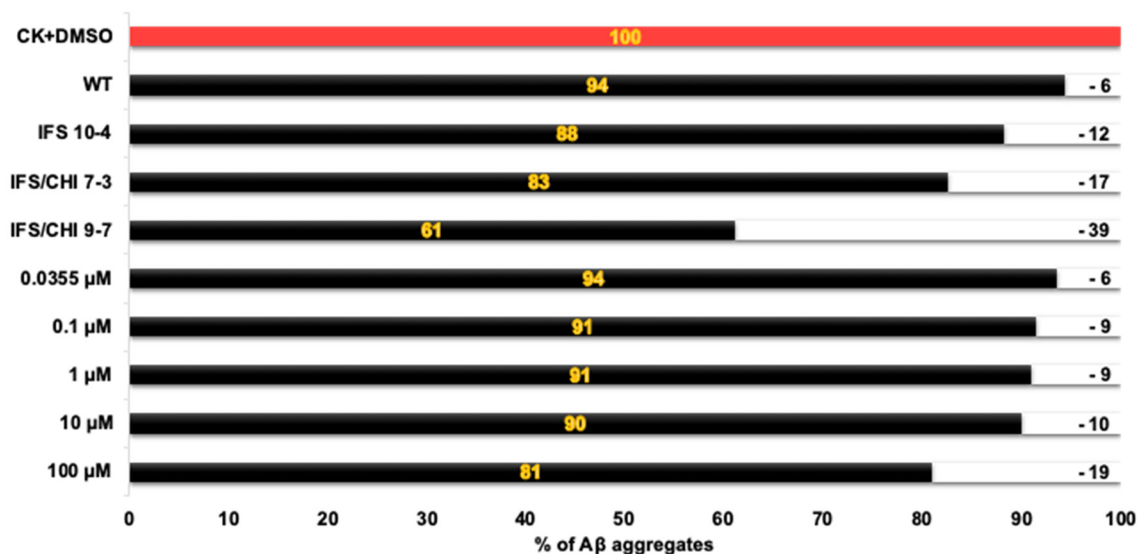


Figure 4.8. Quantification of A β aggregates by thioflavin-T fluorescence staining to illustrate the potential inhibitory effect of A β aggregates formation when *C. elegans* was fed with different crude extracts from transgenic samples and different concentrations of a pure genistein standard. Quantitation assay was carried out post 36 hours of temperature upshift (16 °C to 23 °C) to induce the A β ₁₋₄₂ expression and deposition. The fluorescence signal was quantified using Biotek Synergy 4 Plate Reader with excitation at 440 nm and emission at 482 nm. Experiments were repeated with three independent sample sets and data were averaged. The averaged data were expressed as percentage of A β aggregates and CK+DMSO (control with 0.6% DMSO) as the baseline.

Discussion

Over the past three decades, dietary supplements include vitamins, metabolites, minerals, and enzymes have gradually become an integral component in our health and wellness regime as well as daily meals to provide sufficient nutrients for replenishing our body. Nevertheless, taking supplements can be very intimidating due to some of the harmful effects of taking supplements in excess or mixing supplements [38]. While dietary supplements are the mainstays of current health and wellness programs, getting nutrients from food is always a better alternative to circumvent any unforeseen negative effects from supplement intake. Thus, having food that contains multiple types of nutrients would be a more ideal way to nurture our body instead of supplements. In this study, we attempt to integrate genistein into a food that is widely consumed in Western diets, namely, tomato.

A decade ago, researchers from Hong Kong University produced a transgenic tomato line expressing soybean *IFS* gene driven by the 35S promoter. Genistein production in their transgenic tomato, nonetheless, was unsatisfactory, with the highest yield of genistein in fruit peel at 0.45 nM/g of its fresh weight [12]. In comparison, our highest yield of genistein in IFS/CHI 9-7 fruit peel (78.5 nM/g of its fresh weight) is approximately 174-fold higher than those observed in their highest expressing transgenic line. This striking outcome is very likely due to the co-expression of *IFS* and *CHI* gene within our transgenic tomato. Expression of the endogenous *CHI* gene in both WT and transgenic tomato are weakly expressed and the computed fold-change in log₁₀ scale ranging from 0.3 to 0.7, merely comparable to the transgene expression as shown in Figures 4.4 and 4.5. Since naringenin is the precursor of genistein (Figure 4.9) [39], a weakly expressed endogenous *CHI* gene might not be able to produce the CHI enzyme to make enough precursors available for synthesizing genistein even if the *IFS* transgene is highly expressed. Expression of the *CHI* transgene may allow the plant to isomerize naringenin chalcone to naringenin making it available for synthesizing genistein. Even though naringenin will be available, there is still a possibility of competition for this compound as a substrate for flavonol and anthocyanin biosynthesis [40]. This might explain why some IFS/CHI transgenic lines were unable to synthesize a significant amount of genistein. For the IFS group, the initial idea of deploying a tomato fruit-specific *E8* promoter to drive *IFS* gene expression aimed to increase the accumulation of genistein in fruit tissues [41]. However, an insufficient amount of precursor might have been a limiting factor for genistein production in these IFS lines. Previous studies reported that co-expression of the Arabidopsis transcription factor (*AtMYB12*) with other structural genes can substantially enhance the production of

isoflavones [13, 42]. Researchers from John Innes Centre has reported that co-expression of *AtMYB12* with *IFS* gene driven by *E8* promoter can enhance the genistein level in MicroTom tomato fruit. *AtMYB12* transcription factor is a transcriptional regulator of *chalcone synthase (CHS)* and *flavonol synthase (FLS)* in planta and can enhance the synthesis of flavonoid compounds [43]. The total genistein yield on a dry weight basis from WT and their highest expressing lines of *IFS* and *AtMYB12 IFS* were 0.112 mg/g, 0.284 mg/g and 7 mg/g respectively [13]. Their co-expression line contains a relatively high amount of genistein, with a 39-fold increase, compared to WT. In comparison with their result, expression of the *CHI* gene in transgenic *IFS/CHI* tomato plants in the present studies has validated our hypothesis that it may increase the efficiency of genistein synthesis by making available higher levels of pathway precursors. The higher genistein content present in two of our *IFS/CHI* lines might indicate the involvement of other structural gene modulators that redirect the flux into isoflavone synthesis. Co-expression of *AtMYB12* with *IFS* and *CHI* genes could be another ideal strategy to generate transgenic tomato with higher level of genistein.

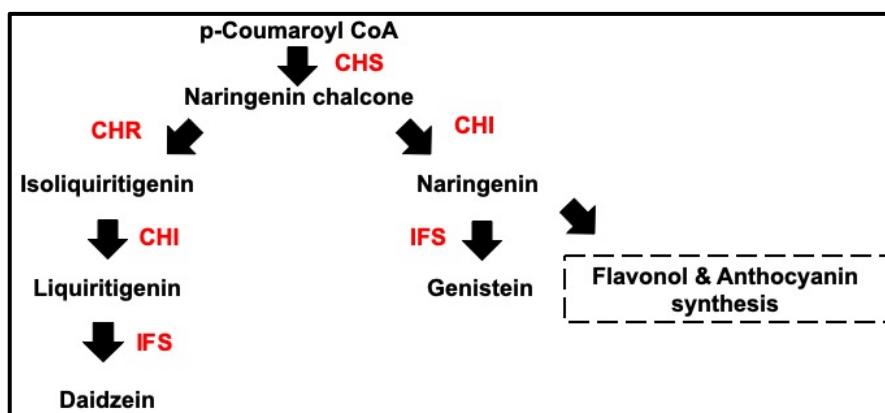


Figure 4.9. Simple illustration of the isoflavone synthesis pathway showing intermediates and enzymes mentioned in this study. CHS, chalcone synthase; CHI, chalcone isomerase; CHR, chalcone reductase; IFS, isoflavone synthase.

In order to get a realistic perspective on the generation of 2 in 1 (genistein and lycopene) transgenic tomato, we set up a comparison chart with foods that contain a significant amount of isoflavone. Table 4.4 illustrates some of the common foods that generally known to have a high level of genistein and daidzein. All this food nutrient information was obtained from the USDA Food Composition Database website under the Special Interest Databases of isoflavones [44]. Information regarding isoflavone content in raw tomato was obtained from another source [45]. Our best line of transgenic tomato, IFS/CHI 9-7, constituents only 11.85% (in 1g of tomato dried peel) of genistein content in 1 g of raw soybean seeds whereas the amount of daidzein in transgenic tomato is no way comparable to soybean because tomato does not have the *chalcone reductase (CHR)* gene to convert naringenin into precursor for daidzein synthesis (refer to Figure 4.9). Despite the transgenic tomato lines generated in this study did not produce amounts of genistein that are on par with soy products, we have made a great breakthrough in enhancing the genistein content in transgenic tomato fruit by no less than 150-fold, compared to WT tomato.

Food	Daidzein (ng/g)	Genistein (ng/g)
Soybeans, mature seeds, raw	620700	809900
Soymilk, made from soy isolate	28000	31000
Soy drink	27500	51000
Soy yogurt	137700	165900
Soy cheese, American	57500	87000
Tempeh	226600	361500
Tofu yogurt	57000	94000
Tofu, soft, VITASOY-silken	85900	206500
Miso	164300	232400
Black bean, sauce	59600	40400
Peanuts, all types, raw	200	2400
Tomato, raw	0	32.5
IFS/CHI 9-7, dried peel	28	95935
IFS/CHI 9-7, fresh peel	5	21201
IFS/CHI 9-7, dried flesh	25	19578
IFS/CHI 9-7, fresh flesh	2	1390

Table 4.4. List of selected foods that contain significant level of isoflavone, particularly in genistein and daidzein. Bottom box sample is the best line of our transgenic tomato, IFS/CHI 9-7, serving as a comparison. The value listed above is for a general guidance since isoflavone content of foods can vary considerably between food sources and brands.

Genistein has been known for a long time to have a protective effect for many chronic diseases especially cancer, diabetes, obesity, neurodegenerative and HIV-infection [2, 46-49]. Genistein is the most biologically active phytoestrogen found in soy and it interacts with estrogen receptors ER α and ER β but more selective to ER β [50, 51]. Its antioxidant property and ability to bind to ER β may contribute to its anti-inflammatory, anti-osteoporosis and anti-cancer effects [52]. In our study, we focused on investigating the effects of genistein on neurodegenerative illnesses especially Alzheimer's disease. The

production and accumulation of toxic amyloid β ($A\beta$) peptide and tau tangles has been long speculated to be linked with the pathogenesis factor of neurodegenerative disorders [53]. While there is no cure for neurodegenerative diseases or a way to slow it down, genistein and lycopene might be an alternative for delaying the disease progression. Our results have showed that the crude extract from our best yield transgenic line, IFS/CHI 9-7, could delay the paralysis time by 75% compared to non-treated control set and its performance is 50% better than genistein standard alone at the same concentration (0.035 μ M). These results indicated that crude extract of IFS/CHI 9-7 could reduce $A\beta$ -induced toxicity in human by 75%. Based on Figure 4.7a-b, genistein itself acts on a dose-dependent pattern and a similar trend can be seen in transgenic lines as well. The higher concentration of genistein content can have a substantial effect in inhibiting the $A\beta$ -induced toxicity and allows *C. elegans* to maintain its mobility after exposing to serotonin. Genistein and lycopene were previously proved to have strong antioxidant property and powerful reactive oxygen species (ROS) scavenging activities [2, 54, 55]. This is possibly due to their antioxidant property that has reduced the oxidative damage induced by $A\beta$ accumulation. Similar to *Ginkgo biloba* extract which has a strong protective effect on $A\beta$ aggregation [56, 57], genistein, through its binding to the estrogen receptor, can suppress the endoplasmic reticulum stress and $A\beta$ -induced toxicity by preventing neuron cell death [58]. Hence, our results further indicate that the combination therapy using the mixture of genistein and lycopene, even at a small amount, can gain a greater protective effect on disease progression. Consequently, we are interested to see if genistein has a direct effect on the formation of $A\beta$ aggregates. Based on our thioflavin-T quantitative staining results (Figure 4.8), IFS/CHI 9-7 displayed a striking reduction in $A\beta$ aggregates by 39% which is double the effect of 100 μ M.

Generally, transgenic lines (IFS/CHI 7-3 and IFS 10-4) have a better outcome compared to genistein alone. The synergistic effect of genistein and other antioxidant compounds within the transgenic tomato on reducing the formation of toxic aggregates is evident. It is possible that they can indirectly or directly modulate the formation of non-toxic A β monomer. A recent study has shown that genistein can dose-dependently inhibit or slow down the oligomerization of A β in the *in vitro* tests [59]. If genistein is capable of interrupting the formation of toxic A β aggregates upon ingestion, it would be interesting as well to study if genistein can modulate amyloid precursor protein (APP) and γ -secretase expression for attenuating neurodegenerative diseases. Even though our results confirmed that the combination of genistein, lycopene and other antioxidant compounds have protective effect on alleviating the disease symptoms, additional experiments are needed to strengthen our interpretation. Oxidative stress assay and quantitation of gene expression on genes involved in the disease progression will provide a clearer understanding of genistein molecular mechanism acting on neurodegenerative diseases.

References

1. Dixon, R.A. and D. Ferreira, *Genistein*. Phytochemistry, 2002. **60**(3): p. 205-11.
2. Matsuda, S., et al., *Chapter 93 - Neuroprotection of Genistein in Alzheimer's Disease*, in *Diet and Nutrition in Dementia and Cognitive Decline*, C.R. Martin and V.R. Preedy, Editors. 2015, Academic Press: San Diego. p. 1003-1010.
3. Pawlowski, J.W., et al., *Impact of equol-producing capacity and soy-isoflavone profiles of supplements on bone calcium retention in postmenopausal women: a randomized crossover trial*. Am J Clin Nutr, 2015. **102**(3): p. 695-703.
4. Mukund, V., et al., *Genistein: Its role in metabolic diseases and cancer*. Crit Rev Oncol Hematol, 2017. **119**: p. 13-22.

5. Devi, K.P., et al., *Molecular and Therapeutic Targets of Genistein in Alzheimer's Disease*. Mol Neurobiol, 2017. **54**(9): p. 7028-7041.
6. Wang, Y., et al., *Genistein suppresses the mitochondrial apoptotic pathway in hippocampal neurons in rats with Alzheimer's disease*. Neural Regen Res, 2016. **11**(7): p. 1153-8.
7. Mirahmadi, S.M., et al., *Soy isoflavone genistein attenuates lipopolysaccharide-induced cognitive impairments in the rat via exerting anti-oxidative and anti-inflammatory effects*. Cytokine, 2018. **104**: p. 151-159.
8. Zhao, L. and R.D. Brinton, *Estrogen receptor alpha and beta differentially regulate intracellular Ca(2+) dynamics leading to ERK phosphorylation and estrogen neuroprotection in hippocampal neurons*. Brain Res, 2007. **1172**: p. 48-59.
9. Zhao, L., et al., *17beta-Estradiol regulates insulin-degrading enzyme expression via an ERbeta/PI3-K pathway in hippocampus: relevance to Alzheimer's prevention*. Neurobiol Aging, 2011. **32**(11): p. 1949-63.
10. Zhao, L., S.K. Woody, and A. Chhibber, *Estrogen receptor beta in Alzheimer's disease: From mechanisms to therapeutics*. Ageing Res Rev, 2015. **24**(Pt B): p. 178-90.
11. Rizzo, G. and L. Baroni, *Soy, Soy Foods and Their Role in Vegetarian Diets*. Nutrients, 2018. **10**(1): p. 43.
12. Shih, C.H., et al., *Accumulation of isoflavone genistin in transgenic tomato plants overexpressing a soybean isoflavone synthase gene*. J Agric Food Chem, 2008. **56**(14): p. 5655-61.
13. Zhang, Y., et al., *Multi-level engineering facilitates the production of phenylpropanoid compounds in tomato*. Nat Commun, 2015. **6**: p. 8635.
14. Li, X., et al., *Metabolic engineering of isoflavone genistein in Brassica napus with soybean isoflavone synthase*. Plant Cell Rep, 2011. **30**(8): p. 1435-42.
15. Sreevidya, V.S., et al., *Metabolic engineering of rice with soybean isoflavone synthase for promoting nodulation gene expression in rhizobia*. J Exp Bot, 2006. **57**(9): p. 1957-69.
16. Beecher, G.R., *Nutrient content of tomatoes and tomato products*. Proc Soc Exp Biol Med, 1998. **218**(2): p. 98-100.
17. U.S. Department of Agriculture, A.R.S. *USDA National Nutrient Database for Standard Reference*. Full Report (All Nutrients): 11529, Tomatoes, red, ripe, raw, year round average 2018; Available from: <https://ndb.nal.usda.gov/ndb/>.
18. Dixon, R.A., *A two-for-one in tomato nutritional enhancement*. Nature Biotechnology, 2005. **23**(7): p. 825-826.
19. Livak, K.J. and T.D. Schmittgen, *Analysis of relative gene expression data using real-time quantitative PCR and the 2(-Delta Delta C(T)) Method*. Methods, 2001. **25**(4): p. 402-8.
20. Champagne, C.E., et al., *Compound leaf development and evolution in the legumes*. Plant Cell, 2007. **19**(11): p. 3369-78.
21. Doyle, J.J. and M.A. Luckow, *The rest of the iceberg. Legume diversity and evolution in a phylogenetic context*. Plant Physiol, 2003. **131**(3): p. 900-10.
22. Frary, A. and J. Van Eck, *Organogenesis from transformed tomato explants*. Methods Mol Biol, 2005. **286**: p. 141-50.

23. Sun, H.J., et al., *A highly efficient transformation protocol for Micro-Tom, a model cultivar for tomato functional genomics*. Plant Cell Physiol, 2006. **47**(3): p. 426-31.
24. Cruz-Mendivil, A., et al., *A Simple and Efficient Protocol for Plant Regeneration and Genetic Transformation of Tomato cv. Micro-Tom from Leaf Explants*. 2011. **46**(12): p. 1655.
25. Kimura, S. and N. Sinha, *Tomato transformation*. CSH Protoc, 2008. **2008**: p. pdb prot5084.
26. Gupta, S.C., et al., *Role of nuclear factor kappaB-mediated inflammatory pathways in cancer-related symptoms and their regulation by nutritional agents*. Exp Biol Med (Maywood), 2011. **236**(6): p. 658-71.
27. Valles, S.L., et al., *Estradiol or genistein prevent Alzheimer's disease-associated inflammation correlating with an increase PPAR gamma expression in cultured astrocytes*. Brain Res, 2010. **1312**: p. 138-44.
28. Bagheri, M., et al., *Genistein ameliorates learning and memory deficits in amyloid beta(1-40) rat model of Alzheimer's disease*. Neurobiol Learn Mem, 2011. **95**(3): p. 270-6.
29. Chen, D., C. Huang, and Z. Chen, *A review for the pharmacological effect of lycopene in central nervous system disorders*. Biomed Pharmacother, 2019. **111**: p. 791-801.
30. Luo, Y., et al., *Caenorhabditis elegans Model for Initial Screening and Mechanistic Evaluation of Potential New Drugs for Aging and Alzheimer's Disease*. 2009.
31. Chase, D. and M. Koelle, *Biogenic amine neurotransmitters in C. elegans*. WormBook : the online review of C. elegans biology, 2007. **20**: p. 1-15.
32. Nuttley, W.M., K.P. Atkinson-Leadbetter, and D. van der Kooy, *Serotonin mediates food-odor associative learning in the nematode Caenorhabditis elegans*. Proceedings of the National Academy of Sciences, 2002. **99**(19): p. 12449-12454.
33. Arya, U., H. Dwivedi, and J.R. Subramaniam, *Reserpine ameliorates A β toxicity in the Alzheimer's disease model in Caenorhabditis elegans*. Experimental Gerontology, 2009. **44**(6): p. 462-466.
34. Wu, Y., et al., *Amyloid- β -Induced Pathological Behaviors Are Suppressed by Ginkgo biloba Extract EGb 761 and Ginkgolides in Transgenic Caenorhabditis elegans*. The Journal of Neuroscience, 2006. **26**(50): p. 13102.
35. Zhi, D., et al., *Dianxianning improved amyloid β -induced pathological characteristics partially through DAF-2/DAF-16 insulin like pathway in transgenic C. elegans*. Scientific Reports, 2017. **7**(1): p. 11408.
36. Dostal, V. and C.D. Link, *Assaying β -amyloid toxicity using a transgenic C. elegans model*. Journal of visualized experiments : JoVE, 2010(44): p. 2252.
37. Xin, L., et al., *Acetylcholinesterase-inhibiting alkaloids from Lycoris radiata delay paralysis of amyloid beta-expressing transgenic C. elegans CL4176*. PLoS One, 2013. **8**(5): p. e63874.
38. Deldicque, L. and M. Francaux, *Potential harmful effects of dietary supplements in sports medicine*. Curr Opin Clin Nutr Metab Care, 2016. **19**(6): p. 439-445.
39. Dixon, R.A. and G.M. Pasinetti, *Flavonoids and isoflavonoids: from plant biology to agriculture and neuroscience*. Plant Physiol, 2010. **154**(2): p. 453-7.

40. Liu, C.J., et al., *Bottlenecks for metabolic engineering of isoflavone glycoconjugates in Arabidopsis*. Proc Natl Acad Sci U S A, 2002. **99**(22): p. 14578-83.
41. Kurokawa, N., et al., *An E8 promoter-HSP terminator cassette promotes the high-level accumulation of recombinant protein predominantly in transgenic tomato fruits: a case study of miraculin*. Plant Cell Rep, 2013. **32**(4): p. 529-36.
42. Pandey, A., et al., *Co-expression of Arabidopsis transcription factor, AtMYB12, and soybean isoflavone synthase, GmIFS1, genes in tobacco leads to enhanced biosynthesis of isoflavones and flavonols resulting in osteoprotective activity*. Plant Biotechnol J, 2014. **12**(1): p. 69-80.
43. Mehrrens, F., et al., *The Arabidopsis transcription factor MYB12 is a flavonol-specific regulator of phenylpropanoid biosynthesis*. Plant physiology, 2005. **138**(2): p. 1083-1096.
44. U.S. Department of Agriculture, A.R.S. *USDA Database for the Isoflavone Content of Selected Foods, Release 2.1*. 2015; Available from: <http://www.ars.usda.gov/nutrientdata/isoflav>.
45. Liggins, J., et al., *Daidzein and genistein contents of vegetables*. Br J Nutr, 2000. **84**(5): p. 717-25.
46. Gilbert, E.R. and D. Liu, *Anti-diabetic functions of soy isoflavone genistein: mechanisms underlying its effects on pancreatic beta-cell function*. Food Funct, 2013. **4**(2): p. 200-12.
47. Guo, J. and Y. Wu, *Chapter 11 - Genistein and HIV Infection*, in *HIV/AIDS*, V.R. Preedy and R.R. Watson, Editors. 2018, Academic Press. p. 125-134.
48. McLaughlin, J.M., et al., *Effects of tomato- and soy-rich diets on the IGF-I hormonal network: a crossover study of postmenopausal women at high risk for breast cancer*. Cancer Prev Res (Phila), 2011. **4**(5): p. 702-10.
49. Rockwood, S., T.L. Broderick, and L. Al-Nakkash, *Feeding Obese Diabetic Mice a Genistein Diet Induces Thermogenic and Metabolic Change*. J Med Food, 2018. **21**(4): p. 332-339.
50. Kuiper, G.G., et al., *Interaction of estrogenic chemicals and phytoestrogens with estrogen receptor beta*. Endocrinology, 1998. **139**(10): p. 4252-63.
51. Morito, K., et al., *Interaction of phytoestrogens with estrogen receptors alpha and beta*. Biol Pharm Bull, 2001. **24**(4): p. 351-6.
52. Spagnuolo, C., et al., *Genistein and cancer: current status, challenges, and future directions*. Adv Nutr, 2015. **6**(4): p. 408-19.
53. Bloom, G.S., *Amyloid-beta and tau: the trigger and bullet in Alzheimer disease pathogenesis*. JAMA Neurol, 2014. **71**(4): p. 505-8.
54. Tvrdá, E., et al., *Antioxidant efficiency of lycopene on oxidative stress - induced damage in bovine spermatozoa*. J Anim Sci Biotechnol, 2016. **7**(1): p. 50.
55. Wei, H., et al., *Antioxidant and antipromotional effects of the soybean isoflavone genistein*. Proc Soc Exp Biol Med, 1995. **208**(1): p. 124-30.
56. Janssen, I.M., et al., *Ginkgo biloba in Alzheimer's disease: a systematic review*. Wien Med Wochenschr, 2010. **160**(21-22): p. 539-46.
57. Yang, G., et al., *Ginkgo Biloba for Mild Cognitive Impairment and Alzheimer's Disease: A Systematic Review and Meta-Analysis of Randomized Controlled Trials*. Curr Top Med Chem, 2016. **16**(5): p. 520-8.

58. Park, Y.J., Y.M. Jang, and Y.H. Kwon, *Isoflavones prevent endoplasmic reticulum stress-mediated neuronal degeneration by inhibiting tau hyperphosphorylation in SH-SY5Y cells*. *J Med Food*, 2009. **12**(3): p. 528-35.
59. Ren, B., et al., *Genistein: A Dual Inhibitor of Both Amyloid β and Human Islet Amylin Peptides*. *ACS Chemical Neuroscience*, 2018. **9**(5): p. 1215-1224.

Chapter **5**

Summary

Summary

The main objectives of this thesis were to utilize novel genetic engineering approach to study plant disease resistance and plant nutrient enhancement. The first objective was to investigate the involvement of the two susceptibility genes (*2OGO* and *EIN2*) in *Fusarium* head blight disease and examine the involvement of barley orthologues in *Fusarium graminearum* infection. The second objective was to engineer Moneymaker tomato with high level of genistein expression and study its therapeutic effect on Alzheimer's disease.

Based on our study on *Fusarium* head blight disease, both susceptibility gene knock-out Arabidopsis mutants were confirmed to confer resistance to fungal infection given that both gene knock-outs succeeded to delay or even impede the fungal colonization as compared to the susceptible wildtype. In addition, the complementation of barley orthologue genes in each of the knock-out mutants recovered the susceptible phenotype, thus implicating involvement of these genes in *Fusarium* resistance. Translational research in the Arabidopsis model provides a foundation for studying *Fusarium* head blight disease in barley.

The engineering of Moneymaker tomato with genistein expression has achieved a great breakthrough in generating a transgenic tomato with higher yield of genistein which is about 250-fold more than the non-transformed tomato. Even though the resulting genistein level is not comparable to soybeans, the success of upshifting the genistein production has led us to gain more ideas about optimizing the yield of this and other secondary products.

Moreover, the protective effect observed in Alzheimer's disease assays suggests that perhaps both genistein and lycopene, even at small amount or lower concentration, may slow down the disease progression and reduce neuronal damage at a greater extent.

In conclusion, the studies discussed in this thesis have achieved the overall objectives and manage to address some of the pressing challenges in producing disease resistance plants and food crops with a higher nutrition profile.